Crosstalk between Mesenchymal Stem/Stromal Cells and Host Immune Cells as a Critical Mechanism of Immunomodulation in Severe Viral Lung Infection and Sepsis

Yuan Tan

Thesis submitted to the University of Ottawa
in partial fulfillment of the requirements for the Doctorate in Philosophy (PhD) program in Cellular and Molecular Medicine

Department of Cellular and Molecular Medicine
Faculty of Medicine
University of Ottawa

Abstract

Sepsis is characterized by a systemic dysregulated immune response to severe infection. Research has shown that mesenchymal stromal/stem cells (MSCs) exert immune-modulatory functions *in vitro* and therapeutic benefits in various animal models of severe immune diseases. These promising results have driven the translation of MSCs as cellular therapy into clinical settings. The host sepsis environment, including the pathogens and the host immune response (cells and soluble factors), may play a crucial role in modifying the therapeutic efficacy of infused MSCs. Here, we aim to investigate the interplay between MSCs and the host microenvironment in three disease contexts: 1) severe SARS-CoV-2 infection (COVID-19), 2) acute lung injury (ALI) induced by H1N1 influenza A virus (IAV) infection and 3) human sepsis caused by heterogenous organisms.

First, we hypothesized that, in severe COVID-19, priming MSCs with a viral mimic would improve their abilities to rebalance the dysregulated immune responses. Transcriptome analysis of Poly(I:C)-primed MSCs (pIC-MSCs) revealed upregulation of pathways involved in antiviral and immunomodulatory responses. Together with increased expression of antiviral proteins, these changes translated into greater MSC effector functions in regulating monocytes and granulocytes, while enhancing their ability to block SARS-CoV-2 pseudovirus entry into epithelial cells. Importantly, the addition of pIC-MSCs to COVID-19 patient whole blood significantly reduced inflammatory neutrophil populations, increased the proportion of M2 monocytes and enhanced their phagocytic function.

In the second study, deep immune profiling was performed on airway and circulating immune cells to examine the effect of immunomodulation and therapeutic outcomes of MSCs therapy in mice with H1N1-induced ALI. Immune cell populations and phenotypic shifts were mapped in whole blood by mass cytometry, showing altered immune responses in animals receiving MSCs vs vehicle treatment. Compared to sham animals, IAV infection induced a significant increase in BAL total cell counts. MSC administration significantly decreased BAL total cell counts and altered immune infiltrations in IAV-infected mice. Phenotypic immune cell profiling of blood and BAL revealed a significant increase in the monocyte population with M2 phenotype in MSCs-treated animals. However, MSCs treatment did not improve survival of infected mice or reduce viral titres in the lungs of infected mice. Further investigation revealed that MSCs were highly susceptible to H1N1 IAV infection, leading to increased cell death and potentially reduced their efficacy.

Lastly, *ex vivo* human and *in vivo* animal models were utilized to investigate neutrophil and monocyte modulation by MSCs in sepsis. Results showed phenotypic and functional improvements of myeloid cells after coculture with MSCs. Interestingly, transcriptomic and cytokine analyses revealed adaptive reprograming of MSCs in response to the sepsis milieu. This activation of caspase-1 pathway of MSCs was subsequently confirmed as an essential molecular mechanism for the immunomodulatory effects of MSCs on dysfunctional neutrophils and monocytes. Caspase-1 activation in MSCs enhanced their therapeutic benefits in treating sepsis in vivo.

Overall, my work suggests that the function and efficacy of MSCs vary depending on types of infection induced by different pathogens and the host immune microenvironment.

These findings highlight the importance of understanding the adaptive responses of MSCs to the host environment in order to better tailor MSC-based therapy for severe viral and bacterial infections.

Acknowledgement

I would like to extend my deepest gratitude to all those who have supported me throughout the journey of my PhD thesis project.

First and foremost, I am profoundly grateful to my supervisors, Drs. Shirley Mei and Duncan Stewart. Dr. Stewart, I thank you for your guidance, continuous encouragement, and insightful feedback. Shirley, you have been a fantastic supervisor, I am sincerely appreciative of the time and effort that you have invested in my work. Since I starting as a technician back in 2016, your invaluable guidance and mentorship have been pivotal to my tremendous growth, both personally and professionally.

I would also like to express my heartfelt thanks to my colleague and dear friend, Dr. Luciana Souza-Moreira, for your unwavering support and friendship. Your help has been invaluable. And your birthday celebration was always a memorable occasion, and I am grateful for the moments we shared. Also, I want to give a big thank you to Mahmoud Salkhordeh, whose encouragement and signature jokes have provided much-needed relief and laughter, making this journey much more enjoyable. Maria, Yan, Pramod, Chi, Aidan, Glinton, Jennifer, Rebecca, Jiapey, and all the lab members, I deeply appreciate all your help and input. And thank you to Dr. Damian Carragher of proteomic core, your help in leading me into world of mass cytometry is important for my thesis development.

More thanks are owed, including to my thesis committee member, Drs. Harold Atkins and Subash Sad, your guidance and expert insights greatly helped in making critical improvements to this thesis. I also had the privilege of working alongside a fantastic intensive care unit (ICU) research team. Dr. Lauralyn McIntyre, Dr. Shane English, Irene Watpool, Rebecca Porteous, and Jessica Haines, I am incredibly thankful for your clinical research expertise in shaping my thesis.

I want to extend my gratitude to all my friends. Betty, Gina, Lucy, Ashley, Chelsea, and Anna, and all, your emotional support, understanding, and the fun times we shared outside lab helped me recharge and provided a great source of relaxation and laughter.

Lastly, I owe my deepest thanks to my family. Their unconditional love, patience, and belief in my abilities have been a constant source of strength. Without their support and understanding, this journey would not have been possible.

Thank you all for your support and encouragement.

Table of Contents

List of Tables

List of Figures

List of Abbreviations

ACE2	Angiotensin-converting enzyme 2
AKI	Acute kidney injury
ALI	Acute lung injury
APACHE II	Acute Physiology and Chronic Health Evaluation II
ARDS	Acute respiratory distress syndrome
BAL	Bronchoalveolar lavage
BM	Bone marrow
CARS	Compensatory anti-inflammatory response syndrome
CCL	Chemokine (C-C motif) ligand
cfDNA	Cell-free DNA
CFSE	Carboxyfluorescein succinimidyl ester
CLP	Cecal ligation and puncture
COVID-19	Coronavirus disease 2019
CXC	Chemokine (C-X-C motif)
CXCL	Chemokine (C-X-C motif) ligand
CXCR	Chemokine (C-X-C motif) receptor
CyTOF	Cytometry by time of flight
DC	Dendritic cell
DMSO	Dimethyl sulfoxide
DNA	Deoxyribonucleic acid
EDTA	Ethylenediaminetetraacetic acid
EV	Extracellular vesicle
FDA	Food and Drug Administration
FlowSOM	Flow Self-Organizing Map
GvHD	Graft-versus-host disease
HA	Hemagglutinin
HAEpi	Human airway epithelial cells
HLA-DR	Human leukocyte antigen - DR isotype
IAV	Influenza A virus
ICU	Intensive care unit
IDO	Indoleamine 2,3-dioxygenase
IFIT1	Interferon-induced protein with tetratricopeptide repeats 1
IFITM3	Interferon-induced transmembrane protein 3
IFN	Interferon
IL	Interleukin
IPA	Ingenuity Pathway Analysis
ISCT	International Society for Cellular Therapy
LN	Lymph node

LPS	Lipopolysaccharide
MAA	Mesenteric artery aneurysm
MHC	Major histocompatibility complex
miRNA	MicroRNA
MODS	Multiple organ dysfunction syndrome
MOI	Multiplicity of infection
MPO	Myeloperoxidase
MSC	Mesenchymal stem/stromal cells
MST	Minimal spanning tree
Mx1	Myxovirus resistance protein 1
NE	Neutrophil elastase
NK cells	Natural killer cells
NO	Nitric oxide
OAS1	2'-5'-Oligoadenylate synthetase 1
PBMC	Peripheral blood mononuclear cells
PBS	Phosphate-buffered saline
PD-1	Programmed cell death protein 1
PD-L1	Programmed death-ligand 1
PFU	Plaque-forming units
PGE2	Prostaglandin E2
PLA	PlasmaLyte A
PLF	Peritoneal fluid
polyI:C	Polyinosinic acid
RNA	Ribonucleic acid
RNase L	Ribonuclease L
ROS	Reactive oxygen species
SIRS	Systemic inflammatory response syndrome
SNA	Sialic acid-binding immunoglobulin-like lectin
SP	Spleen
Th	T helper cells
TLR	Toll like receptor
TNF	Tumor necrosis factor
Treg	Regulatory T cells
TRIM	Tripartite motif-containing
tSNE	t-distributed stochastic neighbor embedding
UMAP	Uniform Manifold Approximation and Projection
WB	Whole blood

Contributors and funding agencies

This dissertation is written as a thesis by articles, and contains findings from the following manuscripts:

Manuscript 1 (Chapter 2): Souza-Moreira, L.*, **Tan, Y.***, Wang, Y., Wang, J.-P., Salkhordeh, M., Virgo, J., Florian, M., Murray, A.B.P., Watpool, I., Mcintyre, L., English, S., Stewart, D.J., Mei, S.H.J., 2022. Poly(I:C) enhances mesenchymal stem cell control of myeloid cells from COVID-19 patients. iScience 25, 104188. https://doi.org/10.1016/j.isci.2022.104188
*Equal contribution (Published)

Manuscript 2 (Chapter 3): **Tan, Y.***, Wang, Y.*, Souza-Moreira L, Wang C, Murray ABP, Salkhordeh M, Florian M, McIntyre L, Stewart DJ, Mei SHJ. Mesenchymal stem cells induce dynamic immunomodulation of airway and systemic immune cells in vivo but do not improve survival for mice with H1N1 virus-induced acute lung injury. Front Bioeng Biotechnol. 2023 Jun 8;11:1203387. doi: 10.3389/fbioe.2023.1203387.
*Equal contribution (Published)

Manuscript 3 (Chapter 4): **Tan, Y***, Souza-Moreira, L*; Sahadevan, P; Wang, Y; Hanover, G; Florian, M; Salkhordeh, M; Murray, A; Virgo, J; Haines, J; Watpool, I; McIntyre, L; Stewart, D.J.; Mei, S.H.J, Adaptive Reprogramming of Mesenchymal Stem Cells by the Sepsis Microenvironment Enhances Immunomodulatory Effects on Myeloid Cells via a Caspase-1 Dependent Mechanism.
*Equal contribution (Submitting)

Thanks to the following core service providers: StemCore laboratories at the Ottawa Hospital Research Institute (OHRI), in particular, Dr. Damian Carragher for preparing and running samples, providing analytical support for mass cytometry.

Funding Sources:
- Ontario Graduate Scholarship (Recipient: Yuan Tan) 2023-2024
- Ontario Graduate Scholarship (Recipient: Yuan Tan) 2022-2023
- Ontario Graduate Scholarship (Recipient: Yuan Tan) 2021-2022
- University of Ottawa Excellence Scholarship (Recipient: Yuan Tan) 2019-2024

Thesis Advisory Committee Members
Dr. Harold Atkins
Dr. Subash Sad
Dr. Shirley Mei

List of Publications

Souza-Moreira, L.*, **Tan, Y.***, Wang, Y., Wang, J.-P., Salkhordeh, M., Virgo, J., Florian, M., Murray, A.B.P., Watpool, I., Mcintyre, L., English, S., Stewart, D.J., Mei, S.H.J., 2022. Poly(I:C) enhances mesenchymal stem cell control of myeloid cells from COVID-19 patients. iScience 25, 104188. https://doi.org/10.1016/j.isci.2022.104188
*Equal contribution

Tan, Y.*, Wang, Y.*, Souza-Moreira L, Wang C, Murray ABP, Salkhordeh M, Florian M, McIntyre L, Stewart DJ, Mei SHJ. Mesenchymal stem cells induce dynamic immunomodulation of airway and systemic immune cells in vivo but do not improve survival for mice with H1N1 virus-induced acute lung injury. Front Bioeng Biotechnol. 2023 Jun 8;11:1203387. doi: 10.3389/fbioe.2023.120338
*Equal contribution

Tan, Y.*, Salkhordeh M.*, Murray ABP, Souza-Moreira L, Stewart DJ, Mei SHJ. Key Quality Parameter Comparison of Mesenchymal Stem Cell Product Cryopreserved in Different Cryopreservation Solutions for Clinical Applications. Front. Bioeng. Biotechnol. 12:1412811. doi: 10.3389/fbioe.2024.1412811
*Equal contribution

Chapter 1 General Introduction

Sepsis is one of the most prevalent conditions requiring treatment in intensive care units (ICUs) and carries a stubbornly high mortality rate owing to its complex underlying pathogenesis. Sepsis was defined by consensus at the 3rd International Sepsis Conference in 2016 as a " life-threatening organ failure produced by an unbalanced host response to infection"[1]. This systemic inflammatory response can lead to conditions such as disseminated intravascular coagulation, multiple organ dysfunction syndromes (MODS), and ultimately death[2]. With significant advancements in sepsis diagnosis, treatment, and management over recent decades with updated recommendations, the mortality rate has notably decreased (by approximately 20–30 percent)[2,3]. Nonetheless, early sepsis detection, prevention of multiple organ failure, specific treatments, and enhanced prognosis remain critical challenges.

Sepsis frequently induces organ dysfunction, including acute kidney injury (AKI), cardiovascular dysfunction (septic shock) and acute lung injury (ALI), which can escalate to acute respiratory distress syndrome (ARDS). Consequently, ARDS is often considered a severe outcome of sepsis, occurring in about 32% of sepsis cases[4]. A primary histological feature of ARDS is profound diffuse alveolar damage, often driven by endothelial injury and local inflammation[6]. As a heterogeneous condition, ARDS typically presents with abrupt exacerbations of non-cardiogenic pulmonary edema, severe hypoxemia, and necessitates mechanical ventilation[5,6].

ARDS, first described in 1967[7], can arise from a variety of pulmonary or extrapulmonary conditions. Severe infections, the leading cause of ARDS, account for about half of the cases[8]. These infections can be localized, such as pneumonia, or systemic, including sepsis and septic shock [9]. ARDS may also occur due to viral lung infections. The common causes of viral lung infection in intensive care unit include community-acquired respiratory viruses (e.g. seasonal viruses) or nosocomial viral infections[8]. Viruses were responsible for approximately 10% of community-acquired pneumonia cases[10,11], and influenza A virus (IAV) was the most frequent detected pathogen[12,13]. Over the past decades, global outbreaks of two major viruses were responsible for acute respiratory failure and ARDS: novel coronavirus (SARS-CoV-1 in 2002[14] and SARS-CoV-2 in 2019[15]) and new influenza viruses (avian IAV H5N1[16] in 1997 and swine IAV H1N1 in 2009[17-19]). The recent emergence of SARS-CoV-2 caused a global pandemic affecting over 150 countries, emphasizing the multifaceted and complex nature of ARDS and sepsis[20]. In a minority of patients, SARS-CoV-2 infection triggers an excessive and abnormal immune response, leading to ARDS and multi-organ dysfunction.

1.1 Pathogenesis of Sepsis

1.1.1 Controversies in host immune response of severe infection and sepsis

The current paradigm regarding host immune responses in sepsis is still under heated debate. In 1997, Roger Bone brought out the concepts of systemic inflammatory response syndrome (SIRS) and compensatory anti-inflammatory response syndrome (CARS) for the pathogenesis of sepsis, and argued that one or the other would be predominating in the

progression of sepsis[2]. This biphasic concept of sepsis has been widely accepted for nearly a decade and used to explain the dual mortality peaks in septic patients. However, the assumption of two-wave concept for sepsis, with SIRS appearing before CARS, has since been disputed by new evidence from genomic analysis of septic patient tissues, which identified the protracted and concurrent pro-inflammatory and anti-inflammatory states[3]. Investigators showed circulating leukocytes from patient suffering trauma and burns exhibited a sustained increase in expression of genes related to upregulation of innate immunity and a concomitant decrease in genes regulating adaptive immunity[3]. Sepsis impacts the immune system directly by altering the life span, production and function of different immune effector cells responsible for homeostasis and immune surveillance against offending pathogens[4] (Figure. 1.1).

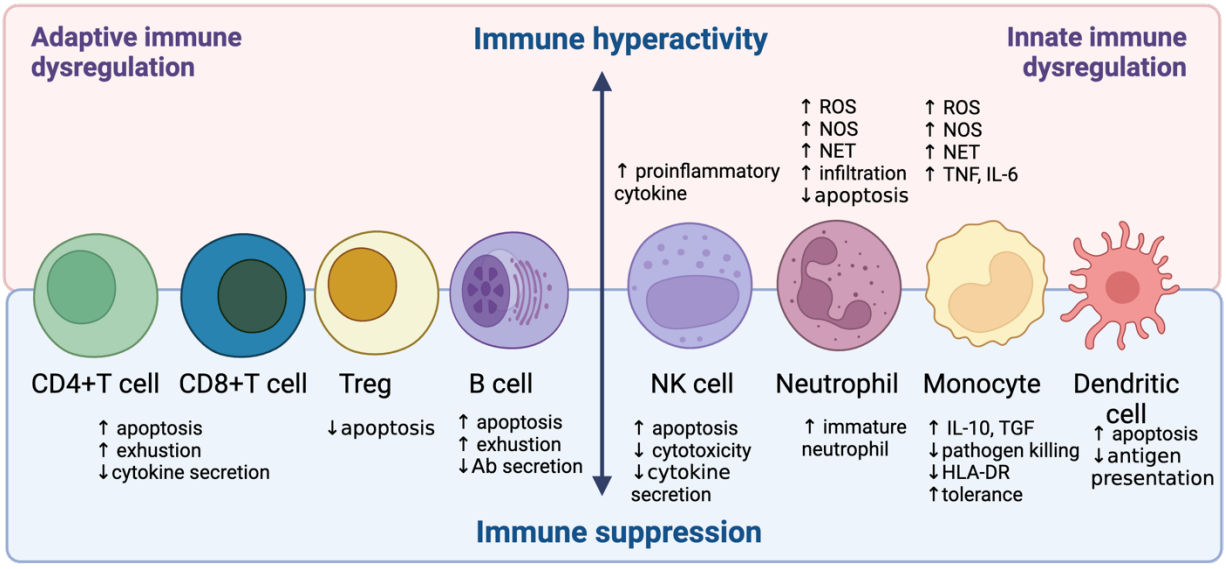

Figure 1.1 Dysregulated adaptive and innate immune cells in sepsis. A schematic illustrating functional dysregulation of various type of immune cells in sepsis (created by Biorender).

1.1.2 *Neutrophil Dysfunction*

Neutrophils are the first-line responder to invading pathogens. Neutrophils are cells with short life span after maturation and release from bone marrow. Studies on neutrophils obtained in the early hours of sepsis uncovered various abnormalizes, including: 1) increased numbers of circulating neutrophils with different stage of maturation[7], and 2) increased resistance to apoptosis[8]. However, neutrophils may play multiple, and sometimes conflicting, roles in sepsis. One study reported a dysregulated immune response characterized by activation of circulating neutrophils and the release of cytokines and reactive oxygen species (ROS) at sites remote to the focus of infection, leading to multiorgan failure[9]. Yet, other studies have shown that neutrophil dysfunction, such as deficiency in respiratory burst, may also lead to nosocomial infections[10] by reducing pathogen clearance. Indeed, experimental preclinical and clinical studies have revealed altered neutrophil function in sepsis, including impaired clearance of bacteria[11], and other reports have found loss of neutrophil chemotactic activity[21,22]. Cummings *et al*. demonstrated that nitric oxide (NO) mediates suppression and downregulation of CXC-chemokine receptor 2 (CXCR2) in neutrophils of septic patients[12]. Studies of both septic patients[13] and mouse model of polymicrobial sepsis[14] have confirmed the association between impaired neutrophil functions and secondary infection in sepsis.

1.1.3 Monocytes/Macrophage Dysfunctions

Monocytes are another critical component of innate immune response. They have pivotal functions in the host response to infection, including phagocytosis, antigen presentation,

context-dependent activation or inhibition of lymphocytes, and production of inflammatory cytokines and chemokines. In early sepsis, studies have shown that monocytes are largely responsible for releasing inflammatory mediators and, in severe cases, initiating the cytokine storm[3]. As disease progresses, monocytes lose the capacity to release cytokines in response to lipopolysaccharides (LPS), also known as endotoxin tolerance, which has been considered a hallmark of monocyte dysfunctions in sepsis[4]. While monocytes isolated from sepsis patients showed a reduced ability to release pro-inflammatory cytokines (i.e. tumor necrosis factor [TNF], IL-1a, IL-6 and IL-12), their ability to release anti-inflammatory mediators (i.e. IL-10, IL-1RA)[5] was unchanged. Furthermore, the lowered expression of the antigen presenting moiety, HLA-DR, has been suggested to be a surrogate marker for impaired monocyte function[6].

1.1.4 NK Cell Dysfunction

Natural Killer (NK) cells are not well studied in human sepsis due to the fact that they preferentially reside in tissues and have low circulating numbers. The number of $CD56^{high}$ and $CD56^{low}$ NK cells has been reported to be markedly decreased in circulation in sepsis[19] which was positively associated with mortality[20]. Moreover, NK cells exhibit suppressed cytotoxic activity after Toll-like receptor (TLR) stimulation, similar to the monocyte endotoxin tolerance state[21].

1.1.5 T Cell Dysfunction

T cell exhaustion is a hallmark of sepsis induced immunosuppression. Studies uncovered a reduction in both T helper 1 (Th1) and Th2 cell associated cytokine production[22] and gene expression (T-bet for Th1 and GATA-3 for Th2)[23] in the early phase of sepsis. Response from Th17 cells was also reduced in sepsis, which contributes to increase susceptibility of septic patients to nosocomial fungal infection[23]. Circulating T cells from septic patients exhibit increased expression of program death 1 (PD-1) and thus decreased proliferative capacity[24], and inhibition of PD-1 and PD-L1 interaction improved the survival in animal models of sepsis[25,26]. Earlier studies suggested an increase in circulating Treg cells in septic shock patients; however, further investigated showed that this relative increase was due to a significant decrease in the effector T cell population[27].

1.2 Therapies for Sepsis

To date, even though the extensive refinement of supportive care of patients with severe sepsis has reduced the overall mortality, no specific or curative therapy has been successful in improving outcomes [28]. The first modern interventional trial for sepsis was conducted by William Schumer in 1976, showing a significant survival benefit of high-dose corticosteroid compared to placebo[29]. The rational for the use of corticosteroid in sepsis is that this type of drugs dampens the exuberant pro-inflammatory response and limits anti-inflammatory response[30,31]. However, the use of high-dose corticosteroids as an adjunctive treatment for sepsis has remained controversial due to its association with increased risks of complications and death. In 2001, the success of activated protein C treatment instigated the field of sepsis researches and was approved by the Food and Drug

Administration (FDA) for the reduction of mortality due to severe sepsis in adult patients at a high risk of death group[32]. The effects of activated protein C were believed to reduce adverse microvascular effects of sepsis via its anticoagulant activity. However, a subsequent phase 3 sepsis trial failed to show a survival benefit comparable to the previous trial[33]. Activated protein C treatment was subsequently withdrawn from a worldwide market.

Other approaches for treating sepsis have directly target the immune aspects of sepsis. Earlier research focused on dampening hyperinflammatory responses by targeting a single microbial activator (e.g. blocking LPS) or inflammatory cascade (anti-TNF or anti-IL1$\boldsymbol{\beta}$), all of which have failed to show improvement[34]. Bone *et al.* used monoclonal antibodies against lipid A of LPS, but no significant benefit was observed[35]. Another wide known target for sepsis is TNF-α, a potent pro-inflammatory cytokine, that has been correlating with patient outcomes. Studies by Beutler *et al.* showed protective effects of TNF-α neutralization in animals of endotoxic shock[36]. Regrettably, clinical trials did not confirm this strategy is efficacious in human sepsis[37].

All in all, considering the complexity of host immune response in sepsis, targeting one specific component of immune responses may not have sufficient therapeutic efficacy for such a severe systematic disease as sepsis. Therefore, it is important to search for an immunomodulatory therapy that targets multiple aspects of immune responses in sepsis.

1.3 Mesenchymal Stromal/stem Cells (MSCs)

MSCs are adult somatic stem-like cells that can be isolated from various tissues and extensively expanded *in vitro*[38]. Friedenstein *et al*. first demonstrated the formation of ectopic bone from isolated and *in vitro* cultured bone marrow cells[39]. In the following years, numerous groups have also successfully harvested cells from bone marrow and other tissues with bone formation capacity[40–42] leading to the concept of a stem cell population with the capacity of forming bone, cartilage and other mesenchymal tissues. In the subsequent studies, mesenchymal stem/stromal cells (MSCs) were successfully derived *in vitro*, and have demonstrated the capacity to differentiate into tissues of various lineages, including osteoblasts, chondrocytes, and adipocytes[43,44]. MSCs were later confirmed to have the differentiation potential into other cell types as well, including muscle[45], neural precursor cells[46], cardiomyocytes[47,48], among other cell types[49,50].

In addition to their regenerative potential, MSCs exhibit important "immunomodulatory" properties. It has been reported that human MSCs have low expression of HLA major histocompatibility complex (MHC) class I expression[51,52] and lack MHC class II expression. Furthermore, MSCs do not exhibit surface expression of costimulatory molecules, B7-1, B7-2, CD40 and CD40 ligand and, therefore, do not have the ability to activate alloreactive T cells[51], which make these cells a candidate for allogeneic therapy. Additionally, MSCs exert direct immunosuppressive effects on various types of immune cell. *In vitro* studies have demonstrated that MSCs, and their secreted mediators, inhibit T cell proliferation[53,54],

regulate B cell functions[55], induce tolerance in dendritic cell and regulatory T cell[56,57] and skew macrophage polarization (i.e. M1/M2)[58,59] (Figure 1.2).

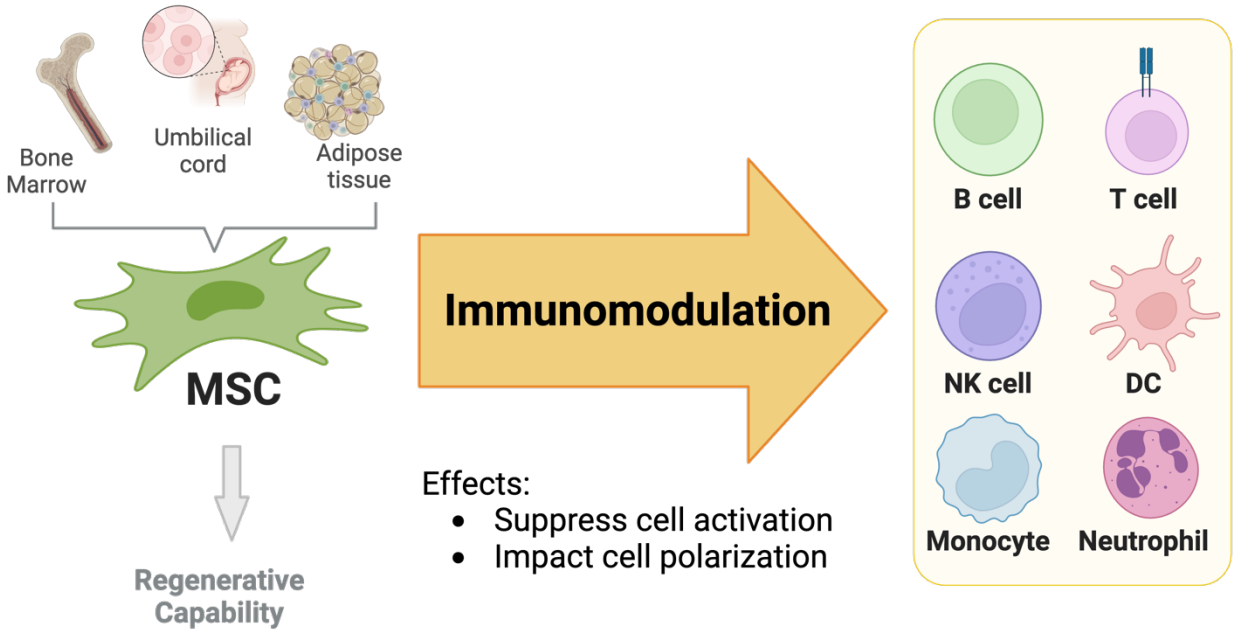

Figure 1.2 Isolation sources and therapeutic function of MSCs. A schematic illustrating various sources for the derivation of MSCs and immunological properties associated with MSCs (created by Biorender).

1.3.1 MSC-mediated Immunomodulatory Effects on Neutrophils

Nitric oxide production in activated neutrophil was significantly reduced when co-cultured with MSC[23]. While MSCs inhibited the proliferation of various types of immune cells, viability of neutrophil, which had a half-life of 6-8 hours *in vitro*, was prolonged in the presence of MSCs [23].

1.3.2 MSC-mediated Immunomodulatory Activity on Monocytes and Macrophages:

MSCs have been shown to promote the polarization of monocytes/macrophages towards an anti-inflammatory/regulatory phenotype, type 2[20]. Secretion of IL-1RA by MSCs directly drive type 2 macrophage polarization[21]. Anti-inflammatory monocytes are characterized by increased IL-10 and decreased IL-12, TNF-a and IL-17 secretion. Apart from polarization, monocytes co-cultured with MSCs expressed higher levels of MHC class II, CD45R and CD11b, which suppress T-cell activation[23].

1.3.3 MSC-mediated Modulation of NK Cell Activity.

MSC have inhibitory effects on NK cell proliferation similar to T cells[68]. The cytotoxicity of NK cells was significantly dampened after co-culturing with MSCs[69].

1.3.4 MSC-mediated modulation of T cell activity.

It is well documented that MSCs suppress T cell proliferation (both CD4+ and CD8+ T cells subsets) in mixed lymphocyte reactions in a dose-dependent fashion[53,70]. MSCs drives a Th1 to Th2 shift in effector T cells [71,72], and increases Treg polarization[61]. Secretion of indoleamine 2,3-dioxygenase (IDO) by MSCs was increased upon stimulation by INF-γ. Consequently, IDO-induced tryptophan depletion leads to an inhibition of allogeneic T cell responses, stimulates the secretion of IL-4 in Th2 cells and decreases the IFN-γ production by Th1 cells[70,73]. Upregulation of galectin-1[74], PD-L1/B7-H1[75], FAS-ligand[76] represents another mechanisms for MSC-induced T cell hypo-responsiveness and apoptosis.

1.4 Objective and Hypothesis

Research on the role of MSCs in sepsis and other critical illnesses has mainly focused on the examination of MSC-mediated immunomodulation, usually on one or two specific immune cell populations of interest. Studies performed by our group and others have shown MSCs exert beneficial therapeutic effects by improving survival preclinical models of sepsis [77,78]. Considering that the host immune environment can be decisive in driving MSC phenotypes, it is important to increase our understanding of precisely how MSCs respond to a complex infectious environment and how this influences their immunomodulatory activities in viral ALI and sepsis. This study will address a knowledge gap related to the mechanism by which MSCs interact with and modulate the host immune system in viral lung injury and sepsis. Notwithstanding the promising immunomodulatory functions of MSC, the evidence supporting whether these functions have beneficial effects on outcomes in a complex immune disease such as sepsis is still lacking.

General hypothesis: We hypothesize that there is a crosstalk between MSCs and host environment in the contexts of viral lung infections and sepsis. Specifically, exposure of MSCs to whole blood from infected animals or human patients, leads to molecular and functional adaptations in MSCs. These changes underly an enhanced ability of MSC to modulate multiple host immune cell population and therefore alter overall outcome.

General Objectives:

1. To investigate the changes in the host immune responses in viral infection (COVID-19 in Manuscript 1 and H1N1 IAV-induced ALI in Manuscript 2) and sepsis (Manuscript 3) and the effects of MSCs on immune cell populations and functions, using ex vivo human and in vivo animal models.

2. To study the impact of MSCs after exposure to host environment (immune cells, plasma/serum) and how this changes their ability to modulate immune cells upon exposure using an ex vivo model of viral infection (COVID-19 in Manuscript 1 and H1N1 IAV-induced ALI in Manuscript 2) and sepsis (Manuscript 3).

Specific Hypotheses:

Manuscript 1 (Chapter 2): We hypothesized that double-stranded RNA (dsRNA [viral mimic])-primed MSCs can improve and more efficiently rebalance the dysregulated immune system associated with viral infection in COVID-19 compared to unprimed MSCs.

Manuscript 2 (Chapter 3): In our previous study, we revealed that viral-mimic priming augmented the immunomodulatory capacity of MSCs in an *ex vivo* co-culture system with whole blood from severe COVID-19 patients [24]. In this study, we hypothesized that MSCs can modulate host immune cells, including both innate and adaptive immune cell populations, in the context of active H1N1 IAV infection.

Manuscript 3 (Chapter 4): We hypothesized that sepsis microenvironment induces molecular changes within MSCs, which positively contributes to an enhanced capacity of MSCs to modulate host innate immune cells and therefore improve overall outcome in sepsis.

Chapter 2 Poly(I:C) Enhances Mesenchymal Stem Cell Control of Myeloid Cells From COVID-19 Patients

Luciana Souza-Moreira#1; Yuan Tan#[1,2]; Yan Wang[1]; Jia-Pey Wang[1]; Mahmoud Salkhordeh[1]; Jennifer Virgo[1]; Maria Florian[1]; Aidan B.P. Murray[1]; Irene Watpool[3]; Lauralyn McIntyre[2,3,4]; Shane English[3,4]; Duncan J. Stewart[1,2] and Shirley H.J. Mei*[1]

1 Regenerative Medicine Program, Ottawa Hospital Research Institute, Ottawa, K1H 8L6, ON, CANADA,
2 Faculty of Medicine, University of Ottawa, Ottawa, ON, K1H 8L1, CANADA
3 Critical Care, The Ottawa Hospital, Ottawa, ON, K1H 8L6, CANADA.
4 Clinical Epidemiology Program, Ottawa Hospital Research Institute, Ottawa, ON, K1H 8L6, CANADA.

#These authors contributed equally.
*Corresponding Author and Lead Contact: smei@ohri.ca

Preamble:
Since the emergence of COVID-19 pandemic, MSC therapy has been investigated in clinical trials as a potential treatment for severe COVID-19 patients. This chapter presents my exploration of how MSCs modulate immune responses in COVID-19, and how viral mimic-primed MSCs could offer better outcomes in rebalancing the dysregulated immune system associated with COVID-19. I hypothesize that viral mimic, double-stranded RNA, priming can enhance the antiviral and immunomodulatory effects of MSCs to better address the complex immune dysregulations associated with COVID-19.

Author Contributions: L.S.M. and Y.T contributed equally to all aspect of this work, including conceptualization, data curation, model setup, investigation, visualization, data analysis, and writing of original draft. Y.W., J.W. and A.M helped in methodology and data validation. M.S. and M.F contributed to resources gathering. J.V. worked on data upload and curation. I.W. contributed to participants recruitment. L.M. and S.E. were involved in clinical supervision, and review & editing of the manuscript. D.J.S. contributed to the supervision and review & editing of the manuscript. S.H.J.M. were involved in conceptualization, funding acquisition, supervision, and review & editing of the manuscript.

2.1 Summary

Mesenchymal stem cells (MSCs) are being studied for the treatment of COVID-19 associated critical illness, due to their immunomodulatory properties. Here, we hypothesized that viral mimic-priming improves MSCs' abilities to rebalance the dysregulated immune responses in COVID-19. Transcriptome analysis of Poly(I:C)-primed MSCs (pIC-MSCs) showed upregulation of pathways in antiviral and immunomodulatory responses. Together with increased expression of antiviral proteins like MX1, IFITM3, and OAS1, these changes translated to greater effector functions in regulating monocytes and granulocytes while further enhancing MSCs' ability to block SARS-CoV-2 pseudovirus entry into epithelial cells. Most importantly, the addition of pIC-MSCs to COVID-19 patient whole blood significantly reduced inflammatory neutrophils and increased M2 monocytes while enhancing their phagocytic effector function. We reveal for the first time that MSCs can be primed by toll-like receptor 3 agonist to improve their ability to rebalance the dysregulated immune responses seen in severe SARS-CoV-2 infection.

Keywords: Mesenchymal Stem Cells, Cell Therapy, Immunomodulation, COVID-19

2.2 Introduction

The coronavirus disease 2019 (COVID-19), caused by a novel coronavirus SARS-CoV-2, was declared a pandemic by the World Health Organization in 2020. Severe illness and even death associated with COVID-19 are primarily related to the patients who develop acute respiratory distress syndrome (ARDS), sepsis, and/or multiorgan failure, resulting from dysfunctional immune, endothelial, and coagulation responses triggered by viral

infection[15]. Although monoclonal antibody therapy has shown to be effective yet transiently protective against early SARS-CoV-2 infection, they are only available to those who are not severely ill[25]. Given the lack of specific treatment for severely ill patients once they are in the intensive care unit (ICU), mesenchymal stem/stromal cells (MSCs) have been investigated in clinical trials as a potential treatment for severe COVID-19[26,27], with currently more than 96 trials registered on clinicaltrial.org.

Currently, there are over 1,200 registered clinical trials studying MSCs in a variety of inflammatory diseases, including but not limited to graft-versus-host disease, rheumatoid arthritis, colitis, and sepsis[28-30]. Leng et al. was the first to report improved pulmonary function in COVID-19 patients who received MSCs[26]. A recent double-blind, randomized controlled trial also showed that MSC treatment was safe, improved survival, and shortened time to recovery in COVID-19 patients[31]. In addition to the above-mentioned trials using MSCs in COVID ARDS, there are other trials that examined the safety and efficacy of MSCs in patients with non-COVID ARDS, most notably the START trial that also demonstrated the safety of administration of MSCs[32,33]. Although the results from these early trials are consistent with the known ability of MSCs to dampen hyperinflammatory response, it is not known how MSCs modulate host immune responses in COVID-19 and whether more can be done to improve MSC therapies.

We hypothesized that double-stranded RNA (dsRNA [viral mimic])-primed MSCs, compared to unprimed MSCs, can improve and more efficiently rebalance the dysregulated immune

system associated with viral infection. We primed MSCs with Poly(I:C) (pIC), a TLR3 agonist that mimics dsRNA viral stimuli, and provide the first evidence showing an improved molecular and functional profile of primed MSCs in the context of SARS-CoV-2, leading to recalibration of the dysregulated immune response in a virus-induced inflammatory environment. Additionally, pIC-MSCs showed greater inhibition of SARS-CoV-2 pseudovirus entry to human pulmonary epithelial cells *in vitro*. Compared to unprimed MSCs, pIC-MSCs further enhanced phenotypic and functional impacts on myeloid-derived populations, particularly on granulocytes and monocytes, towards less inflammatory phenotypes. These observations demonstrate that MSCs can be induced to upregulate antiviral protein expression and enhance the ability to modulate host immune responses, including direct evidence for the effects of MSCs on immune cells in the context of SARS-CoV-2, utilizing a unique *ex-vivo* MSC co-culture system with whole blood from severe COVID-19 patients. Our data offers critical insights into the actions of primed MSCs in viral infections that could be leveraged for further clinical investigations.

2.3 Result

2.3.1 Poly(I:C) Stimulus Enhances Immunomodulatory, Antiviral, and Transcriptomic Profile of MSCs.

To study the underlying molecular changes in MSCs primed with viral mimic Poly(I:C) (pIC-MSCs), we first analyzed the global transcriptome via Next Generation RNA Sequencing (RNAseq) at 6h after priming. A total of 989 genes were identified to be differentially expressed, among three different donors of MSCs that had been primed with Poly(I:C).

Results revealed 794 upregulated and 195 downregulated genes that were modulated in pIC-MSCs compared to non-primed cells (Ctrl-MSCs) based on Log2 fold change cut-off criteria, < -1 indicating downregulation and > 1 upregulation, with significance indicated by an adjusted p-value < 0.05 (Fig. 2.1A). Ingenuity Pathway Analysis (IPA) and Gene Ontology (GO) were conducted to gain insight into potential biological functions of the transcriptome changes. Significant enrichment (adjusted p value < 0.05) of GO terms related to defense response to the virus and interferon signalling were seen in the upregulated gene set (Fig. 2.1B). The IPA analysis predicted a strong regulation of several canonical pathways, upstream regulators (key transcriptional regulators), and biological functions related to antiviral response ($p < 0.05$, Fig. 2.1C). Negative z-score (predicts inhibition) was seen for terms such as replication of coronavirus and viral life cycle, while positive z-score (predicts activation) was seen for terms such as interferon signaling and maturation of blood cells. Using IPA terms to filter the dataset, we confirmed that genes induced by a pIC priming approach are primarily associated with activation of immune (411 genes) and antiviral (75 genes) responses (shown as unsupervised cluster heatmap, Fig. 2.1D). Indeed, the most significantly upregulated genes (Top 25) included several antiviral proteins and interferon-stimulated cytokines (ISG). The protein-protein interaction analysis of these 25 upregulated protein-coding genes in pIC-MSCs suggested a relevant protein interaction (strong computational prediction) among these genes (Fig. 2.1E). Furthermore, with UniProt Knowledgebase[34], which consists of all known protein sequence data linked to functional information about that protein, we found that compared to non-primed MSCs, pIC priming specifically increased expression of gene coding for secreted antiviral factors (Fig. 2.1F).

This data was consistent among three different MSC donors. Altogether, our data revealed dynamic transcriptome changes induced by pIC in MSCs, specifically on genes and proteins responsible for enhancing antiviral response and immunomodulatory functions.

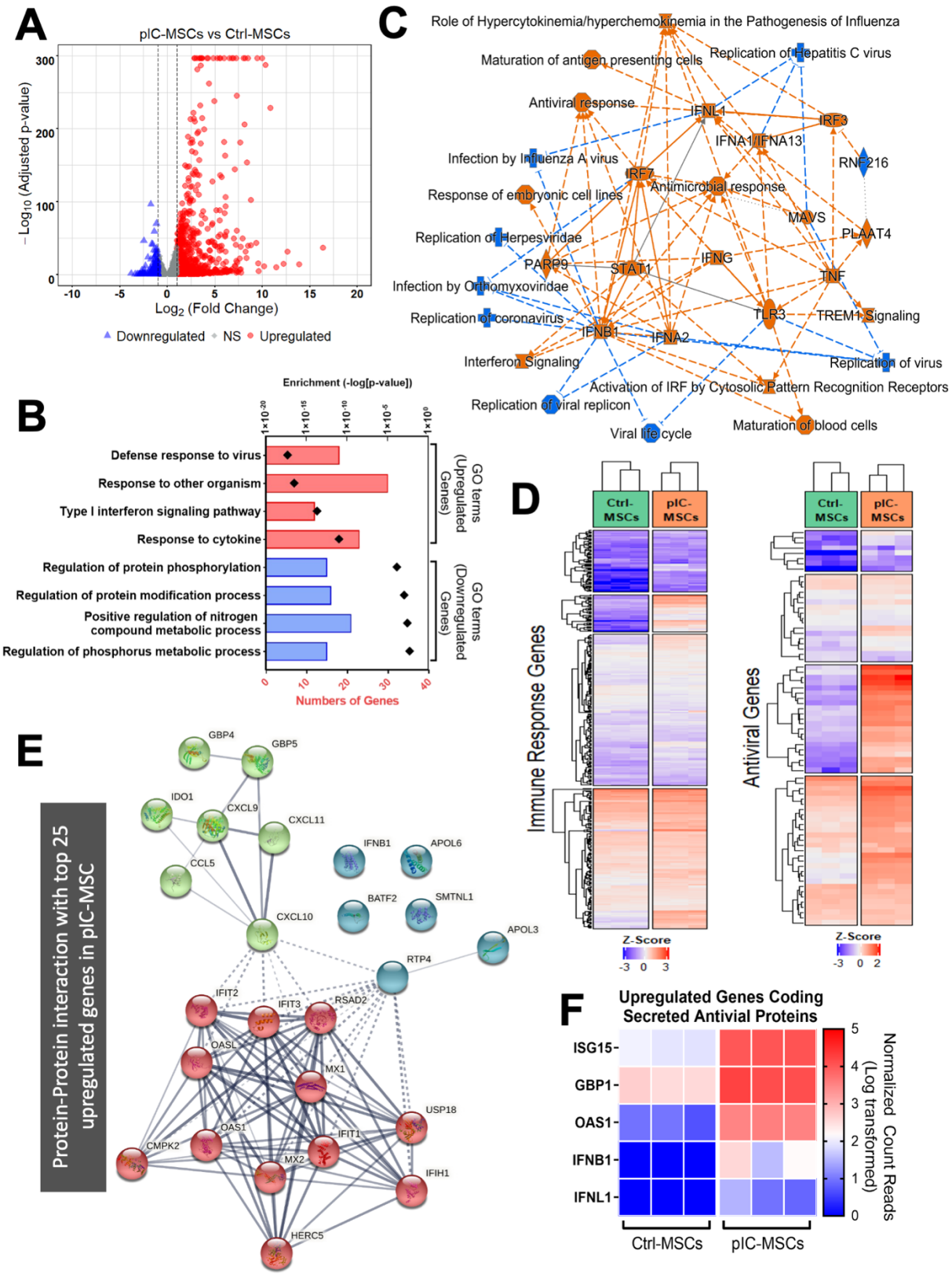
A
pIC-MSCs vs Ctrl-MSCs
−Log10 (Adjusted p-value)
Log2 (Fold Change)
Downregulated
NS
Upregulated
B
Enrichment (-log[p-value])
Defense response to virus
Response to other organism
Type I interferon signaling pathway
Response to cytokine
Regulation of protein phosphorylation
Regulation of protein modification process
Positive regulation of nitrogen compound metabolic process
Regulation of phosphorus metabolic process
GO terms (Upregulated Genes)
GO terms (Downregulated Genes)
Numbers of Genes
C
Role of Hypercytokinemia/hyperchemokinemia in the Pathogenesis of Influenza
Maturation of antigen presenting cells
Replication of Hepatitis C virus
Antiviral response
IFNL1
IRF3
IFNA1/IFNA13
Infection by Influenza A virus
IRF7
RNF216
Antimicrobial response
Response of embryonic cell lines
MAVS
Replication of Herpesviridae
PLAAT4
PARP9
STAT1
IFNG
TNF
Infection by Orthomyxoviridae
Replication of coronavirus
TLR3
TREM1 Signaling
IFNB1
IFNA2
Interferon Signaling
Replication of virus
Activation of IRF by Cytosolic Pattern Recognition Receptors
Replication of viral replicon
Viral life cycle
Maturation of blood cells
D
Ctrl-MSCs
pIC-MSCs
Immune Response Genes
Antiviral Genes
Z-Score
E
Protein-Protein interaction with top 25 upregulated genes in pIC-MSC
GBP4
GBP5
IDO1
CXCL9
CXCL11
CCL5
IFNB1
APOL6
BATF2
SMTNL1
CXCL10
APOL3
RTP4
IFIT2
IFIT3
RSAD2
OASL
MX1
USP18
OAS1
IFIT1
CMPK2
MX2
IFIH1
HERC5
F
Upregulated Genes Coding Secreted Antivial Proteins
ISG15
GBP1
OAS1
IFNB1
IFNL1
Ctrl-MSCs
pIC-MSCs
Normalized Count Reads (Log transformed)

Figure 2.1 pIC Priming Enhances Antiviral and Immunomodulatory Transcriptomic Profile of MSCs.

(A) Volcano plot shows differentially expressed genes (log2 fold change >1 or < -1 and adjusted p-value <0.05) with 794 genes upregulated (red) and 195 downregulated (blue); NS: non-significant change (grey). Each dot represents one gene.

(B) Ingenuity Pathway Analysis of the differential expressed genes data set showed the most significant canonical pathways, molecules, diseases, and functions. Blue icon: negative z-score (predicts inhibition); orange icons: positive z-score (predict activation).

(C) Relevant Gene Ontology terms for the top 50 upregulated (red) and downregulated (blue) genes in pIC-MSCs compared to unprimed MSCs.

(D) Heatmaps of unsupervised clustering show gene expression (normalized counts) of Ctrl-MSCs and pIC-MSCs, illustrating the variation of genes (each row) annotated for immune or antiviral response. Each column represents MSCs derived from 1 bone marrow donor, with a total of 3 donors.

(E) Protein-Protein interaction network shows top 25 upregulated protein-coding genes in pIC-MSCs (cluster [k-means] numbers estimated to 3). The thickness of the network edge line indicates the strength of publicly available data that support the specific interaction, with the thicker line indicating stronger evidence support.

(F) Heatmap showing upregulated genes in pIC-MSCs coded for secreted antiviral proteins. For RNA-seq, n=3 biological replicates.

2.3.2 pIC-Primed MSCs Show Enhanced Inhibition of SARS-Cov-2 Pseudoviruses Viral Entry In Vitro.

To validate antiviral and immune response pathways identified in the aforementioned RNAseq analysis, proteins coded by these related genes were measured in the supernatant or cell lysate from pIC-MSCs and Ctrl-MSCs at 24h after priming. Cytokines, including CCL2, CXCL10, CXC11, CXCL8, and IL-6, showed significantly increased levels in conditioned media from pIC-MSCs (vs. Ctrl-MSCs, Fig. 2.2A). Western blot analysis of antiviral proteins confirmed the elevation of IFIT1 (Interferon Induced Protein with Tetratricopeptide Repeats 1), IFITM3 (Interferon Induced Transmembrane Protein 3), Mx1 (MX Dynamin Like GTPase 1), OAS1 (2'-5'-Oligoadenylate Synthetase 1), but not TRIM-5α (Tripartite motif-containing protein 5) or RNase L (Ribonuclease L) antiviral proteins in pIC-MSCs (Fig. 2.2B, see summarized data in Fig. S2.1). The secretion of IFITM3, a virus host restriction factor that has been described to be released by extracellular vesicles and inhibit infections in dengue [35] and zika [36] viral models, was increased by pIC-MSCs compared to Ctrl-MSCs. (Fig. 2.2C).

Next, to examine the potential antiviral effect of MSCs in coronavirus, SARS-CoV-2 pseudovirus tagged with a fluorescent reporter was used to evaluate viral entry in human alveolar epithelial cells (HAEpi). MSCs have been reported to not be permissive to coronavirus infection due to their lack of angiotensin-converting enzyme 2 (ACE2) expression[37]. We exposed MSCs to the SARS-CoV-2 pseudovirus and confirmed a minimal level of pseudovirus entry could be detected in MSCs (Fig. 2.2D). In HAEpi, SARS-CoV-2

pseudovirus exhibited efficient viral entry, with fluorescence detected in 68.3±5.2% of cells. In contrast, HAEpi cells incubated with conditioned media from Ctrl-MSCs had significantly reduced viral entry with 52.3±3.7% of HAEpi SARS-CoV-2 pseudovirus positive, while conditioned media of pIC-MSC further augmented the ability to suppress viral entry, showing only 38.8±3.3% of HAEpi cells positive for fluorescent signals (Fig. 2.2E). Our results demonstrate that antiviral effects of MSCs can be further improved with dsRNA pIC priming.

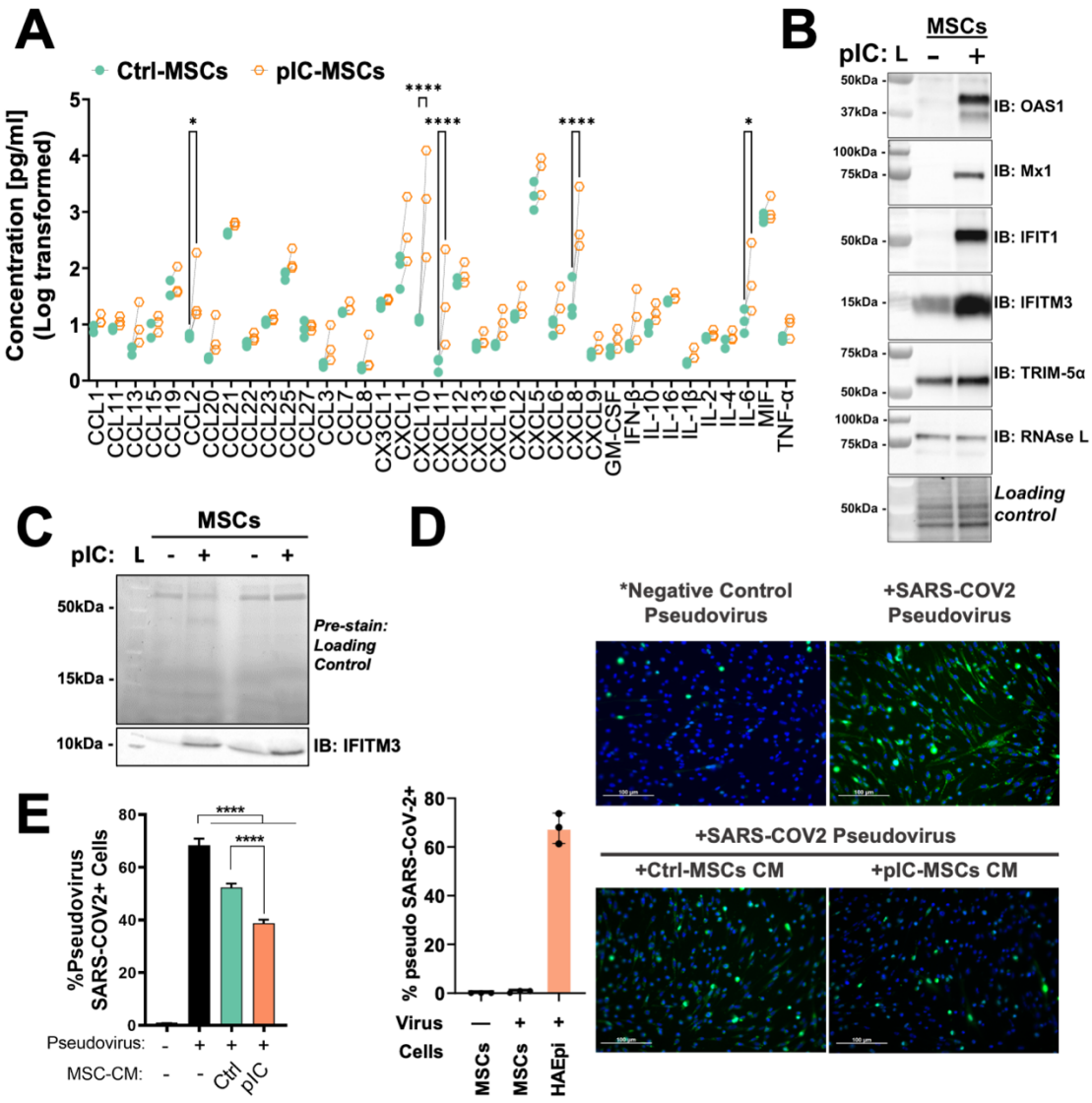
A
Ctrl-MSCs
pIC-MSCs
Concentration [pg/ml] (Log transformed)
CCL1 CCL11 CCL13 CCL15 CCL19 CCL2 CCL20 CCL21 CCL22 CCL23 CCL25 CCL27 CCL3 CCL7 CCL8 CX3CL1 CXCL1 CXCL10 CXCL11 CXCL12 CXCL13 CXCL16 CXCL2 CXCL5 CXCL6 CXCL8 CXCL9 GM-CSF IFN-β IL-10 IL-16 IL-1β IL-2 IL-4 IL-6 MIF TNF-α
B
MSCs
pIC: L - +
IB: OAS1
IB: Mx1
IB: IFIT1
IB: IFITM3
IB: TRIM-5α
IB: RNAse L
Loading control
C
MSCs
pIC: L - + - +
Pre-stain: Loading Control
IB: IFITM3
D
*Negative Control Pseudovirus
+SARS-COV2 Pseudovirus
+SARS-COV2 Pseudovirus
+Ctrl-MSCs CM
+pIC-MSCs CM
% pseudo SARS-CoV-2+
Virus
Cells
MSCs
MSCs
HAEpi
E
%Pseudovirus SARS-COV2+ Cells
Pseudovirus:
MSC-CM:
Ctrl
pIC

Figure 2.2 pIC Priming Enhances Antiviral and Immunomodulatory Profile of MSCs.

(A) Cytokines were measured using MSC supernatant collected after 24h of pIC stimulation. Secretome profile showing 37 soluble factors measured in the supernatant with log-transformed data shown. Each dot represents one MSC donor, with a total of 3 donors included.

(B) Representative Image of western blot analysis showing increased intracellular antiviral proteins in MSC lysate after 24h of pIC priming (compared to non-pIC primed). Images obtained from chemiluminescent and colorimetric channel were merged to show molecular weight ladder position (left lane). Total proteins (ran on stain-free gel) shown on bottom panel was used as loading control.

(C) Western blot analysis showing expression of secreted antiviral protein IFITM3 in MSC supernatant from two independent experiments. Images obtained from chemiluminescent and colorimetric channel were merged to show molecular weight ladder position (left lane). Total proteins (ran on stain-free gel) shown on bottom panel was used as loading control.

(D) Fluorescently tagged SARS-CoV-2 pseudovirus was incubated with MSCs or human alveoli epithelial cells (HAEpi), which showed MSCs were not permissible to pseudovirus entry.

(E) Fluorescently tagged SARS-CoV-2 pseudovirus was incubated with human alveoli epithelial cells with or without MSC-conditioned media, which showed pIC-MSCs had greater effects in blocking pseudovirus entry into epithelial cells. Event was quantified by flow cytometry, and images were taken with fluorescent microscope (scale bars, 100 μm).

Summary data of the protein expression is in Fig. S2.1. For all experiments, n=4-6 of independent experiments with the data shown as mean ± SEM. $*p<0.05$, $**p<0.01$, $***p<0.005$, $****p<0.001$. For western blot images, L = molecular weight ladder and IB = immunoblotting.

2.3.3 pIC-Primed MSCs More Effectively Modulate Granulocytes and Monocytes Towards Less Inflammatory Phenotypes.

To confirm that pIC priming enhances the immunomodulatory effect of MSCs, we employed an *ex vivo* acute inflammation system (lipopolysaccharide [LPS]-stimulated whole blood from healthy donors incubated with or without MSC co-culture), followed by mass cytometry (CyTOF) analysis to deep profile the immune cell populations. A t-distributed stochastic neighbor embedding (tSNE) analysis was first conducted on the pan-leukocyte population identified from CyTOF, followed by Self-Organizing Maps (FlowSOM), which showed that granulocytes formed the large metaclusters in a Minimum Spanning Tree (MST), color mapped with CD66b expression to identify neutrophil clusters (Fig. S2.2). Stimulation of whole blood with LPS upregulated CD14 and CD64 expression in CD66b+ neutrophils (indicative of inflammatory phenotype), while both MSCs and pIC-MSCs suppressed this response (Fig. 2.3A & Fig. S2.2). Other granulocyte associated markers, including CD33, CD13, CD15, and HLA-DR, were also analyzed and showed no significant changes with or without MSC (Ctrl- or pIC-) treatments after LPS stimulation. A subsequent t-SNE and FlowSOM analysis of CD66b- mononuclear cells identified 10 metaclusters of immune cell subpopulations (Fig. 2.3B), with monocytes (CD14+) as metacluster 1, 2, 4, 5, 6, and 7, of which expression of M1 (CD64) and M2 (CD206) polarization markers were extracted and presented as pie charts within each note (Fig. 2.3C). Notably, we observed shifts in nodes of monocytic regions (in dotted circles) of MSTs among LPS-stimulated whole blood with or without Ctrl-MSC or pIC-MSC co-culturing (Fig. 2.3C). In particular, pIC-MSCs significantly increased CD206 and decreased CD64 expression on monocytes,

implying a further shift towards M2 polarization (Fig. 2.3D). We next sought to determine whether this shift was associated with functional improvement in phagocytic capacity. Co-culture with pIC-MSCs more significantly improved phagocytosis ability of CD14+ monocytes ($p < 0.0001$ between Ctrl-MSC vs. pIC-MSC, Fig. 2.3E). We next examined changes in CD4+ and CD8+ T cell populations after MSC co-culture. Both Ctrl- or pIC-MSCs did not change the size of the CD4+ or CD8+ populations, nor the expression of activation marker HLA-DR (Fig. 2.4A). Furthermore, in MSC and PBMC co-culture experiments, we found priming of MSCs by pIC did not impair their ability to suppress T cell proliferation or activation, compared to Ctrl-MSC (Fig. 2.4B and 2.4C). Taken together, these data show that pIC priming enhanced the ability of MSCs to modulate monocytes and neutrophils towards less inflammatory phenotypes, as well as improve their phagocytic capacities under an *ex vivo* model of acute inflammation.

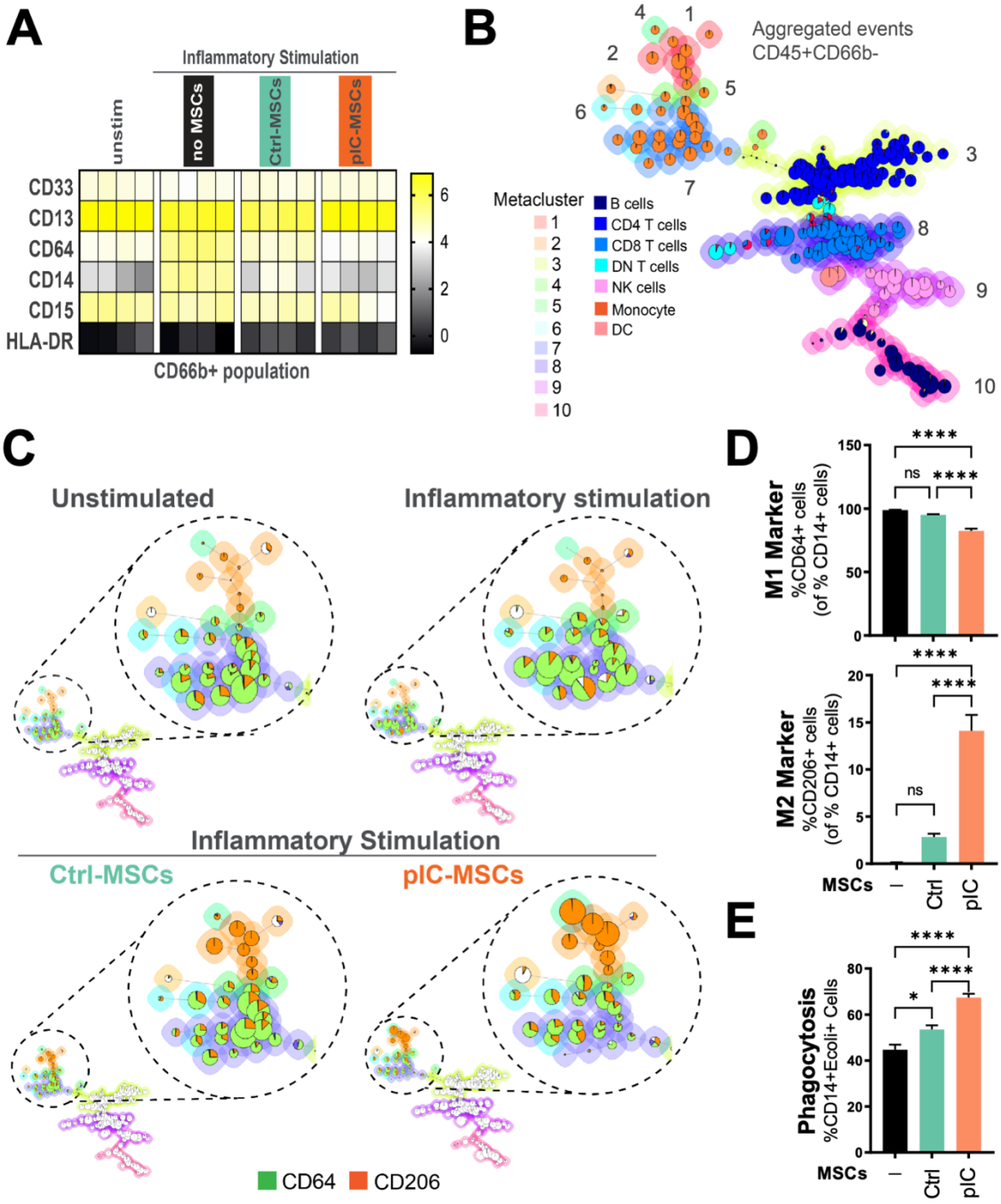
A
Inflammatory Stimulation
unstim
no MSCs
Ctrl-MSCs
pIC-MSCs
CD33
CD13
CD64
CD14
CD15
HLA-DR
6
4
2
0
CD66b+ population
B
Aggregated events
CD45+CD66b-
Metacluster
1
2
3
4
5
6
7
8
9
10
B cells
CD4 T cells
CD8 T cells
DN T cells
NK cells
Monocyte
DC
C
Unstimulated
Inflammatory stimulation
Inflammatory Stimulation
Ctrl-MSCs
pIC-MSCs
CD64
CD206
D
M1 Marker
%CD64+ cells
(of % CD14+ cells)
****
ns
****
M2 Marker
%CD206+ cells
(of % CD14+ cells)
****
****
ns
MSCs
—
Ctrl
pIC
E
Phagocytosis
%CD14+Ecoli+ Cells
****
*
****
MSCs
—
Ctrl
pIC

Figure 2.3 Enhanced Ability of pIC-Primed MSCs to Modulate Innate Immune Cell Responses Ex Vivo.

(A) Heatmap represents changes of phenotypic markers on CD66b+ cells with or without MSC co-culture upon inflammatory (LPS) stimulation.
(B) Cell subsets (10 clusters) of CD45+/CD66b- mononuclear cell population were identified by FlowSOM algorithm, with total aggregated events (100,000 single cells) shown.
(C) MST plots of unstimulated and stimulated whole blood, with or without MSCs (Ctrl-MSCs, pIC-MSCs) were shown, with details of monocytic population enlarged in dash circle. Expression of CD64 and CD206 were extracted and overlaid on MST shown as pie chart to visualize the shifts in monocyte phenotype with LPS stimulation under different co-culturing conditions.
(D) Quantification of CD64 (M1 marker) and CD206 (M2 marker) expressions of monocytes identified in (C).
(E) Phagocytic capacity of CD14+ monocytes measured with pHrodo bioparticles, showing increased phagocytosis after Poly(I:C)-MSC co-culture.

For all experiments, n=4 of independent experiments with data shown as bar graphs as mean ± SEM (panel D, E). ns=non-significant, $*p<0.05$, $**p<0.01$, $***p<0.005$, $****p<0.001$. See also Fig. S2.3.

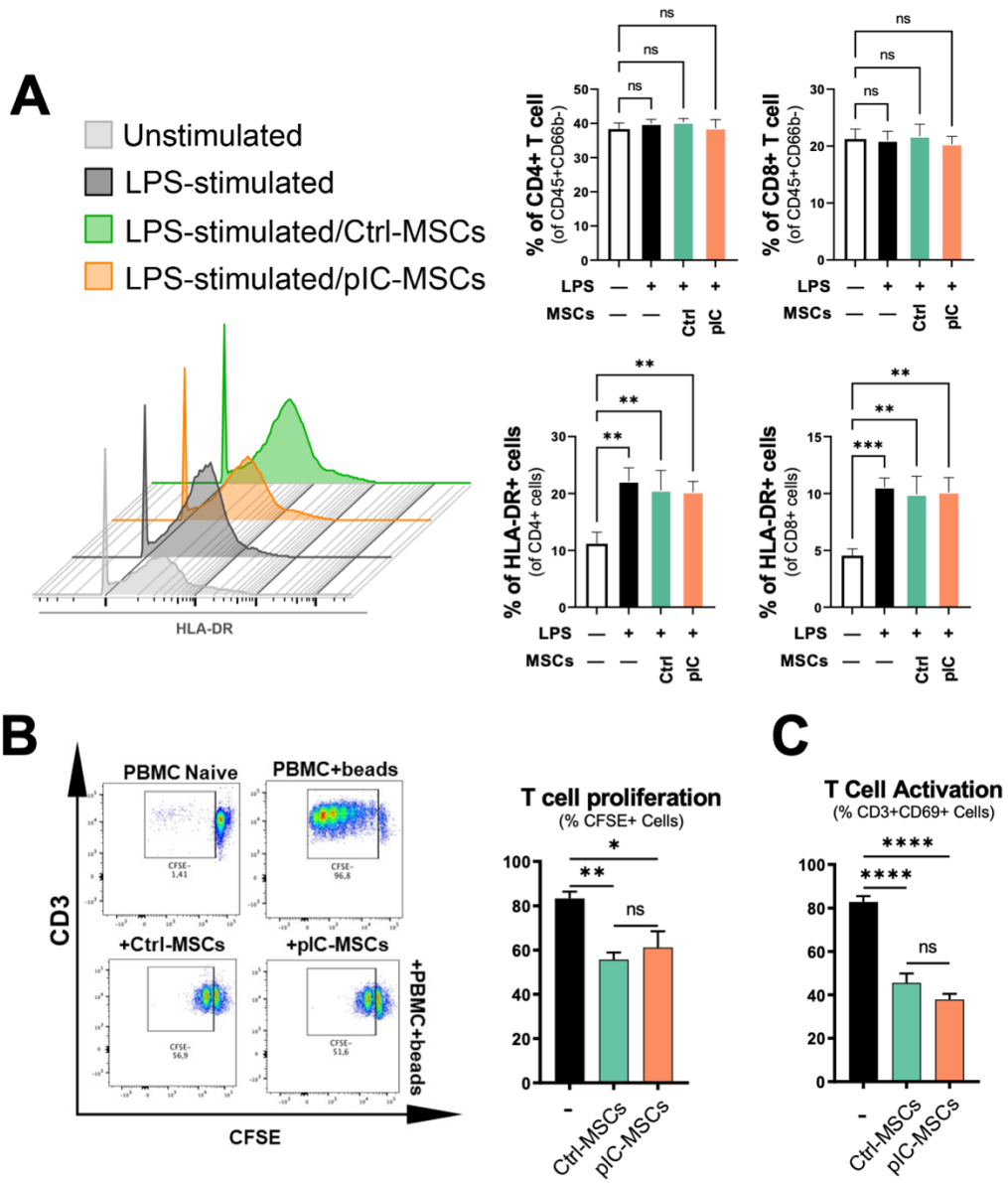
A
Unstimulated
LPS-stimulated
LPS-stimulated/Ctrl-MSCs
LPS-stimulated/pIC-MSCs
HLA-DR
% of CD4+ T cell
(of CD45+CD66b-)
% of CD8+ T cell
(of CD45+CD66b-)
% of HLA-DR+ cells
(of CD4+ cells)
% of HLA-DR+ cells
(of CD8+ cells)
LPS
MSCs
Ctrl
pIC
ns
B
PBMC Naive
PBMC+beads
+Ctrl-MSCs
+pIC-MSCs
CD3
CFSE
+PBMC+beads
C
T cell proliferation
(% CFSE+ Cells)
T Cell Activation
(% CD3+CD69+ Cells)
Ctrl-MSCs
pIC-MSCs

Figure 2.4 pIC Priming Did Not Affect MSC's Ability to Modulate T Cells.

(A) Qualification of CD4+ and CD8+ T cell showed no effects on cell population by LPS stimulation with Ctrl- or pIC-MSC co-culturing. Expression of HLA-DR, activation marker, on CD4+ and CD8+ T cell of CyTOF data in Fig. 2.3A were also quantified, which showed no impact on T cell activation by MSCs (either by MSCs with or without pIC-priming) co-culturing.

(B) Effect of inhibition on T cell (CFSE stained) proliferation by MSCs (Ctrl vs. pIC-treated). MSCs were co-cultured with the PBMCs activated with Dynabeads Human T-Activator CD3/CD28 for 5 days. On day 5, cells were stained with CD3 followed by measurement of proliferation of T cell (CD3+CFSE+) by flow cytometry (showing representative dot plots). Flow cytometric analysis showed comparable extent of inhibition on T cell proliferation by either Ctrl- or pIC-MSCs, with % T cell proliferation plotted as bar graph.

(C) Effect on T cell activation by MSCs (by Ctrl-MSCs vs. pIC-MSCs). MSC were co-cultured with the activated PBMCs for 2 days, followed by measurement of CD3 and CD69 to detect T cell activation status by flow cytometry.

For all experiments, n=4-6 of independent experiments with the data shown as bar graph as mean ± SEM. $*p<0.05$, $**p<0.01$, $***p<0.005$, $****p<0.001$

2.3.4 pIC-MSCs Better Modulate Severe COVID-19 Patient Immune Cell Responses in an Ex Vivo Model.

To evaluate whether MSCs modulate host cell responses in the context of immune dysfunction in COVID-19, we utilized an *ex vivo* co-culture system using Ctrl- or pIC-MSCs with whole blood collected from critically ill COVID-19 patients (see Table S1 for patient characteristics), followed by CyTOF analysis. The tSNE algorithm was conducted on CD45+ leukocytes, followed by PhenoGraph algorithm for cluster generation (Fig. 2.5A, Fig. S2.3A and B). Phenotypic changes were identified by CyTOF to segregate major leukocyte lineages in whole blood via expression of 23 markers. On the t-SNE map, neutrophil populations formed the largest clusters (cluster 1, 2, 3, 4, 5, and 7) (Fig. 2.5A). Using density analysis, we identified that cluster 1, 2, 3, 4, and 5 were neutrophils uniquely present in COVID-19 patients (Fig. 2.5B) while neutrophils from healthy donors were in cluster 7 (Fig. S2.3A). Furthermore, distinct phenotypic shifts in neutrophil populations in COVID-19 immune responses were observed after co-culturing with pIC-MSCs (Fig. 2.5B). We then extracted the median intensities of neutrophil-relevant markers and generated a dot plot (Fig. 2.5C). A side-by-side comparison of neutrophil-related marker expression in these clusters confirmed the presence of neutrophils at various levels of immaturity, with reduced expressions of CD66b and CD16 in COVID-19 patients (Fig. 2.5C). Furthermore, we identified inflammatory neutrophil populations (CD66b+ cells; clusters 4 and 5) in COVID-19 patients that exhibited high expression of CD64, a biomarker correlated with sepsis, infectious diseases, and tissue damage[38]. In contrast, pIC-MSCs increased non-activated neutrophils (cluster 1) and reduced inflammatory neutrophil populations with

high CD64 expression (cluster 4, 5) (Fig. 2.5D). Total monocyte numbers in whole blood (cluster 6) were not affected in the presence of MSCs (Fig. 2.5D). However, while exerting no effects on CD86 and CD64 expression, Ctrl-MSCs and to a larger extend, pIC-MSCs, did shift the monocyte population towards a more M2 phenotype (higher CD206 and HLA-DR) (Fig. 2.5E), consistent with our observations from LPS-stimulated healthy whole blood (Fig. 2.3C).

Having established that pIC-MSCs exhibited enhanced modulatory effects on neutrophils and monocytes, we investigated how these phenotypic changes could translate to biological functions. After pIC-MSC co-culture, total leukocytes showed a trend in reduction of apoptosis in blood from severe COVID-19 patients ($p = 0.55$ for COVID-19 vs. COVID-19/Ctrl-MSC, $p = 0.093$ for COVID-19 vs. COVID-19/pIC-MSC) (Fig. 2.5F). Furthermore, phagocytic capacity of CD66b+ neutrophils and CD14+ monocytes were improved by Ctrl-MSC, and more so by pIC-MSC co-culture (vs. non-MSC treated, $p < 0.01$ for monocytes and $p < 0.005$ for neutrophils, Fig. 2.5G).

Altogether, we found that pIC-MSCs shifted neutrophil and monocyte populations in whole blood from COVID-19 patients towards a more modulatory phenotype, with enhanced phagocytic effector function. The data corroborate our findings seen in the acute inflammatory model with healthy donor whole blood stimulated by LPS, while further demonstrating that pIC priming renders an enhanced immunomodulatory activity of MSCs in pathogenic viral infections.

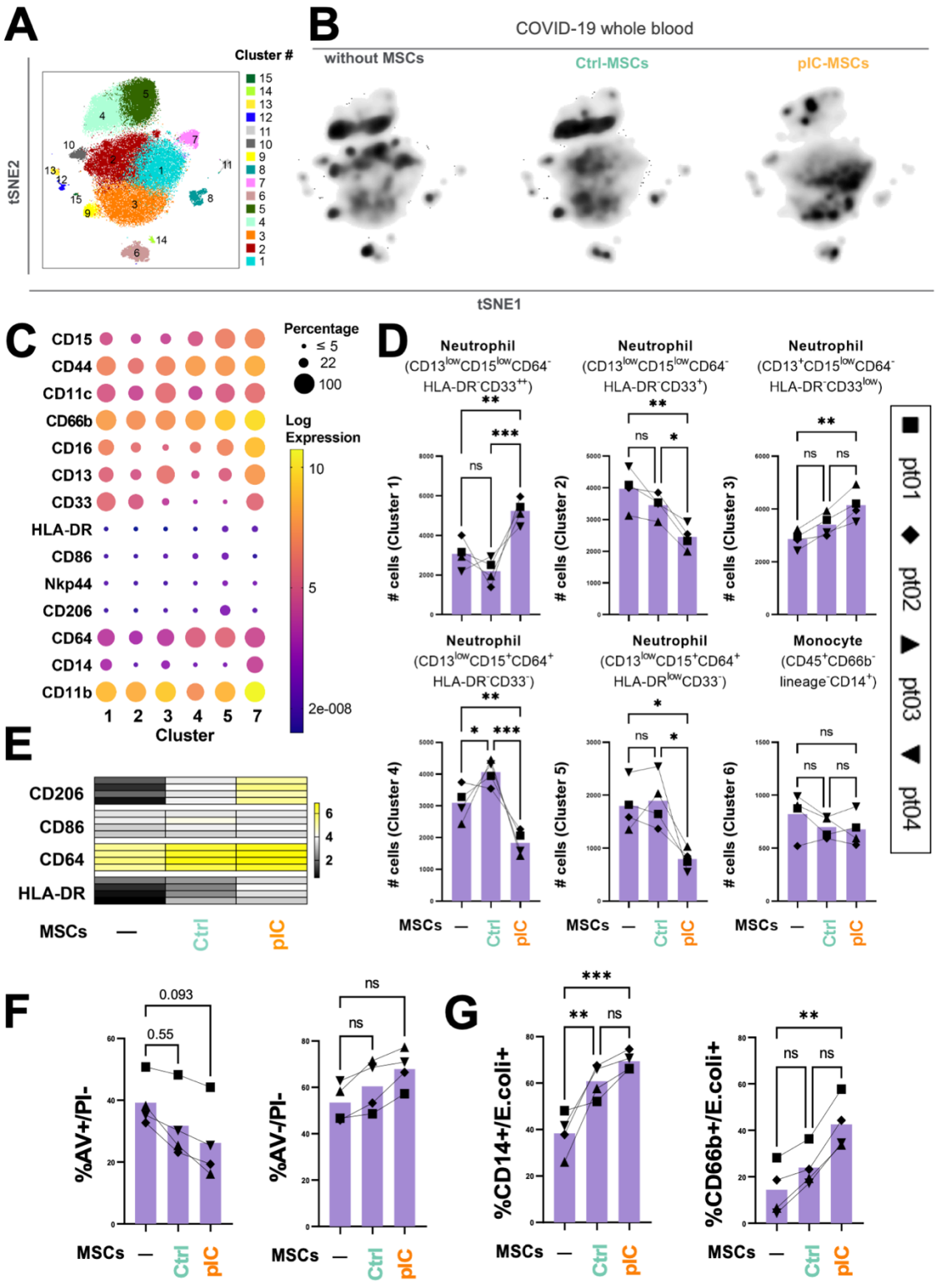
A
Cluster #
15
14
13
12
11
10
9
8
7
6
5
4
3
2
1
tSNE2
tSNE1
B
COVID-19 whole blood
without MSCs
Ctrl-MSCs
pIC-MSCs
C
CD15
CD44
CD11c
CD66b
CD16
CD13
CD33
HLA-DR
CD86
Nkp44
CD206
CD64
CD14
CD11b
1 2 3 4 5 7
Cluster
Percentage
≤ 5
22
100
Log Expression
10
5
2e-008
D
Neutrophil (CD13lowCD15lowCD64- HLA-DR-CD33++)
Neutrophil (CD13lowCD15lowCD64- HLA-DR-CD33+)
Neutrophil (CD13+CD15lowCD64- HLA-DR-CD33low)
Neutrophil (CD13lowCD15+CD64+ HLA-DR-CD33-)
Neutrophil (CD13lowCD15+CD64+ HLA-DRlowCD33-)
Monocyte (CD45+CD66b- lineage-CD14+)
cells (Cluster 1)
cells (Cluster 2)
cells (Cluster 3)
cells (Cluster 4)
cells (Cluster 5)
cells (Cluster 6)
ns
*
**
***
MSCs — Ctrl pIC
pt01
pt02
pt03
pt04
E
CD206
CD86
CD64
HLA-DR
6
4
2
MSCs — Ctrl pIC
F
%AV+/PI-
%AV-/PI-
0.093
0.55
ns
MSCs — Ctrl pIC
G
%CD14+/E.coli+
%CD66b+/E.coli+
***
**
ns
MSCs — Ctrl pIC

Figure 2.5 MSCs Primed with Viral Stimuli Support Greater Immunomodulation in Severe COVID-19.

(A) Cell subsets were identified of CyTOF data by unsupervised clustering with the PhenoGraph algorithm. Each dot represents one cell (100,000 cells total). The t-SNE plot overlayed with PhenoGraph clusters was shown.
(B) Density analysis of t-SNE maps demonstrated distinct phenotypic shift of clusters after co-culturing of pIC-MSCs with whole blood of severe COIVD-19 patient samples.
(C) Dot plot showed median fluorescent level of neutrophil related markers in clusters 1, 2, 3, 4, 5, and 7 with the size of dot representing percentage of positive cells (size scale shown either as ≤5, 22, or 100%) and color of dot representing median intensity of corresponding markers (color scale shown as log expression).
(D) Quantification of number of cells expressing markers specified in (C) with selected clusters of myeloid cells (cluster 1 to 6).
(E) Heatmap of marker showing CD206, CD86, CD64, and HLA-DR expression levels of CD14+ monocytes in Cluster 6 of Fig. 2.5B from mass cytometry data (fluorescent intensity scale shown on the right).
(F) Flow cytometry analysis of Annexin V and PI staining showed a trend of reduction in total leukocytes apoptosis by pIC-MSCs.
(G) Flow cytometry analysis showed the improved phagocytosis capacity of CD14+ monocyte and CD66b+ neutrophils after pIC-MSC co-culture (compared to non-MSC treated).

For all experiments, n=4 patients (pt) per group, with each patient represented by different symbol (legend on the far right of panel C) with the data shown as bar graph as mean ± SEM, $*p<0.05$, $**p<0.01$, $***p<0.005$, $****p<0.001$. See also Fig. S2.3.

2.4 Discussion

Our study uncovers upregulation of antiviral and immunomodulatory pathways in MSCs using an *in vitro* priming strategy, leading to an improved ability for MSCs to modulate the immune landscape in acute inflammation and in COVID-19. It has been suggested that the innate potential of MSCs can be influenced by diverse extrinsic factors such as oxygen concentration and the presence/absence of various cytokines[39]. Herein, we first demonstrated that an altered transcriptome and cytokine profile towards an antiviral and improved immunomodulatory phenotype can be acquired when MSCs are primed with pIC, a viral stimuli mimic. Second, of particular importance, the present study is the first to explore how pIC-MSCs regulate antiviral protein expression while exhibiting augmented ability to modulate host innate immune responses. Third, by using an innovative *ex vivo* co-culture model with COVID-19 patient blood combined with a deep immune profile approach, we demonstrate that antiviral and immunomodulatory functions of MSC features are augmented by pIC priming on global immune cells and therefore lead to better modulation of immune responses, resulting in less inflammatory neutrophils and more M2 monocytes. Results presented here advance our understanding on how MSCs contribute their beneficial effects at the cellular and molecular level during viral infection, with important implications that may guide the design of a next-generation MSC therapy in critically ill patients with SARS-CoV-2 infection or different underlying viral aetiologies.

Studies have shown that stimulation of specific TLRs affects the immune modulating responses of MSCs[40]. For example, TLR3 stimulation of human MSCs establishes their

immunosuppressive effects, while TLR4 activation elicits proinflammatory effects[40]. The pIC-activated MSCs were more effective in reducing sepsis-induced inflammation and organ dysfunction while improving overall survival in a mouse model of polymicrobial sepsis via upregulated miRNA-143[41]. Pierce *et al*. confirmed that priming MSCs with pIC enhances expression of proteins related to host defense and innate immunity in extracellular vesicles[42]. In the current study, we further demonstrate that the empowerment of MSCs by pIC priming could be a valid therapeutic approach to improve the immunomodulatory and antiviral effectiveness of MSCs to treat COVID-19. It is worth mentioning that pIC-primed MSCs exhibit an enhanced antiviral and modulated secretome profile, which ultimately stimulate greater host defense, contributing to the blocking of SARS-CoV-2 virus entry to epithelial cells.

Unlike more lineage committed cells, MSCs are known to have an inherent ability to resist viral infection with endogenous expression of interferon-stimulated cytokines, including OAS1, Mx1, and the IFITM family[43], targeting different stages of viral cycle[44]. Herein, we highlight the upregulation of those proteins in pIC-MSC. The OAS1 protein can bind double-stranded RNA and subsequently activate the latent RNAse L that, when activated, can cleave single-stranded RNAs[45]. Zhou *et al*. provided evidence that increased OAS1 levels in humans is strongly associated with reduced risks of very severe COVID-19 hospitalization and susceptibility[46]. The Mx proteins belong to the dynamin family and have been shown to display activity against several viruses[47,48]. As for the IFITM family, it has been reported these proteins can block cytosolic entry of SARS-CoV-1 and SARS-CoV-2 as well as MERS-

CoV[49,50]. Kirchhoff and colleagues recently demonstrated that exogeneous overexpression of IFITM proteins in HEK293T cells prevents spike protein-mediated fusion and SARS-CoV-2 entry.

Some preclinical studies have indicated beneficial effects of MSCs in different viral infections. A study by Qian and colleagues reported antiviral activity of MSCs against hepatitis C virus, mainly conferred by non-coding miRNAs[51]. In our study, we further demonstrate that by priming MSCs with viral stimuli, pIC-MSCs can exert superior effect in blocking viral entry. Altogether, pIC-MSCs show an augmented antiviral phenotype that could contribute to more efficient inhibition of SARS-CoV-2 infection in COVID-19. Additionally, the current study provides the first evidence that, coupled with upregulated antiviral pathways, pIC priming renders MSCs with improved modulatory abilities on host immune cellular responses that can be beneficial in the context of severe SARS-CoV-2 infections, likely due to elevated secretion of cytokines like CCL2(MCP1), CXCL10(IP-10), CXC11(I-TAC), IL-6, and CXCL8 (IL-8). These cytokines are pleotropic cytokines in an infectious setting. There is direct evidence supporting the importance of IL-6 during viral infections, shown experimentally using IL-6-deficient mice[52,53]. IL-6 has been shown to be essential for survival of mice infected with an influenza virus by promoting optimal regulation of the T cell response, inflammatory resolution, tissue remodeling promoting lung repair, migration, and phagocytic activities of macrophages, preventing viral-induced apoptosis in lung epithelial cells, and regulation of IgG isotype switching[52,53]. Trifilo *et al.* further demonstrated that CXCL10 expression played a pivotal role in defense following

coronavirus infection of the CNS by recruitment and activation of NK cells that reduced viral replication[54]. Furthermore, CCL2 is important in coordinating the immune response following microbial infection by regulating T cell polarization as well as leukocyte migration and accumulation within infected tissues[55].

In our *ex vivo* model, pIC-MSCs more effectively modulate dysfunctional neutrophils towards a less inflammatory phenotype with higher phagocytic activities, while polarizing monocytes towards an M2 phenotype, which plays an important role in the resolution phase of inflammation and the repair of damaged tissues. A previous report documented a myeloid-driven immunopathology in COVID-19, in which hyperactivated neutrophils and an ineffective adaptive immune system act as mediators of the cytokine storm that worsens disease severity[56]. Patients with severe COVID-19 show dysfunction in myeloid cells, with a particularly large population of immature and dysfunctional neutrophils and monocytes with an inflammation-promoting phenotype (lack of HLA-DR)[57]. Hyperactivated neutrophils not only play an important role in systemic COVID-19 disease manifestations, but also contribute to severe COVID-19 associated pneumonia and tissue damage[58]. Consistent with the existing literature, we observed that COVID-19 patients display a high level of immature neutrophils and inflammatory monocytes.

The cellular signature in severe COVID-19 patients feature a surge of HLA-DR^{low} classical monocytes, reminiscent of an immune paralysis phenotype seen in severe ARDS and sepsis. HLA-DR^{low} classical monocytes, which exhibit increased capacity in cytokine

production, are a key determinant of the severity of COVID-19. These dysregulated monocytes may contribute to an insufficient antiviral immune response or may arise as a by-product of a hyperinflammatory environment[59]. We find that MSCs primed with viral mimic pIC were enhanced in their ability to suppress neutrophil activation and skew the monocyte phenotype towards M2 phenotype (increase of CD206 and HLA-DR expression). Importantly, Trombetta *et al*. reported that, in samples from ICU discharged patients, M2-like monocyte subsets were increased and contributed to an acquired myeloid cell immune-regulatory phenotype that aided in patient recovery from severe SARS-CoV-2 infection[60]. Their data corroborate our findings that the use of a therapeutic agent, such as pIC-primed MSCs, with a capacity to induce innate immune system regulatory shift could represent a viable strategy to combat severe COVID-19[60]. In addition to phenotypic changes, monocytes co-cultured with pIC-MSC exhibited greater functional ability to phagocytose, which could ultimately lead to better pathogen clearance.

In summary, here we present important evidence that pIC-MSCs possess improved antiviral and immunomodulatory functions. This study highlights the immense potential of pIC-MSCs to be explored as a next generation cell therapy for infectious diseases. Our results illustrate the ability of pIC-MSCs to reshape the immune cell landscape in severe COVID-19 directly in a disease-relevant human cellular context.

2.5 Limitations of Study

In the current study, we utilized bone marrow-derived MSCs to investigate how pIC preconditioning affects the antiviral and immunomodulation functions of MSCs.

Differences in molecular profiles have been reported among MSCs derived from various tissue sources. Here, we utilized a pseudovirus-based in vitro model to explore the inhibitory effect of MSCs on SARS-CoV-2 viral entry into the epithelial cells. To date, there are still limited animal models available for studying SARS-CoV-2 infection, and most require the ability to access a biosafety level 3 facility. Future studies may be needed to further explore actions of MSCs or pIC-MSCs in other pathogenic aspects of virus cycle, including transmission and replication.

2.6 Author Contributions

L.S.M. and Y.T: Conceptualization, Data curation, Methodology, Investigation, Visualization, Formal analysis, and Writing – original draft; Y.W., J.W. and A.M: Investigation, Methodology, and Validation; M.S. and M.F: Resources; J.V: Software and Data curation; I.W: Resource - participants recruitment; L.M. and S.E: Clinical Supervision, and Writing – review & editing; D.J.S: Supervision and Writing – review & editing; S.H.J.M: Conceptualization, Funding acquisition, Project administration, Supervision, Writing – review & editing.

2.7 Acknowledgments

The authors gratefully acknowledge the support of Drs. Gareth Palidwor and Christopher Porter of the Bioinformatics Core Facility of Ottawa Hospital Research Institute for technical support on RNAseq data analysis; Dr. Damian Carragher (mass cytometry proteomic core) for providing help in CyTOF data analysis; Rebecca Porteous for supporting participant recruitment. The work was supported by Emergent Ventures, Thistledown

Foundation (Fast Grant, S.H.J.M.), The Ottawa Hospital Foundation COVID-19 Emergency Response Fund (S.H.J.M.), and Ontario Institute of Regenerative Medicine - Disease Team Grant (S.H.J.M. & L.M.).

2.8 Declaration of Interests

The funding institution had no role in the conception, design or conduct of the study, data collection or analysis, interpretation or presentation of the data, or preparation, review or approval of the manuscript. We also like to declare the following conflicts of interest: D.J.S. is co-founder and holds equity in Northern Therapeutics Inc., and S.H.J.M. is a part-time employee of Northern Therapeutics Inc. for work outside of this study. However, these conflicts are not relevant for any of the work included in submission. The remaining authors have no disclosures.

2.9 EXPERIMENTAL MODEL AND SUBJECT DETAILS

2.9.1 Healthy Volunteer and COVID-19 Cohort

This study was approved by the Research Ethics Board (REB) (Ottawa Health Science Network REB, REB ID: 20200312-01H and #20190401-01H). After providing written informed consent, 4 health donors and 4 COVID-19 patients were included in the study. Information on age, sex, and blood analysis of healthy volunteers and COVID-19 patients were listed in Table S1. COVID-19 patients who tested positive for SARS-CoV-2 were recruited in intensive care unit of The Ottawa Hospital between June 2020 and February 2021.

2.9.2 Bone Marrow Aspirates and MSC Culture

Bone marrow aspirates were obtained from commercial vendor (Lonza) or at The Ottawa Hospital (with informed written consent and ethical approval granted by the Ottawa Health Science Network Research Ethics Board, REB ID: 20120929-01 H). Human bone marrow-derived MSC (n=3 different donors; 2 females and 1 male) were cultured, characterized, and cryopreserved. Briefly, the human bone marrow aspirates were diluted, counted, and plated on T-175 flasks (Corning) with complete MSC Nutristem xeno-free media (Biological Industries) with gentamicin reagent solution [Gibco]). All cells were maintained at 37°C, 5% (v/v) CO2. Upon >80% confluence, MSCs were harvested and cryopreserved at $2.5x10^6$ cells/mL in freezing media (Biological Industries) with storage in liquid nitrogen[28,61]. MSCs have been characterized to meet all the criteria (plastic adherence, differentiation potential, and cell surface antigen expression) proposed by the International Society for Cellular Therapy (ISCT)[62] as previously described[28,61].

Cryopreserved MSCs were thawed and cultured in Nutristem complete media (Biological Industries) for 24-72 hours prior to being lifted and plated for *in vitro* or *ex vivo* assays. MSCs were maintained at 37°C in a humidified incubator containing 5% CO_2. All experiments used cells between passages 3 to 5.

For viral stimulus priming, MSC were incubated with or without 10 µg/mL of Poly(I:C) (pIC) for 6 hours for sample collection for RNAseq analysis, or 24 hours for protein expression (total cell lysate and secreted protein in the supernatant).

2.10 METHOD DETAILS

2.10.1 Library Preparation and Sequencing

MSCs (n= 3 different donors) were incubated with or without pIC for 6 hours, then cell pellets were collected and sent to Qiagen NextGeneration Service for RNA isolation and library preparation. In summary, the libraries' size distribution was validated and quality inspected on a Bioanalyzer 2100 or BioAnalyzer 4200 TapeStation (Agilent Technologies); Sequencing was performed on an Illumina NextSeq500 instrument (76 cycles) generating single end reads; Qiagen service reported an average 38.2 million reads were obtained for each sample.

2.10.2 RNAseq Data Analysis

In summary, raw counts were compiled into FASTQ format and the reads containing adapter sequences or qualified as low-quality reads were filtered from the dataset. All samples passed the FASTQC Quality Scores (i.e., per sequence quality scores, sequence quality histograms and adapter content). Quality controlled FASTQ files were aligned to human reference genome GRCh38.p13 using HISAT2 aligner software [63] to obtain the raw counts matrix. Data was mapped and count matrix were generated by Bioinformatics Department at OHRI. The R programming language (R version 3.6.3 and RStudio version 1.2.5033) was used to perform the gene expression analysis of the reads. Differential expression analysis was performed using the default parameters of R DEseq2 package version 1.26 (results summarized in a volcano plot)[64]. RNAseq heatmaps were drawn using Complex heatmap package [65] and illustrate the variation of selected genes (each row); each column

represents MSC derived from 1 bone marrow donor (n=3 donor). The g:GOSt (g:Profiler) was used for Gene Ontology analysis and to identify the enriched terms of biological process. Ingenuity Pathway Analysis software (IPA; Qiagen) was used to identify canonical pathways. String-db was used to visualize the protein-protein interaction network of the up-regulated differentially expressed genes[66].

2.10.3 Conditioned Media and Secretome Profile

MSCs were primed for 24 hours without or with pIC (10 µg/mL) for 24h. The supernatant was harvested and cell debris eliminated by spining down at 5,000g 5 min at room temperature. Supernatant was collected and stored at -80°C. Cytokines, chemokines, and growth factors contents were detected by Multiplex Immunoassay System (Bio-Rad) in the supernatant following manufacturers' recommended protocols. Assays were conducted by personnel blinded to the identities of the sample. Alternatively, after the treatment, the supernatant was removed, and the cells were washed 3 times with PBS. Fresh media was added, and the supernatant was collected 24 hours later to produce the MSC-conditioned media.

2.10.4 Immunomodulatory Assays to Assess MSC Functions

For *ex vivo* assays, whole blood (sodium citrate as anticoagulant) from healthy volunteers were obtained from commercial vendor (StemCell Technologies) or from healthy volunteer and COVID-19 patient at OHRI. Whole blood was directly co-cultured with MSCs (primed with or without pIC) for 24 hours. Blood obtained from health volunteers were used to

establish *ex vivo* acute inflammation system. In summary, whole blood was co-cultured with or without MSCs in the presence of lipopolysaccharide (100 ng/mL). Whole blood and MSC co-culture were conducted in ratio of 0.5 mL of whole blood to 100,000 MSCs. After co-culture, part of whole blood was saved for CyTOF (details below), the rest of whole blood samples underwent red blood cell lysis (ThermoFisher) to obtain total white blood cells. Cells were washed with flow cytometry washing buffer (PBS supplemented with 2% fetal bovine serum). For apoptosis staining, cells were incubated with AnnexinV (BD Biosciences) and PI (ThermoFisher) for 15 minutes at room temperature followed by flow cytometry analysis (Attune NxT acoustic focusing cytometer, ThermoFisher).
For phagocytosis analysis, pHrodo *E.coli* bioparticle (ThermoFisher) was added to whole blood culture system and incubated for 15 minutes at 37ºC. Cells were then washed and stained with anti-human CD14 and anti-human CD66b (BD Biosciences) for 30 minutes at 4ºC. After staining, washed cells were analyzed by flow cytometry (LSRFortessa cytometer, BD Biosciences).

In addition, the inhibition of T cell proliferation assay used peripheral blood mononuclear cells (PBMCs) stained with carboxyfluorescein succinimidyl ester (CFSE) (ThermoFisher) and activated with Dynabeads Human T-Activator CD3/CD28 (Gibco). MSCs were co-cultured with the activated PBMCs for 5 days, then the proliferation of T cell was measured by flow cytometry (Attune NxT acoustic focusing cytometer, ThermoFisher). Alternatively, cells were cultivated for 2 days and CD3 and CD69 were used to detect T cell activation status by flow cytometry. Data analysis was done using FlowJo X software (FlowJo, LLC).

2.10.5 Mass Cytometry-Based Immune Cell Profiling (CyTOF)

For CyTOF sample processing, 250 µL of human whole blood (sodium citrate) was lysed in 350 µL of stable-lyse V2 and then fixed in 1 mL of stable-store V2 (Smart Tube Inc., San Carlos, US) as described in the user's manual and stored at -80ºC until further processing. Further, whole blood samples were thawed and washed, followed by barcoding using Cell-ID 20-Plex Pd Barcoding Kit (Fluidigm). Up to 4 individual samples were barcoded for 30 minutes at room temperature. Cells were then washed and pooled for surface staining. For surface staining, cells were resuspended in diluted human Fc-block (BDbioscience) for 10 minutes and incubated with antibody staining cocktails for 30 minutes at room temperature. After incubation, cells were washed with staining buffer and fixed overnight in MaxPar Fix-I buffer with iridium intercalator (Fluidigm). Immediately prior to data acquisition, samples were washed once with each of Cell Staining Buffer (Fluidigm) and Cell Acquisition Solution (Fluidigm). Samples were then resuspended at a concentration of $5x10^5$ cells per mL in Cell Acquisition Solution containing EQ Four Element Calibration Beads (5:1 Ratio) (Fluidigm). The samples were acquired on a Helios Mass Cytometer equipped with a wide-bore sample injector at a rate of 300-500 events per second. After acquisition, repeat acquisitions of the same sample were concatenated as necessary and normalized using the Fluidigm software. Normalized fcs files were gated to exclude debris, doublets, and dead cells using Cytobank software.

2.10.6 Antibodies Used for Mass Cytometry

All anti-human pre-conjugated to metal isotopes were obtained from Fluidigm Corporation (San Francisco, US). All remaining antibodies were obtained from the indicated companies as purified antibodies and in-house conjugation was completed using the MaxPar X8 labeling kit (Fluidigm) following manufacturers' recommended protocols. A detailed list of all antibodies is shown in the Key Resource table (Supplementary Table 2.1).

2.10.7 Mass Cytometry Data Analyses

Files were processed following Fluidigm recommendation, including randomization and normalization using EQ Beads signal. Files were then concatenated, debarcoded, and randomized according to Fluidigm's instructions using the CyTOF Software. Gating to identify and export single cells was completed in Cytobank[67]. Clustering analysis was completed with either FlowSOM (Cytobank)[68] or PhenoGraph [69] as stated as part of the R Bioconductor package Cytofkit [70] and Flowjo X using the markers listed in the Key Resource Table with up to 50,000 cells per sample. The transformation method used was cytofAsinh, and the visualization method was t-SNE. The t-SNE map overlaid with PhenoGraph-defined cell populations (Figures S2.3B and 2.4B) was generated using ggplot2 package in RStudio (open-source) and FlowJo (BD Biosciences).

2.10.8 Pseudovirus Assay

Human pulmonary alveoli epithelial cells (HAEpi) (ScienCell Research Laboratories) were thawed and expanded in Alveolar Epithelial Cell Medium (AEpiCM) (ScienCell Research

Laboratories) between passage 3-8. HAEpi were passaged into a 24-well plate overnight. On the next day, MSC-conditioned media was mixed 1:1 with AEpiCM and added to HAEpi. After one day, SARS-CoV-2 pseudovirus (Montana Molecular) was added according to manufacturer's instructions. On the following day, pseudovirus entry was measured in the harvested and washed HAEpi using flow cytometry (Attune NxT acoustic focusing cytometer, ThermoFisher).

2.10.9 Immunoblot Analysis

Cells were collected after stimulation pIC by cell scraper and addition of sample lysis buffer (Sigma-Millipore). Protein quantification was performed using Bradford reagent (Bio-Rad). Loading buffer was added to the cell lysate, and immediately heated at 95°C for 5 minutes. Samples (10-15 µg of protein/lane) were resolved by electrophoresis on pre-cast SDS-PAGE(Bio-Rad). After electrophoresis, separated proteins were transferred to low fluorescence PVDF membranes and blocked with PBS-T (PBS plus 0.1% Tween 20) and 5% of non-fat dry milk for 2 hours at room temperature. Membranes were washed 5× with PBS-T and incubated with primary antibodies diluted (1:500 or 1:1,000) in PBS-T and 5% BSA for 18 hours at 4°C under gentle agitation. After washing 5× with PBS-T membranes were incubated with horseradish peroxidase (HRP)-conjugated secondary antibodies (1:5,000) for 1 hour at room temperature. Clarity and Clarity Max Western ECL (Bio-Rad) was used to detect HRP signal using digital-based imaging system (Chemidoc, Bio-Rad). Images were further analyzed using Image Lab software (Bio-Rad). Total protein (Stain free gel technology) was used as Loading control.

2.10.10 Immunoblot Analysis of Secreted Proteins

MSC were primed with pIC for 24 hours. After that, supernatant was collected and centrifuged at 3,000 g for 15 minutes to remove cells and cell debris. Supernatant was transferred to a new tube then stored at -80°C for further analysis. Lastly, MSC supernatant was thawed on ice, then 1 ml of ExoQuick-TC (SBI) was added per 5 ml of supernatant, and tubes remained upright overnight at 4°C. ExoQuick-TC/supernatant mixtures were centrifuged at 1,500 g for 30 minutes. The supernatant solution was aspirated and residual solution spun down by centrifugation at 1,500 g for 5 minutes. All traces of fluid were removed by aspiration without disturbing the precipitated pellet. Pellets were resuspended in RIPA lysis buffer (ThermoFisher) with protease inhibitor (Sigma-Aldrich). Protein quantification and expression in the lysates were performed as described in Immunoblot analysis section.

2.10.11 QUANTIFICATION AND STATISTICAL ANALYSIS

Statistical analysis was performed using GraphPad PrismV9.0 software (GraphPad Software). Numerical data are presented as mean ± SEM unless otherwise stated. Multiple groups were analyzed by one-way ANOVA followed by Sidak's or Turkey's multiple comparisons test unless otherwise stated. For the analysis of cytokine data, logarithmic transformation was performed to normalize the data distribution before conducting ANOVA. Statistical significance was set at $p < 0.05$. Graphical abstract created with Biorender.com.

Chapter 3 Mesenchymal Stem Cells Induce Dynamic Immunomodulation of Airway and Systemic Immune Cells *In Vivo* But Do Not Improve Survival for Mice with H1N1 Virus-Induced Acute Lung Injury

Yuan Tan[1, 2]†, Yan Wang[1]†; Luciana Souza-Moreira[1]; Chi Wang[1]; Aidan B.P. Murray[1]; Mahmoud Salkhordeh[1]; Maria Florian[1]; Lauralyn McIntyre[2,3] Duncan J. Stewart[1, 2] and Shirley H.J. Mei[1]*

1 Regenerative Medicine Program, Ottawa Hospital Research Institute, Ottawa, Canada.
2 Faculty of Medicine, University of Ottawa, Ottawa, Canada
3 Clinical Epidemiology Program, Ottawa Hospital Research Institute, Ottawa, Canada
†These authors contributed equally to this work and share first authorship

*** Correspondence:**
Shirley H.J. Mei, smei@ohri.ca

Keywords: Mesenchymal stem cells$_1$, Influenza A$_2$, Immunomodulation$_3$, Acute lung injury$_4$, Viral Infection$_5$, H1N1$_6$, Immune cell profiling$_7$. (Min.5-Max. 8)

Preamble:
In the previous chapter, I revealed that viral-mimic priming improved the antiviral and immunomodulatory capacities of MSCs in context of severe COVID-19. In continuation of my investigation into MSCs in viral infections, this chapter focuses on the role of MSCs in modulating both innate and adaptive immune responses during active H1N1 Influenza A Virus (IAV) infection. Building on previous findings, I hypothesize that MSCs could significantly influence the dynamics of immune cell populations, and these modulatory effects can be impacted by interaction of MSCs with the IAV and infected host environment

Author Contributions: Y.T and Y.W contributed equally to conceptualization, data curation, animal model setup, data analysis, and writing of the original draft. L.S.M., C.W., and A.M were involved in animal model setup and data validation; M.S and M.F contributed to resource gathering. L.M. was involved in clinical supervision, and review & editing of the manuscript. D.J.S. contributed to supervision, funding acquisition, and review & editing of the manuscript. S.H.J.M. were involved in conceptualization, funding acquisition, project administration, supervision, review & editing of the manuscript.

3.1 Abstract

Introduction: Influenza A virus (IAV) induced acute lung injury (ALI) is characterized by pronounced proinflammatory activation and respiratory lung dysfunction. In this study, we performed deep immune profiling on airway and circulating immune cells to examine the effect of immunomodulation and therapeutic outcomes of mesenchymal stem cells (MSCs) therapy in mice with IAV-induced ALI.

Methods: Animals were inoculated intranasally with H1N1 IAV, followed by intravenous administration of vehicle, or human clinical-grade, bone marrow derived MSCs 24-hour later, and monitored for six days to evaluate the survival. In another set of animals, bronchoalveolar lavage (BAL) fluid and whole blood were collected three days after infection for flow or mass cytometry (CyTOF) immune profiling analysis.

Results: Immune cell population and phenotypic shifts in blood were mapped by CyTOF. Increases were observed in granulocytes and myeloid-derived cells in blood from vehicle-treated animals. While MSCs treatment accentuated changes in these populations, naïve B, antibody-secreting B cells and T cells were decreased in MSCs-treated animals at day 3. Compared to sham animals, IAV infection induced a significant 5.5-fold increase total BAL cell counts, including CD4+ and CD8+ T cells, CD19+ B cells, CD11b+Ly6G+ neutrophils, and CD11b+Ly6C+ monocytes. MSCs treatment significantly decreased BAL total cell counts in IAV-infected mice, specifically the number of infiltrating CD4+ T cells and CD11b+Ly6G+ neutrophils. In contrast, there were increases in CD8+ T cells, B cells, and monocytes in the alveolar space in MSCs-treated animals. Phenotypic immune cell profiling of blood and BAL revealed a significantly higher proportion of the monocyte

population with the M2 phenotype (CD206) in MSCs-treated animals; however, this failed to confer protective effects in the survival of infected mice or reduce viral titre in the lung. Further investigation revealed that MSCs were susceptible to IAV infection, leading to increased cell death and potentially affecting their efficacy.

Conclusion: These findings provided *in vivo* evidence that MSCs promote the selective recruitment of immune cells to the site of infection during IAV infection, with reductions in proinflammatory phenotypes. However, MSCs offered no survival benefit in IAV-infected animals, possibly due to MSCs' H1N1 IAV susceptibility and subsequent cell death.

3.2 Introduction

Acute respiratory distress syndrome (ARDS) is a clinical syndrome associated with lung inflammation, increased pulmonary vascular permeability, as well as blood and tissue hypoxemia[71,72]. To date, ARDS remains one of the leading causes of death in critically ill patients, with a mortality rate of up to 40%[73].

Influenza A virus (IAV) is a respiratory virus that primarily infects epithelial cells lining the respiratory tract of humans. Severe IAV infection can result in hospitalization for pneumonia and ARDS [74] and is the most common cause of pneumonia-related death[75,76]. Entry of IAV into host cells is mediated by binding of the viral surface glycoprotein, hemagglutinin (HA), to sialic acid (SA) receptors on the cell membrane[77]. The distribution of different types of sialic acid receptors on host cells determines the tissue tropism and host range of IAV. Upon cell infection, IAV triggers a pronounced activation of the lung's proinflammatory cascade. Uncontrolled, excessive cytokine production and immune cell activation are known to be central to the pathophysiology of influenza-induced ARDS [78]. Treatments for severe IAV-induced ARDS are limited to the use of high dose neuraminidase (NA) inhibitors and aggressive supportive care[75,79], and new therapies are needed to improve the outcomes of patients with severe IAV infections.

Mesenchymal stromal/stem cells (MSCs) are a type of adult stem cells that have the ability to differentiate into various cell types and possess broad immunomodulatory properties[80]. MSCs have been proposed as a promising therapeutic strategy in viral pneumonia because

of their immunomodulation and pro-resolution properties[81-83]. In the context of IAV infection, some preclinical studies showed that systemic administration of MSCs in IAV infection reduced virus-induced mortality, proinflammatory cytokines, and chemokines in the absence of reducing lung virus titers[84,85], while others found that MSCs failed to provide protection[86,87]. Additionally, concerns were raised over the susceptibility of MSCs to IAV infection, resulting in impaired cell functionality. Although known to potently inhibit T-cell and other immune effector cell functions *in vitro*, the knowledge of how MSCs function *in vivo* in the context of IAV-induced pneumonia remains unclear. Therefore, the aim of this study was to understand how MSCs may impact host immune responses during severe IAV-induced acute lung injury, with the goal of using this knowledge to design better therapeutic strategy in the future.

In our previous study, we revealed that viral-mimic priming augmented the immunomodulatory capacity of MSCs in an *ex vivo* co-culture system with whole blood from severe COVID-19 patients[24]. Therefore, we hypothesized that MSCs maintain their ability to modulate host immune cells *in vivo*, including both innate and adaptive immune cell populations, in the context of active H1N1 IAV infection. Here, we undertook a comprehensive analysis of systemic (whole blood) and locally (bronchoalveolar space) immune profiling using a IAV model, in which MSCs were administered after the onset of infection. We also examined the susceptibility of MSCs to H1N1 IAV infection and assessed cell viability of IAV-infected MSCs.

3.3 Materials and Methods

3.3.1 Bone Marrow Aspirates and MSC Culture

Bone marrow aspirates were obtained from a commercial vendor (Lonza) or at The Ottawa Hospital (with informed written consent and ethical approval granted by the Ottawa Health Science Network Research Ethics Board, REB ID: 20120929-01 H). Human bone marrow-derived MSCs (n=3 different donors; 2 females and 1 male) were cultured, characterized and cryopreserved as described previously[28,61]. MSCs have been characterized to meet all the criteria (plastic adherence, differentiation potential, and cell surface antigen expression) proposed by the International Society for Cellular Therapy (ISCT) [62]as previously described[28,61]. MSCs were thawed and cultured in Nutristem complete media (Biological Industries) for 24-72 hours prior to be lifted and plated for *in vitro* assays or *in vivo* studies. MSCs were cultured and maintained at 37°C in a humidified incubator containing 5% CO2. All experiments used cells between passages 3 to 5.

3.3.2 IAV infection animal model

All animal experiments were conducted under the protocol approved by the University of Ottawa Animal Care Committee (ACC, institutional animal protocol #3371). Eight to nine-week-old female C57BL/6N mice were purchased from Charles River Laboratories (Saint Constant, QC, Canada). They were allowed to acclimate in the animal care facility for one week prior to the experiment date. Animals were housed according to Canadian Council on Animal Care (CCAC) guidelines. All animals were housed in groups of either 3 or 4, in conventional breeding cages within the animal care facility. A standard chow diet was

provided within the hopper of the cage to avoid soiling, and water was provided ad libitum. All cage bedding was changed on a weekly cycle. Animals were housed in a 20°C-23°C temperature-controlled room with a 12-hour light, 12-hour dark cycle, and 40%-60% humidity. Daily wellness checks were conducted by the laboratory personnel, as well as the veterinary technicians on site.

For the experimental model, animals were anesthetized with isoflurane (1L/min O2 and 4% isoflurane), and then inoculated intranasally with 500 PFU (survival curve; 6 days) or 1000 PFU (3 days experiments) of IAV strain A/FM/1/47-MA (mouse adapted H1N1 strain, a generous gift from Dr. Earl Brown at University of Ottawa), diluted in 30 µL of sterile PBS. For hydration, mice received 40 mL/kg saline subcutaneously after IAV inoculation. Twenty-four hours post virus infection, animals were anesthetized with isoflurane (1L/min O2 and 1.5- 2% isoflurane) and a suspension of $2.5x10^5$ MSCs in Plasma-Lyte A (PLA) and 5% human albumin (100 µl total volume) or vehicle (PLA + 5% human Albumin) was slowly infused via jugular vein. After cell administration, the incision was closed with a sterilized surgical clip, and a topical pain-relieving cream was administered to the surgical site. Mice were monitored daily by trained laboratory personnel, as well as the veterinary technicians on site, until the end of study. Note that animals were previously randomized (random.org; Randomness and Integrity Services Ltd.) for the treatment groups (vehicle or MSCs); cell infusion, animal wellness, and sample analyses were performed in a blinded fashion, with independent operators blinded for the group assignment. Any correlation between treatment name and nature of the treatment was only revealed following the data collection

and analysis period for graphing purpose. For mass cytometry immunoprofiling analysis, total numbers were n = 6 sham, n=13 IAV/vehicle- and n=11 IAV/MSCs-treated animals, see Figure 3.1A. For survival, a total of n = 15 for IAV +Vehicle group, and n=14 for IAV +MSCs group were used (see Figure 3.6A).

3.3.3 Animal sample collection and processing

Mice were sacrificed 3 days after IAV inoculation to evaluate the therapeutic efficacy by collecting samples for analysis. Mice were anesthetized with Ketamine (200 mg/kg) and Xylazine (10 mg/kg) cocktails through IP injection. Once surgical plane was reached (mice not reactive to toe pinch), blood was collected from the inferior vena cava with 50 mM EDTA-coated syringe.

For immune profile studies and cytokine analysis, Bronchoalveolar lavage (BAL) were performed by inserting a catheter into the trachea, and slowly injecting and aspirating 1 mL of saline three times. Total cell number was determined by 1:1 methylene blue counting by personnel blinded by the identity of animal injury/treatment. BAL was then centrifuged at 800 g for 10 min at 4 °C, and supernatant (BAL fluid; BALF) was collected and stored at -80°C for further analysis. Cell pellets were resuspended in PBS and further fixed with paraformaldehyde 4% for flow cytometry analysis. Cytokine and chemokine levels in BALF were measured using multiplex immunoassays kit (Bio-Rad) according to the manufacturer's instruction and analyzed using Bio-Plex 200 System (Bio-Rad, USA). Total protein and IgM levels in BALF were measured using Bro-Rad DC (detergent compatible)

Protein Assay (Bio-Rad) and a murine specific IgM ELISA kit (Bethyl Laboratories), respectively, according to the manufacturer's instruction. Note that BALF samples were incubated with 1% Triton X-100 at room temperature for one hour to deactivate IAV prior to the assay.

3.3.4 BAL cells staining

After fixation, cells were washed 3 times with staining buffer (PBS supplemented with 2% Fetal Bovine Serum). Cells were subsequently stained with anti-mouse CD11b, Ly6C, Ly6G, CD3, CD4, CD8 and CD19 (BD Biosciences) for 30 minutes at room temperature. Following incubation, cells were washed 3 times and resuspended in staining buffer with CountBright Absolute Counting Beads (ThermoFisher) for flow cytometry analysis (LSR Fortessa cytometer, BD Biosciences). A detailed list of all antibodies is shown in Resource table.

3.3.5 Sample processing and antigen staining of mass cytometry-based immune cell profiling (CyTOF)

For CyTOF sample processing, 250 µL of mouse whole blood (EDTA) via caudal (inferior) vena cava was lysed in 350 µL of stable-lyse V2 and then fixed in 1 mL of stable-store V2 (Smart Tube Inc., San Carlos, US) as described in the user's manual and stored at -80ºC until further processing. Further, whole blood samples were thawed and washed, followed by barcoding using Cell-ID 20-Plex Pd Barcoding Kit (Fluidigm). Up to 4 individual samples were barcoded for 30 min at room temperature. Cells were then washed and pooled for surface staining. Pooled cells were resuspended in diluted human Fc-block (BD bioscience)

for 10 minutes and incubated with antibody staining cocktails for 30 min at room temperature. After incubation, cells were washed with staining buffer and fixed overnight in MaxPar Fix-I buffer with iridium intercalator (Fluidigm). Immediately prior to data acquisition, samples were washed once with each of Cell Staining Buffer (Fluidigm) and Cell Acquisition Solution (Fluidigm). Samples were then resuspended at a concentration of $5x10^5$ cells per mL in Cell Acquisition Solution containing EQ Four Element Calibration Beads (5:1 Ratio) (Fluidigm). The samples were acquired on a Helios Mass Cytometer equipped with a wide-bore sample injector at a rate of 300-500 events per second. After acquisition, repeat acquisitions of the same sample were concatenated as necessary and normalized using the Fluidigm software. Normalized fcs files were gated to exclude debris, doublets and dead cells using Cytobank software.

All antibodies pre-conjugated to metal isotopes were obtained from Fluidigm Corporation (San Francisco, US). All remaining antibodies were obtained from the indicated companies as purified antibodies and in-house conjugation was done using the MaxPar X8 labeling kit (Fluidigm) following manufacturers' recommended protocols. A detailed list of all antibodies used in this study is shown in table 1.

3.3.6 Mass cytometry data analyses

Files were processed following Fluidigm recommendation, including randomization and normalization using EQ Beads signal. Files were then concatenated, debarcoded, and randomized according to Fluidigm's instructions using the CyTOF Software. Gating to

identify and export single cells was completed in Cytobank[67]. Clustering analysis was completed with either FlowSOM (Cytobank)[68] or PhenoGraph [69] as stated as part of the R Bioconductor package Cytofkit [70] and Flowjo X using the markers listed in the Key Resource Table with up to 50,000 cells per sample. The transformation method used was cytofAsinh, and the visualization method was t-SNE. The t-SNE map overlaid with PhenoGraph-defined cell populations (Figures S3.3B and 3.4B) was generated using ggplot2 package in RStudio (open-source) and FlowJo (BD Biosciences).

3.3.7 Automated western blot analysis

MSCs were seeded into 24-well plates (100,000cell/well) and treated the day after with 10% of BALF obtained from control (sham) or IAV infected (sick) animals; in parallel, cells were also infected with IAV (A/FM/1/47-MA) at a multiplicity of infection (MOI) of 0.1. After 24h, cell lysate was collected by adding sample lysis buffer cocktail containing proteinase inhibitor cocktail (Sigma-Millipore) and cell scraper. Protein quantification was performed using Bradford reagent (Bio-Rad). Target protein signal was measured by automated capillary electrophoresis-based western blotting system (Jess, ProteinSimple, San Jose, CA, USA). In summary, samples were diluted to 1ug/ul total protein in simple western sample buffers from the 12-230 kDa Jess Separation Module cartridge kit (cat# SM-W004), heated at 95ºC for 5 minutes, then loaded to the plate. All Jess simple western system experiments were conducted according to the manufacturer's instructions. Compass for SW software (ProteinSimple) was used to analyze and quantify protein band intensities. A detailed list of all antibodies used in this study is shown in table 1.

3.3.8 Sialic acid detection on MSCs

150,000 MSCs were washed 3 times with staining buffer (PBS supplemented with 2% Fetal Bovine Serum). Cells were stained with 100 µL of 100 µg/mL Maackia Amurensis Lectin (MAA) conjugated with Dylight 649 (EY Laboratories, DY649-7801-1), and Sambucus Nigra (Elderberry Bark) Lectin (SNA, EBL) conjugated with fluorescein (FITC) (Thermo Fisher, L32479) for 30 mins at room temperature. Following incubation, cells were washed 3 times and resuspended in staining buffer for flow cytometry analysis (Attune NxT Flow Cytometer, Invitrogen).

3.3.9 In vitro virus infection assays

MSCs were seeded into 48-well plates with the seeding density of 15,000 cells/per well. The day after, cells were infected by H1N1 IAV (A/FM/1/47-MA) at a MOI of 1 diluted in OptiMEM(100 µl/well). After 1h, the infection media were removed cells were washed twice with PBS. MSCs were cultured in Nutristem complete media (Biological Industries) at 37ºC for 24h, 48h and 72h. For LDH assay and testing virus titer, conditioned media of each group were collected at each timepoint, then cells were washed with PBS and fixed using 4% Paraformaldehyde (PFA). Lactate dehydrogenase (LDH) measurement was performed using the CytoTox 96® Non-Radioactive Cytotoxicity Assay (Promega). For virus titer, IAV RNA was isolated from conditioned media using the QIAamp Viral RNA Mini RNA isolation kit (Qiagen), and the qPCR was performed using QuantiTech Virus Kit (Qiagen) and analyzed in CFX384 Thermocycler (Bio-Rad). Cell images were obtained using Incucyte S3, objective 20x (Sartorius). For nuclei counting of attached cells, DAPI (4',6-diamidino-2-phenylindole,

Thermofisher) staining was used to identify nuclei. The fluorescent images were captured and analyzed (Cellomics ArrayScan VTI HCS Reader, Thermo Fisher Scientific, CA, USA). For publication purposes, the brightness of all images was enhanced at the same percentage (+20%) to optimize visualization.

3.3.10 Statistical analysis

Statistical analysis was performed using GraphPad PrismV9.0 software (GraphPad Software). Numerical data are presented as mean ± SEM unless otherwise stated. Analysis was conducted using a two tailed T-test. Multiple groups were analyzed by one-way ANOVA followed by Sidak's or Dunnett's multiple comparisons test unless otherwise stated. For the analysis of cytokine data, logarithmic transformation was performed to normalize the data distribution before conducting ANOVA. Statistical significance was set at $p < 0.05$.

3.4 Results

3.4.1MSCs Induced Immunomodulatory Changes in Circulating Innate Immune Cell Population in an IAV-induced Acute Lung Injury (ALI)

We first investigated whether MSCs can improve host immune responses when exposed to a virus-infected host microenvironment *in vivo*. Mice were challenged with IAV followed by treatment with vehicle or MSCs (Figure. 3.1A). Immune cells in whole blood were profiled at day 3 post-infection by CyTOF, followed by t-SNE analysis and PhenoGraph clustering, revealing 20 distinct populations (Figure 3.1B and C). The density analysis of the t-SNE

maps demonstrates dynamic shifts of circulating immune cell population in IAV-infected mice (vs. sham, Figure 3.1B), while the expression level of individual cluster's surface markers is represented in a heatmap (Figure 3.1C). To analyze the modulation of both innate and adaptive immune cell populations, CD11b expression was used to further subgroup the CD11b+ innate cells (Figure 3.2) and CD11b- adaptive immune cells (Figure 3.3) in the t-SNE analysis. In Figure 3.2A and Figure S3.1A, the innate immune cell population was clustered into t-SNE maps, overlayed with cluster 1, 5, 10, 11, 12, 13, 14, 16 and 20. In vehicle-treated IAV animals, there were significant enrichment of granulocytic (cluster1) and monocytic (cluster 5) myeloid-derived cells, monocytes (cluster 10), granulocytes (cluster 16) and dendritic cells (DCs, cluster 12) compared to sham animals (Figure 3.2B, Supplementary Figure 3.1B). On the contrary, circulating macrophage (cluster 20) was significantly depleted ($p<0.001$ vs. sham, Figure 3.2B). With MSCs administration, we observed distinctive changes of innate cell populations compared to vehicle-treated animals (shown in Figure .2B and Figure S3.1B). MSCs administration significantly potentiated the increase in granulocytic myeloid-derived cells (cluster1) and granulocytes (cluster 16), while decreasing the number of circulating macrophages (cluster 20) and monocyte (cluster 10) in circulation (Figure 3.2B). Natural killer (NK) (cluster 13 and 14) cells and DCs (cluster 12) have no significant changes with MSCs administration (Figure S3.1B). When examining the phenotypic marker profile, the monocyte population in whole blood exhibited a greater M2 (CD206+) and less immune tolerance (high MHC-II) phenotype after MSCs (Figure. 3.2C), compared to vehicle-treated ones.

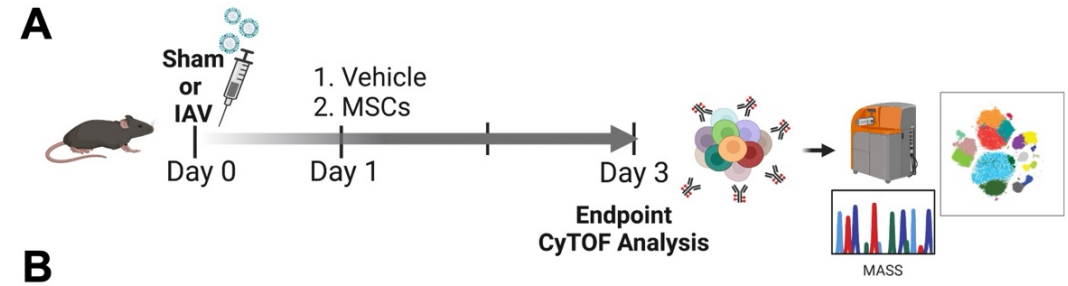

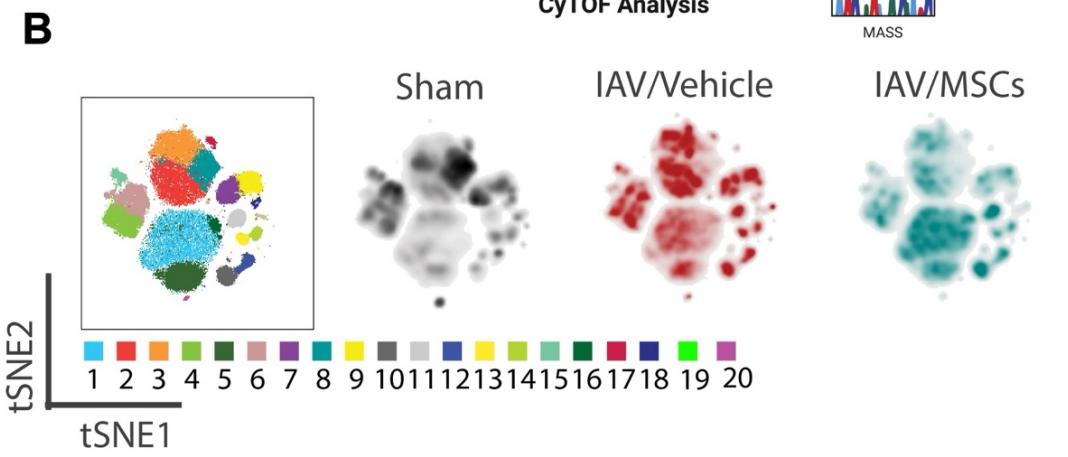

C

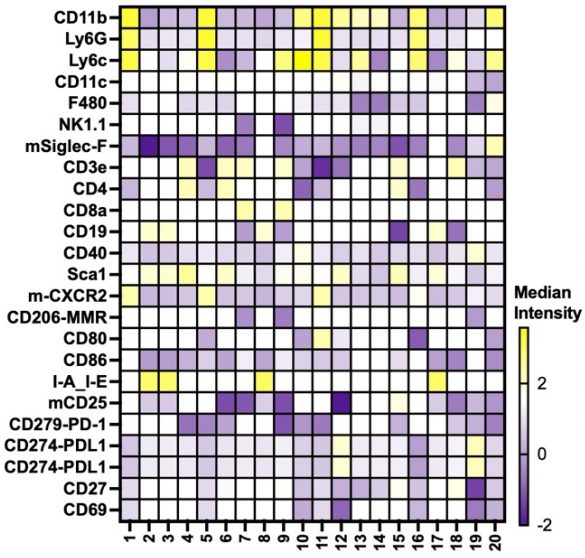

Cluster	Cell type	Lineage expression
1	G-MDSCs	CD11b+Ly6G+Ly6cMID
2	naive B	CD19+Ly6C-
3	Antibody secreting B cell	CD19+Ly6c+Sca1+
4	memory CD4 T	CD3+CD4+Ly6c+
5	M-MDSC	CD11b+Ly6G+Ly6cHIGH
6	naive CD4 T	CD3+CD4+Ly6c-
7	naive CD8 T	CD3+CD8+
8	Resting B cell	CD19+Sca-
9	Memory CD8 T	CD8+Ly6c+
10	monocyte	CD11b+Ly6G-Ly6c+
11	Granulocytes	CD11b+Ly6G+CD80++
12	Dendritic cell	CD11b+CD11c+
13	Mature NK	CD11b+NK1.1+Ly6C+
14	NK	CD11b+NK1.1+Ly6C-
15	Actiivated CD4 T cells	CD3+CD4+SCA1+CD25+
16	Granulocyte	CD11b+Ly6G+Ly6clow
17	Memory B	CD19+Ly6c-CD11b+
18	memory-like CD27 + γδ T cells	CD3+Ly6c+CD27+
19	CD40+ cells	cd40+pd1+
20	Macrophage	CD11b+F4-80+

Figure 3.1 In vivo H1N1-Induced ALI Schematic and Mass Cytometry Analysis of Whole Blood.

(A) In vivo schematic of H1N1 IAV animal model with vehicle or MSCs treatment timeline, followed by endpoint tissue collection for the downstream CyTOF analysis.

(B) Cell clusters were identified from CyTOF data by unsupervised clustering with the PhenoGraph algorithm. Each dot represents a cell (100,000 cells total). t-SNE plot overlayed with PhenoGraph clusters (the first map on the left), and density analysis was conducted (three map on the right).

(C) Heatmap of 25-marker expression for different immune cell types with cluster identification

n = 6 of sham, n=13 of IAV/vehicle- and n=11 of IAV/MSCs-treated animals.

3.4.2 MSCs Modulated Circulating Adaptive Immune Cell Population in IAV infection.

When analyzing the adaptive immune cells (CD11b-), PhenoGraph clusters 2, 3, 4, 6, 7, 8, 9, 15, 17, 18 and 19 were and analyzed into tSNE map (Figure 3.3A). Density maps further revealed distinctive enrichment and depletion of B and T cell populations, as in Figure 3.3A and different B cells subpopulation were identified using markers including Ly6C and Sca1(Figure 3.3B). With H1N1-infection, a marked depletion of naïve T cells (CD8+ T cell in cluster 7) and naïve (resting) B cells (cluster 8) was observed, while MSCs further promoted these changes (Figure 3.3C). Moreover, while there was a marked increase of memory CD8+ T cells (cluster 9) seen in the whole blood of IAV animals (vs. sham), MSCs treatment decreased the levels of these circulating immune cell clusters (vs. IAV/vehicle-treated, Figure 3.3C and Figure S3.2). Interestingly, while percentages of antibody-secreting B cells (ASB) (cluster 3), activated CD4 T cells (CD25+, cluster 15), and gamma-delta T cells (cluster 18) were not significantly altered in vehicle-treated IAV animals (not significant vs. sham). These cell populations were significantly lowered by MSCs (vs. IAV/vehicle-treated, Figure 3.3C). Taken together, MSCs were able to induce early alterations in both innate and adaptive immune responses during H1N1 IAV infection.

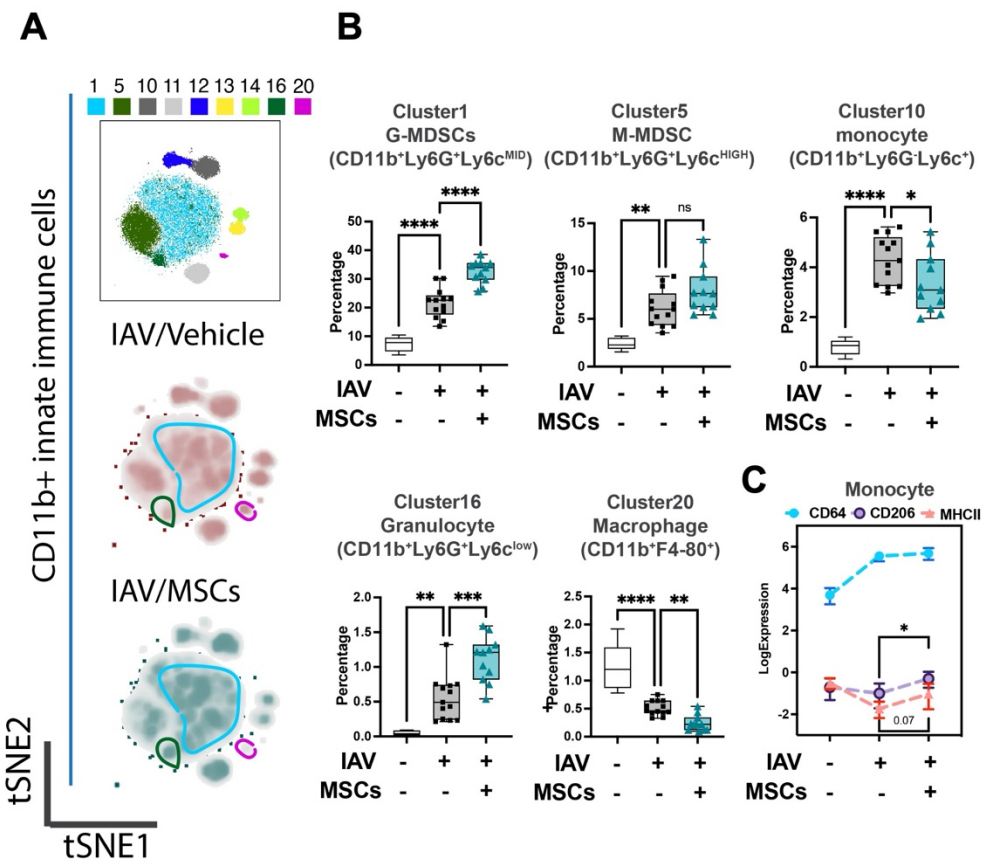

Figure 3.2 MSCs Re-Shapes Innate Host Immune Responses in Circulation (Whole Blood) of IAV Infected Mice.

(A) Subsequent tSNE analysis of CD11b+ innate immune cell population, overlaid with PhenoGraph clustering identified in Figure 3.1A.

(B) Quantification of cell subpopulations, identified by unsupervised clustering with PhenoGraph algorithm of CyTOF data, in whole blood isolated from IAV-infected mice (Fig. S3.1C). Analysis showed modulatory effects of MSCs on host innate immune responses during IAV infection.

(C) Quantification of CD64, CD206 and MHCII expression from CyTOF data showed increased expression of CD206 in MSC-treated groups.

n = 6 of sham, n=13 of IAV/vehicle- and n=11 of IAV/MSCs-treated animals with the data shown as box-and-whisker plots (B), or symbol= mean ± SEM (C). Group comparisons were analyzed by one-way ANOVA with Dunnett's post hoc test. ∗p <0.05, ∗∗p <0.01, ∗∗∗p <0.005, ∗∗∗∗p <0.001. See also Figure S3.1.

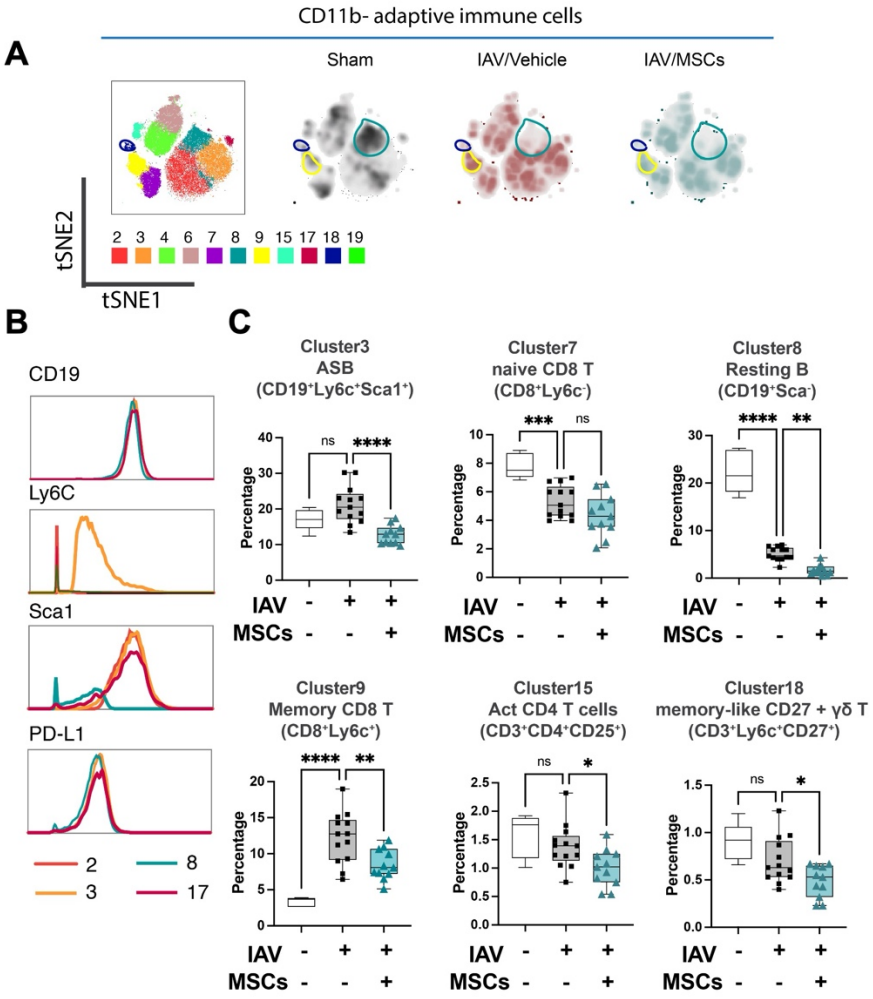

Figure 3.3 MSCs Alters Adaptive Immune Responses in Circulation (Whole Blood) in IAV Infected Mice.

(A) tSNE analysis of CD11b- adaptative immune cell population, overlaid with PhenoGraph clustering identified in Figure 3.1A.

(B) Histogram of various B cell related surface markers expression of cluster 2, 3, 8, and 17.

(C) Quantification of cell subpopulations, identified by unsupervised clustering with PhenoGraph algorithm of CyTOF data, in whole blood isolated from IAV-infected mice.

n = 6 of sham, n=13 of IAV/vehicle- and n=11 of IAV/MSCs-treated animals with the data shown as box-and-whisker plots. Group comparisons were analyzed by one-way ANOVA with Dunnett's post hoc test. $*p$ <0.05, $**p$ <0.01, $***p$ <0.005, $****p$ <0.001. See also Figure S3.2.

3.4.3 Modulation of Immune Cell Airspace Infiltration by MSCs in Airway of IAV-infected Lungs.

Next, we profiled changes of immune cell infiltration to bronchoalveolar space. Total cell counts in BAL were significantly elevated in IAV-infected animals (vs. sham), coinciding with early response to infection, and these were significantly decreased by MSCs treatment (vs. IAV/vehicle-treated, Figure 3.4A). The absolute number of neutrophils, monocytes, B cell, CD4+ and CD8+ T cells were all elevated in vehicle-treated mice (Figure 3.4B and C). MSCs significantly decreased the number of CD11b+Ly6G+ neutrophils (Fig. 3.4B). In contrast, MSCs-treated animals showed significantly increased number of CD11b+Ly6C+ monocytes (Figure 3.4B), CD8+ T and CD19+ B cells (Figure 3.4C) in the BAL, corresponding to a depletion of these populations in circulation (Figure 3.2B and 3C), suggesting MSCs may accelerated their recruitment into the alveolar airspace.

3.4.4 Upregulated Antiviral Protein Expression in MSCs upon Exposure to IAV-infected BALF.

We previously showed that MSCs upregulated antiviral protein expression induced by exposure to the viral mimic, poly(I:C)[24]. Next, the expression level of a range of antiviral proteins was examined in MSCs after exposure to BALF collected from H1N1 IAV-infected animal *ex vivo*. Upon stimulation with H1N1 IAV-infected BALF (BALF sick), MSCs exhibited marked elevation of Mx1, IFIT1, IFITM3, and OAS1 expression, compared to control MSCs or cells treated with BALF from sham animals (BALF Sham, Figure 3.5A and B).

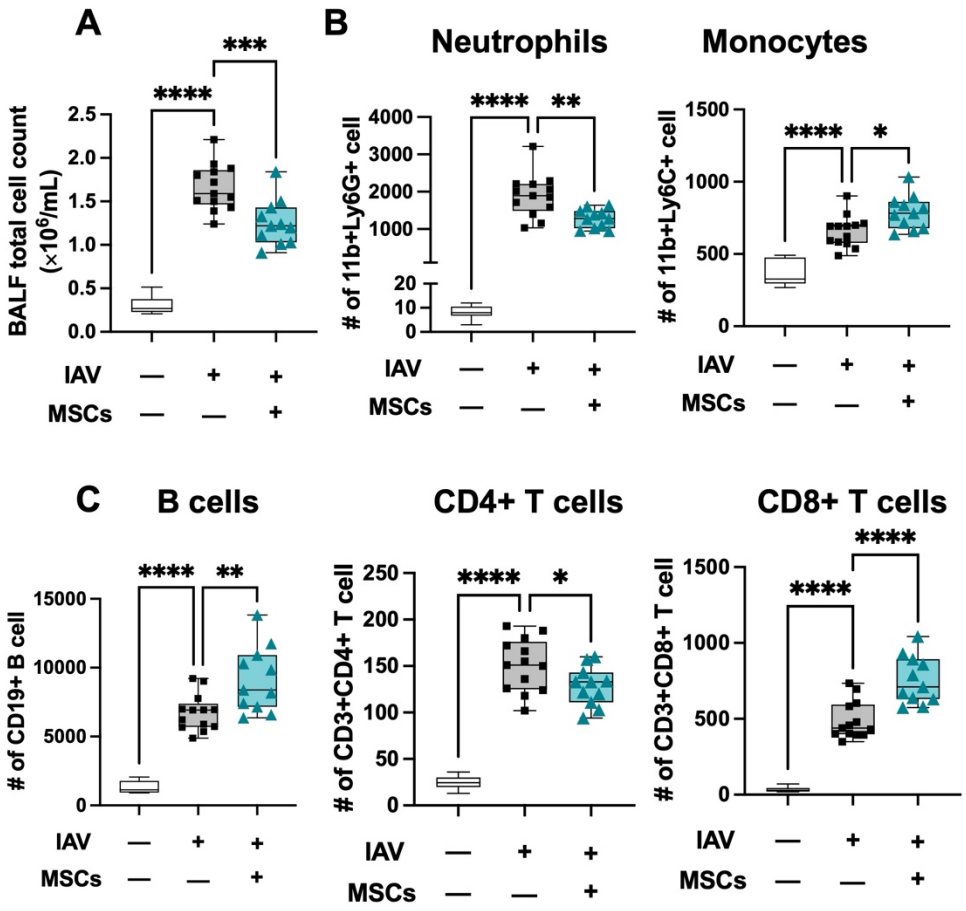

Figure 3.4 MSCs Modulates Immune Cell Infiltration into Localized Bronchoalveolar Spaces.

(A) Cell counts of total BAL infiltrating cells. Flow cytometry analysis of cells collected from BAL of IAV-infected mouse lung with or without MSCs treatment showed immune modulation on (B) innate immune cell (neutrophil and monocyte), and (C) adaptive immune cell (B cells, CD4+ T cells and CD8+ T cells) by MSCs.

n = 6 of sham, n=13 of IAV/vehicle- and n=11 of IAV/MSCs-treated animals with the data shown as box-and-whisker plots. Group comparisons were analyzed by one-way ANOVA with Dunnett's post hoc test. $*p$ <0.05, $**p$ <0.01, $***p$ <0.005, $****p$ <0.001.

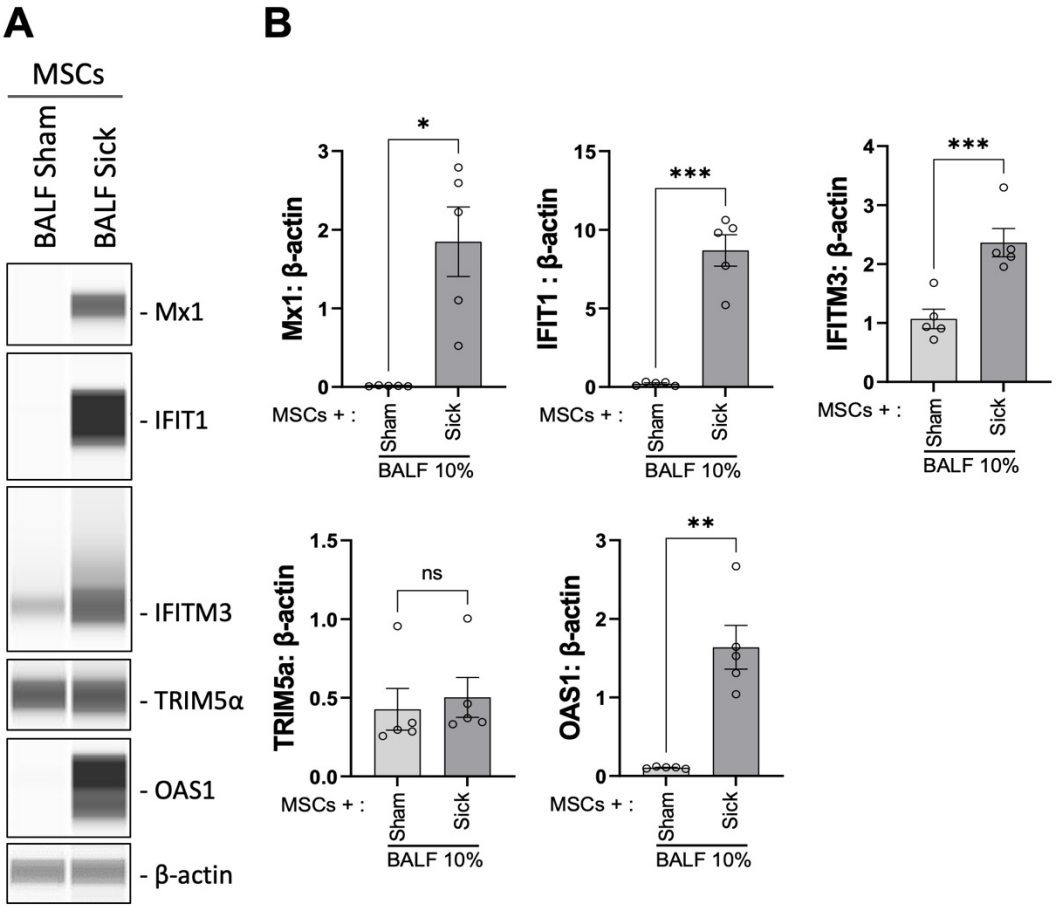

Figure 3.5 Upregulation of Antiviral Protein Expression in MSCs after Exposed to Bronchoalveolar Lavage of H1N1 IAV Infected Animal.

(A) Automated western blot analysis showed increased antiviral protein expressions in MSCs after *in vitro* exposure to BALF (BALF, 10%) from sham or sick (IAV-infected) mice.

(B) Densitometry analysis of protein expression detected using automated western blot. n = 5 with the data shown as mean ± SEM. $*p$ <0.05, $**p$ <0.01, *** p<0.005 using two-tailed t-test.

3.4.5 MSCs Did not Improve Survival of IAV-induced ALI

With the evidence showing that MSCs maintain their capacities to modulate immune cells *in vivo* during H1N1 infection, we further tested the therapeutic potential of MSCs in protecting mice from H1N1-induced mortality (Figure 3.6A). Unexpectedly, no improvement in survival rate was observed in the MSC-treated group compared to vehicle-treated IAV mice (Figure 3.6B). Corresponding to the survival result, MSCs- and vehicle-treated animals showed similar levels of virus load in BALF at day 3 post-virus infection (Figure 3.6C). An aggravated pulmonary vascular permeability was observed in vehicle-treated IAV mice with a significant increase in total protein and IgM in BALF (Figure 3.6D and E). Additionally, BALF from vehicle-treated IAV mice exhibited a significant increase in the cytokine levels (Figure 3.6F). However, MSCs did not induce changes either in the alveolar-capillary membrane barrier integrity (Figure 3.6D and E) or the cytokine levels in BALF compared with vehicle treatment (Figure 3.6F). Taken together, although MSCs exhibited significantly immunomodulatory activities the immune system, our results showed that MSCs did not prevent mortality or lung injury induced by H1N1 IAV infection in mice.

3.4.6 MSCs Highly Expressed H1N1 Binding Receptor and Underwent Cell Death upon IAV Infection.

Having established that MSCs do not protect against animal mortality *in vivo*, we next investigated whether IAV can infect MSCs. Given that MSCs were previously tested in virus-induced ALI using different IAV strains (mammalian H1N1 and avian H5/H9)[85,86] with different degrees of therapeutic efficacy, we examined whether there is differential

expression pattern of α-2,6-linked SA (receptor for mammalian H1N1, by SNA staining) and α-2,3-linked SA (receptor for avian H5 or H9 IAV strains, by MAA staining) on MSCs. Our data demonstrated that MSCs expressed high levels of H1N1 IAV receptor, α-2,6-linked SA (shown as SNA+ stained cells), while significantly smaller population of MSCs expressed level of avian IAV receptor (α-2,3-linked SA, shown as MAA+ stained cells) (Figure 3.7A). Direct H1N1 IAV infection still led to upregulated antiviral protein (Mx1, IFIT1, IFIMIT3, TRIM5a and OAS1) in MSCs (Figure S3.3), corroborating with our data of increased antiviral protein expression by MSCs after being exposed to H1N1-infected animal BALF (Figure. 3.5). Interestingly, we observed a significant increase in viral titer in conditioned media of MSCs at 48h after infection (at 2.70 ± 0.35 x 10^5 PFU/mL), compared to 24h (at 4.96 ± 0.95 x 10^4 PFU/mL, respectively, $p<0.01$; Figure 3.7B). The high virus load plateaued at 72h (3.07 ± 0.34 x 10^5 PFU/mL), possibly due to the high cytopathic effect induced by the H1N1 IAV strain. Indeed, marked morphological changes (Figure 3.7C) and reduced adherent MSCs (identified by nuclei staining, Figure 3.7D) were observed via microscopy post 24h IAV infection. Additionally, LDH level, which is released by cells upon plasma membrane damage or cell death, was significantly elevated at 48h after infection (Figure 3.7E). These results confirmed that the H1N1 strain used in our study can infect and kill MSC, which might limit therapeutic efficacy of MSCs treatment seen *in vivo*.

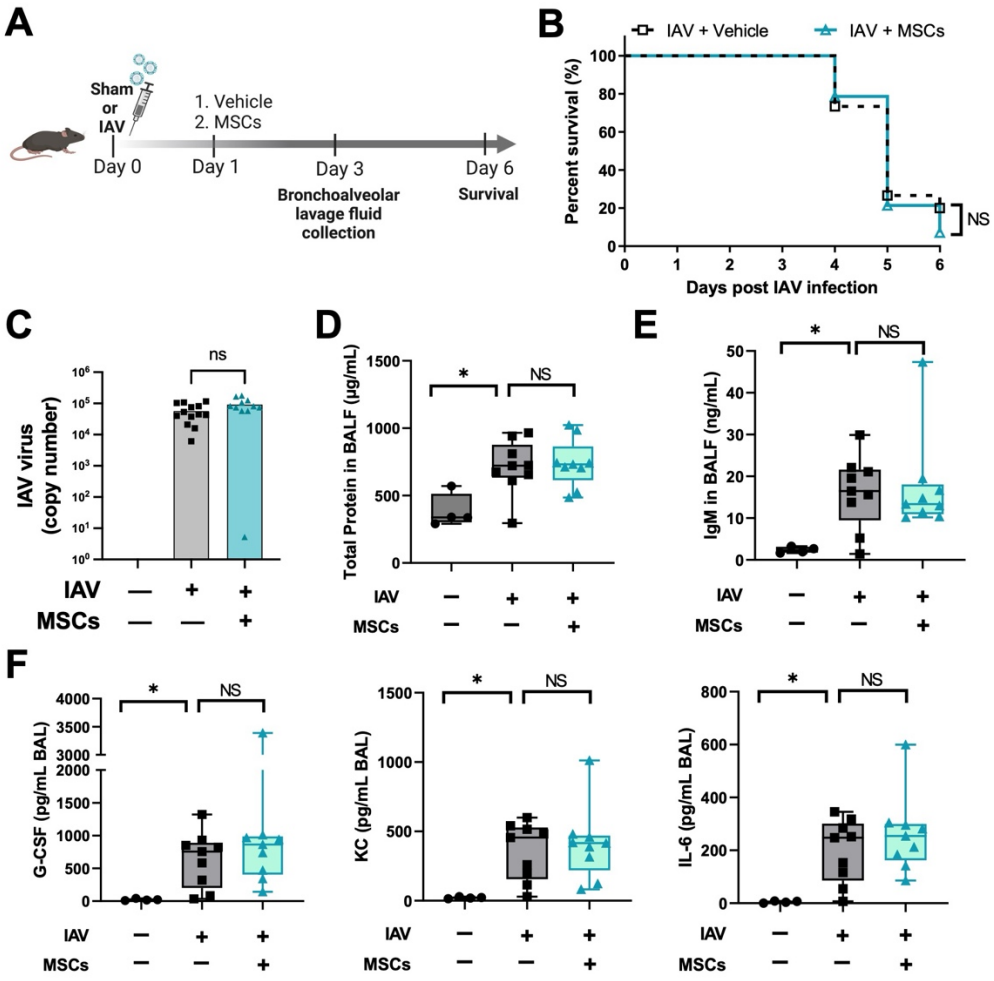

Figure 3.6 MSCs Did Not Rescue IAV-Infected Mice.

(A) *In vivo* schematic of the study. Mice received 500 PFU of influenza A intranasally. One day post-virus, mice received MSCs or vehicle treatment via jugular vein, and were monitored for 6 days post-virus inoculation.

(B) Percentage of animal survival data in vehicle vs. MSCs-treated IAV mice over 6 days.

(C) Virus tilter in mice BALF at day 3 post infection.

(D) Total protein levels in BALF at day 3 post infection.

(E) IgM level in BALF at day 3 post infection.

(F) Cytokines levels (G-CSF, KC and IL-6) in BALF at day 3 post infection.

n = 9-15 for IAV/Vehicle group or IAV/MSCs group, with the data shown as mean ± SEM. Survival result was analyzed by log-rank test (B). Group comparisons were analyzed by one-way ANOVA with Dunnett's post hoc test (D-F), $*p$ <0.05, $**p$ <0.01, $***p$<0.005, $****p$ <0.001.

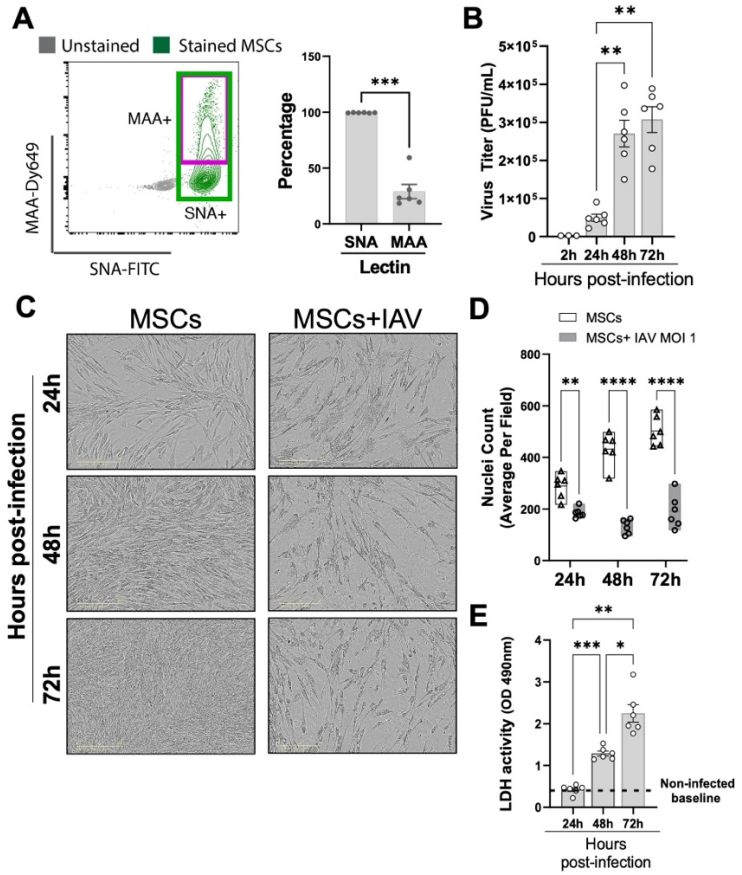

Figure 3.7 Viral Replication in H1N1-infected MSCs.

(A) MSCs were stained with fluorescein (FITC) conjugated Sambucus Nigra Lectin (SNA, EBL) and Dylight 649 conjugated Maackia Amurensis Lectin (MAA), followed by analyzing via flow cytometry for detecting the presence of salic acid on MSCs. n=6 with the data shown as mean ± SEM, ***p <0.0005.

(B) Viral titer measured by copy number (determined by qPCR) in the conditioned media harvested from MSCs infected with IAV. n = 3-6 with the data shown as mean ± SEM, **p <0.005.

(C) Representative phase microscopic images of MSCs with or without IAV H1N1 infection (MOI 1).

(D) Nuclei counting of DAPI-stained cells images. Graph shows average per field; total of 36 fields were imaged per well for each condition per individual experiment. n= 6 with the data shown as mean ± SEM, **p<0.005, ****p<0.0005.

(E) LDH activity showing that MSCs underwent cell death measured after H1N1 infection (MOI 1) over time. n = 6 with the data shown as mean ± SEM, *p <0.05, **p<0.005, ***p <0.0005.

Group comparisons were analyzed by one-way ANOVA with Dunnett's post hoc test (A, B and E) and Sidak's post hoc test (D).

3.5 Discussion

In a model of H1N1 IAV induced ALI, we showed that intravenous administration of MSCs induced a shift of monocyte phenotype in whole blood, enhanced the recruitment of granulocytic myeloid-derived cells, B cells (ASB) and T cells (CD8+) from circulation to the site of infection, while reduced immune cell infiltration into bronchoalveolar space caused by H1N1 IAV infection. Despite this clear evidence of immunomodulatory activities during IAV infection, there was no reduction in mortality, possibly due to infection of MSCs by H1N1 IAV, limiting their overall therapeutic potential.

By deep profiling the immune landscape in whole blood and BAL of IAV-infected mice, we showed evidence that MSC treatment resulted in increases in recruitment of antibody-secreting B cell and CD8+ cytotoxic T cell into the lung. Early activation of B cells contributes to a better host response against influenza viral infection by rapidly generating neutralizing antibodies to blunt the initial infection and help in inflammation resolution[88]. Cytotoxic T cell immunity is also important in limiting the severity and transmission of influenza infection by specifically eliminating infected cells[89]. Although we observed a significant impact of MSCs on the host immune response, there was no reduction in virus titer in BALF and mortality in IAV infected mice treated with MSCs. Nevertheless, as none of the previous studies conducted a comprehensive immune profiling of IAV-infected animals post MSCs treatment, our study provided a clear and definitive evidence of early immunomodulatory bioactivities of MSCs in a IAV induced lung injury model.

Chan et al. reported that MSCs, as an adjunctive therapy with antiviral agent, significantly reduced the impairment of alveolar fluid clearance induced by avian IAV (H5N1) infection and prevented or reduced H5N1-associated acute lung injury (Chan et al. 2016). In addition, MSCs were shown to inhibit the replication of H9N2 IAV *in vitro*, by reducing the expression of viral receptors on host cells and enhancing the antiviral activity of interferons (Li et al. 2016). In contrast, Darwish and colleagues demonstrated that the administration of murine or human MSCs, either prophylactically or therapeutically, failed to improve survival, decrease pulmonary inflammation, or prevent ALI in H1N1-infected mice[86]. Another recent study further confirmed that mouse or human MSCs treatment did not significantly affect H1N1 viral proliferation or mouse mortality in H1N1-induced ALI, despite the evidence of biological activity by blocking influenza-induced thrombocytosis.[87].

In virus-induced ALI, viral tropism needs to be carefully considered for evaluation of MSCs efficacy. We reported in this study that nearly all MSCs (99.43±0.21%) exhibited high expression of α-2,6-linked SA (measured by SNA, Figure 3.7A), H1N1 IAV binding receptors, and were highly permissive to infection by H1N1(swine-origin) strain. The upregulated interferon-stimulated genes such as Mx1, IFIT1 and IFITM3 in MSCs, after H1N1 IAV infection, failed to provide sufficient protection for MSCs from the H1N1 virus induced cytopathic effects and subsequently cell death. Therefore, we observed the similar lack of MSCs efficacy in reducing H1N1 IAV-induced mortality in our study, consistent with other studies reported to date[86,87]. In contrast, the encouraging results of MSCs in avian IAV (H5/H9 strains) [84,85]induced ALI and its associated mortality could be due to the different

strain tested, as a significantly lower expressed of avian IAV receptor (2,3-linked SA, measured by MAA, Figure.3.7A) are found on MSCs. It is likely that MSCs could be primed by avian IAV but not fully susceptible to the cytopathic effects or significant cell death, which could explain the better beneficial effect seen in avian IAV (H5 or H9 strain)-induced models. The lower susceptibility of MSCs to avian IAV infection may mirror the effect of viral mimic priming we previously reported in other viral disease[24]. All in all, function and efficacy of MSCs may vary in ALI induced by different strains of respiratory viruses, and more thorough understandings of the effect of MSCs on immune responses and viral susceptibility are needed to improve MSCs-based therapy.

3.6 Conclusion

In conclusion, we have provided thorough *in vivo* insights that MSCs were capable of inducing significant immune modulatory effects on phenotypic shifts and mobilization of granulocytes, B cell, and T cell subsets, evolving immune response elicited by viral infection. When employing MSCs as a therapy in the context of H1N1 infection, IAV strain-specific tropism need to be carefully considered.

3.7 Conflict of Interest

The funding institution had no role in the conception, design or conduct of the study, data collection or analysis, interpretation or presentation of the data, or preparation, review or approval of the manuscript. We also like to declare the following conflicts of interest: D.J.S. holds a patent for cell-based therapy for the pulmonary system, and S.H.J.M , Y.T, Y.W, and

L.S.M. hold a patent for cell-based therapy for viral disease; S.H.J.M. and L.S.M. have received personal fees from Northern Therapeutics that are outside of this submitted work. The remaining authors have disclosed that they do not have any conflicts of interest.

3.8 Author Contributions

Y.T and Y.W: Conceptualization, Data curation, Methodology, Investigation, Visualization, Formal analysis, and Writing – original draft; L.S.M., C.W., and A.M: Investigation, Methodology, and Validation; M.S and M.F: Resources; L.M: Clinical Supervision, and Writing – review & editing; D.J.S: Supervision, Funding acquisition, and Writing – review & editing; S.H.J.M: Conceptualization, Funding acquisition, Project administration, Supervision, Writing – review & editing.

3.9 Funding

The work was supported by Emergent Ventures, Thistledown Foundation (Fast Grant), The Ottawa Hospital Foundation COVID-19 Emergency Response Fund, and Ontario Institute of Regenerative Medicine (OIRM) - Disease Team Grant.

3.10 Acknowledgments

The authors gratefully acknowledge the support of Dr. Damian Carragher, mass cytometry proteomic core of OHRI, for providing help in CyTOF data analysis; Dr. Earl Brown of

University of Ottawa for providing a kind gift of IAV aliquots; Zeinab Altmieme for providing help in virus animal model.

Chapter 4 Adaptive Reprogramming of Mesenchymal Stem Cells by the Sepsis Microenvironment Enhances Immunomodulatory Effects on Myeloid Cells via a Caspase-1 Dependent Mechanism

Yuan Tan [#1,2], Luciana Souza-Moreira [#1]; Pramod Sahadevan[1]; Yan Wang[1]; Glinton Hanover[1]; Maria Florian[1]; Mahmoud Salkhordeh[1]; Aidan Murray[1]; Jennifer Virgo[1]; Jessica Haines[3]; Irene Watpool[3]; Lauralyn McIntyre[1,2,3]; Duncan J. Stewart[1,2,3]; Shirley H.J. Mei[*1]

[1]Ottawa Hospital Research Institute, Ottawa, ON, CANADA
[2]University of Ottawa, Ottawa, ON, CANADA
[3]The Ottawa Hospital, Ottawa, ON, CANADA

# These authors contributed equally.
[*]Corresponding Author and Lead Contact: smei@ohri.ca

Preamble:
In the previous two chapters, I have demonstrated that function and efficacy of MSCs may vary in ALI induced by two different types of respiratory viruses and highlighted the importance of studying interaction between MSCs and their surrounding environment. In this final chapter, I focus on a third disease setting of sepsis and examine the hypothesis that sepsis environment induces critical molecular changes within MSCs, that enhancing their ability to modulate innate immune responses. By investigating this adaptive reprograming within MSCs, I aim to uncover how MSCs can be better leveraged to improve outcomes in sepsis.

Author Contributions: Y.T and L.S.M contributed equally to the conceptualization, data curation, assay design, visualization, data analysis, and writing of the original draft. P.M, Y.W., and G.H. helped in assay setup and data validation. A.M, M.S, J.V and M.F worked on resource gathering; J.H. and I.W. contributed to participant recruitment. L.M. was involved in clinical supervision, and review of the manuscript. D.J.S. was involved in supervision, funding acquisition, and review & editing of the manuscript; S.H.J.M: contributed to conceptualization, funding acquisition, project administration, supervision, and review & editing of the manuscript.

4.1 Summary

Mesenchymal stem/stromal cells (MSCs) are actively being explored as a potential therapy for disorders associated with immune dysregulation, including sepsis. However, little is known about crosstalk between sepsis environment and MSC-mediated immunomodulation on myeloid cells. We utilized *ex vivo* human and *in vivo* animal models to investigate neutrophil and monocyte modulation by MSCs in sepsis, complemented by temporal analysis of neutrophil markers in septic shock patients who received MSCs therapy. We provided evidence of MSCs altering the phenotypes and improving the functions of myeloid cells. Transcriptomic and cytokine analyses revealed activation of caspase-1 pathway in MSCs by the sepsis milieu, which was identified as an essential molecular mechanism mediating immunomodulatory effects of MSCs on dysfunctional neutrophils and monocytes. Overall, our results demonstrate an adaptive crosstalk between MSCs and host immune environment in sepsis that enhances the therapeutic activity of MSCs. These novel insights can be used to refine MSC-based therapies.

4.2 Introduction

Sepsis is a life-threatening condition resulting from a dysregulated immune response to infection and remains a significant challenge in healthcare[90]. Despite advancements in critical care and antimicrobial therapies, sepsis continues to be a leading cause of morbidity and mortality worldwide[91]. The complex pathogenesis of sepsis presents several challenges for its treatment. In particular, myeloid cell dysregulation plays a significant role in sepsis and contributes to both the inflammatory response and immune dysfunction and

paralysis. Neutrophils are highly motile phagocytic cells that constitute the first line of defense of innate immunity and are considered to have an integral role in sepsis pathobiology; both qualitatively and quantitatively[92-94]. Monocytes, another key member of innate immune defense against infection, rapidly exhibit an impaired production of cytokines in response to secondary bacterial challenge, which represents a state of globally impaired immune functions and correlates with poor clinical outcomes in critically ill patients[95]. These dynamic myeloid dysfunctions exhibited in sepsis necessitate ongoing research and innovative treatment development approaches.

Mesenchymal stem/stromal cells (MSCs) are resident mesoderm-derived cells that can be isolated from various tissue sources and expanded greatly in numbers *in vitro*. While the restricted multipotency of MSCs led to their use as a promising therapy in regenerative medicine, it is their ability to modulate different aspects of the host immune system[96] that has generated tremendous interest for MSC-based therapies in the treatment of a wide variety of immune diseases. Well-documented MSC-mediated immunomodulation includes inhibition of T cell proliferation, tolerance induction in dendritic cells, as well as macrophage polarization (i.e. M1/M2)[97,98]. Combination of *in vitro* studies and promising data from various *in vivo* animal models[81,99] has accelerated the translation of MSC therapy for clinical applications, and the medical utility of MSCs is currently being investigated in over 1,400 clinical trials (clinicaltrial.org).

Despite an increasing number of preclinical studies that have demonstrated efficacy in animal models of sepsis and acute lung injury[100-102], there is a knowledge gap in identifying the global effect of MSCs on neutrophils and monocytes in sepsis, and how this effect could be influenced by adaptive molecular response of MSCs to host sepsis environment. Accumulating evidence suggests that MSCs are endowed with the capacity for environmental sensing and can mount responses adaptively, a key differentiator compared to conventional therapies, such as small molecule compounds, that only target one specific pathway for a given immune disorder. MSCs express a large variety of surface sensory receptors, including toll-like receptors (TLRs)[103], integrins[104], and cytokine receptors[105] etc., that could integrate cellular environmental cues. For instance, we have previously shown that, by activating TLR-3 via double-stranded RNA viral mimic, MSCs reciprocally augmented antiviral and immunomodulatory capacities in severe viral infection[106]. During sepsis, patients suffer from a dysregulated host immune system, which further contributes to a highly complex, imbalanced network of soluble factors (i.e. cytokines, growth factors) and immune cell phenotypes. Yet, how the sepsis microenvironment milieu, which is dynamic and interactive, may influence activities of MSCs is largely unknown.

We hypothesized that sepsis microenvironment induces molecular changes within MSCs, which positively contributes to an enhanced capacity of MSCs to modulate host innate immune cells and therefore improve overall outcome in sepsis. To test this hypothesis, we first aim to identify the key changes in the host neutrophil and monocyte responses in

sepsis and their modulation by MSC delivery, including changes in immune cell populations, phenotypes and functions. We achieved this using a clinically relevant mouse model and an *ex vivo* human blood model of sepsis. Global immune cell profiling was done via mass cytometry (CyTOF) to investigate the distinct modulations by MSCs on neutrophils and monocytes. Secondly, to decipher the molecular mechanism of MSCs in response to sepsis microenvironment, we studied transcriptome and cytokine changes within MSCs after co-culture with sepsis patient whole blood (mimicking physiologically relevant simulation of systematic administration of MSCs to sepsis patients). We discovered significant alterations of multiple genes within the caspase-1 pathway, accompanied by the increased secretion of IL-1□. Pre-activating caspase-1 in MSCs using sepsis-like stimuli, enhanced the ability of MSCs to facilitate myeloid modulation and bacterial clearance *in vivo* and *ex vivo*. In contrast, the knockdown of caspase-1 abolished the ability of MSCs to modulate myeloid cell functions in sepsis, further confirming the essential role of caspase-1 in MSCs.

4.3 Results

4.3.1 Effect of MSCs on Myeloid Cell Activation, Trafficking and Function in Sepsis

Modulation of neutrophil and monocyte responses by MSCs was studied over time using a clinically relevant murine model of polymicrobial sepsis (induced by cecal ligation and puncture [CLP]). We collected whole blood (WB), peritoneal lavage fluid (PLF), and bone marrow (BM) at acute (day 2) and prolonged (day 5) phases of the disease progression to investigate the effects of MSCs on neutrophil and monocyte mobilization to peritoneal

infection. In vehicle-treated septic animals (CLP/vehicle), significant trafficking of neutrophils (Lin-CD11b+Ly6G+) and monocytes (Lin-CD11b+Ly6C+) from circulation (WB) into peritoneum (PLF) was observed in acute response (day 2, shown by the reduced cell number in WB and the significantly increase in PLF (Figure 4.1A and B, CLP/vehicle vs sham). Neutrophil infiltration to PLF remained significantly elevated up to day 5 of sepsis compared to the sham group (Figure 4.1A). This cell migration toward the peritoneum was corroborated by a decrease in myeloid reserve in BM (Figure S4.1A). With in vivo MSC intravenous treatment (CLP/MSCs group), we mapped a pattern of accelerated neutrophil trafficking in early sepsis progression, but this was reduced at day 5 of CLP. CLP/MSCs animals, compared to the CLP/vehicle group, showed a higher number of neutrophils in PLF on day 2, but it was greatly reduced on day 5 (Figure 4.1A). Consistently, neutrophil numbers in BM with MSC treatment were significantly recovered (Figure S4.1A, CLP/vehicle vs CLP/MSCs) to a level similar to the sham. For monocytes, MSCs induced delayed trafficking with lowered cell number at day 2 (PLF) but significantly increased cell number detected in WB and PLF at day 5 (Figure 4.1B, CLP/vehicle vs CLP/MSCs). (Figure 4.1B, CLP/vehicle vs CLP/MSCs).

Next, we explored whether *in vivo* MSCs treatment could improve the functions of neutrophils and monocytes. Two key functions of neutrophils, oxidative burst (ROS) and phagocytosis, were measured in neutrophils isolated from CLP. Neutrophils in early disease (CLP/vehicle at day 2) showed robust ROS production capacity to a similar extent as cells from sham. However, as the disease progressed to day 5, neutrophils lost half of ROS-

producing activities (Figure 4.1C, CLP/vehicle vs sham). With MSCs treatment, a time-dependent modulation of ROS capacity of neutrophils was observed. At acute state (day 2), neutrophils from CLP/MSC had lowered ROS production capacity compared to CLP/vehicle, while MSCs partially rescued ROS production defects of neutrophils at the later phase of the disease (day 5) from both WB (Figure 4.1C) and PLF (Figure S4.1B). For phagocytic function, neutrophils in the CLP vehicle-treated group showed a mild increased activity compared to sham animals, while MSC treatment further significantly potentiated enhanced phagocytosis neutrophils in WB (Figure 4.1C) and PLF (Figure S4.1B) from septic mice, at both day 2 and 5. In addition, monocyte function was also measured. Phagocytosis was severely impaired in monocytes of septic animals without treatment (CLP/vehicle) at both early and late stages of the disease; however, MSCs (CLP/MSCs) significantly rescued monocyte phagocytosis, approaching that of cells in sham animals (Figure 4.1D), suggesting MSCs likely led to improved ability of neutrophils and monocytes to clear pathogens.

As being an important bridge connecting innate and adaptive immunity, monocytes were collected from additional lymphoid tissues: lymph node (LN) and spleen (SP) for a more systematic analysis of monocytic responses. Monocytes from CLP/Vehicle group showed a modest elevation of M2 markers, CD206, expression compared to the sham group. This was further augmented by MSC treatment, leading to greater than 2-fold increase of CD206 in all three collected tissues along disease progression ($p<0.01$, compared to CLP/vehicle, Figure 4.1E). This data suggests that MSCs may assist in dampening acute inflammation by

skewing monocytes to an anti-inflammatory phenotype. Furthermore, MSC treatment led to increases in monocytic MHC-II and CD86 (co-stimulatory molecules) expression in circulation (WB) and lymph tissues (MHC-II and CD86 in LN and MHC-II in SP) at 5 days post-CLP ($p<0.05$, CLP/vehicle vs CLP/MSCs, Figure 1E), supporting that monocytes were less immune tolerant and having higher antigen-presenting capacity. Overall, we provided direct *in vivo* evidence, using a clinically relevant model of polymicrobial sepsis, that there is a time-dependent modulation dynamics of neutrophil and monocyte responses by MSCs. There were acute and late benefits demonstrated by MSCs in promoting neutrophil and anti-inflammatory monocyte/macrophage mobilization, accompanied by augmented functions of these myeloid cells for better bacterial clearance.

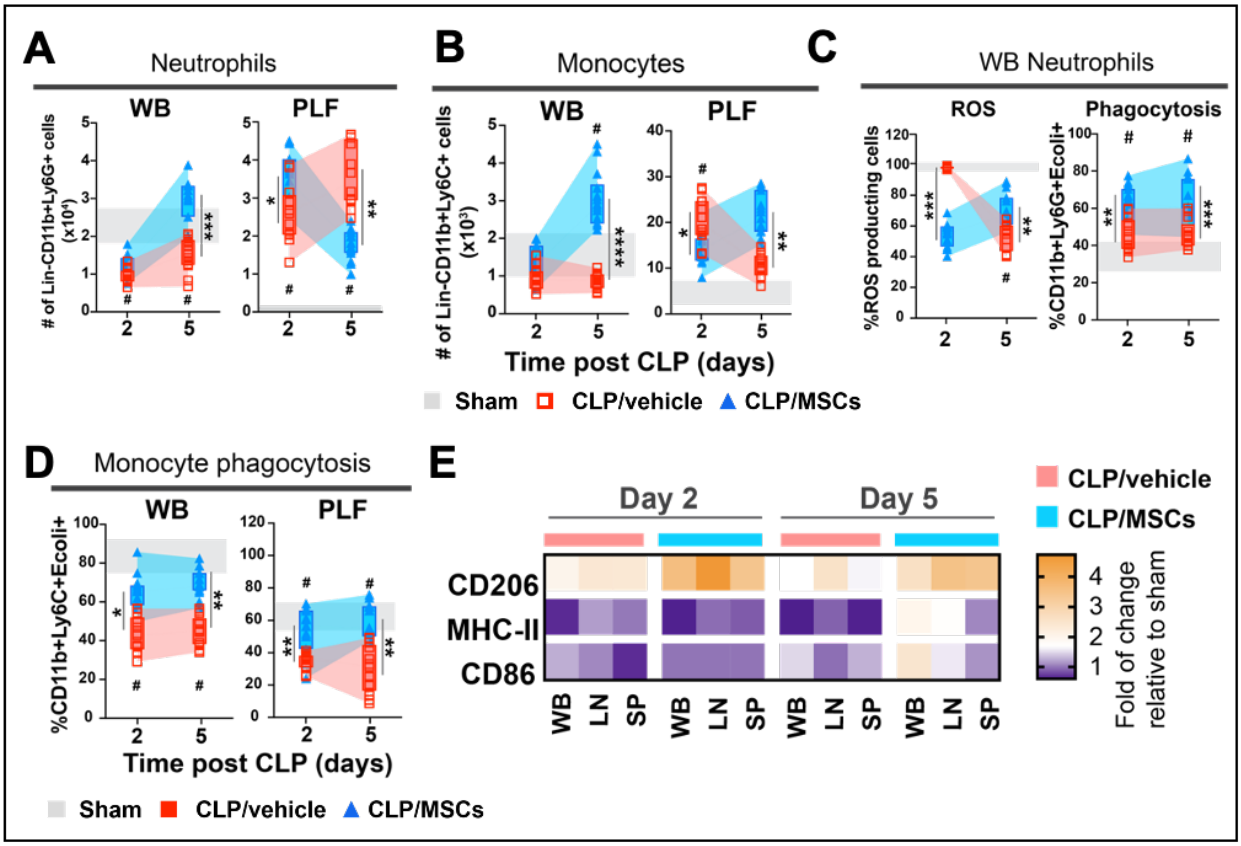
A
Neutrophils
WB
PLF
# of Lin-CD11b+Ly6G+ cells (x10⁴)
B
Monocytes
# of Lin-CD11b+Ly6C+ cells (x10³)
C
WB Neutrophils
ROS
%ROS producting cells
Phagocytosis
%CD11b+Ly6G+Ecoli+
Time post CLP (days)
Sham
CLP/vehicle
CLP/MSCs
D
Monocyte phagocytosis
%CD11b+Ly6C+Ecoli+
E
Day 2
Day 5
CD206
MHC-II
CD86
WB
LN
SP
Fold of change relative to sham

Figure 4.1 Time-Dependent Modulation of Neutrophil and Monocyte Response by MSC Treatment in Polymicrobial Sepsis.

A. Quantification of neutrophil (CD11b+Ly6G+) population in WB and PLF by flow cytometry at day 2 or day 5 post CLP.
B. Quantification of monocyte (CD11b+Ly6C+) population in WB and PLF at day 2 or day 5 post CLP.
C. Measurement of ROS production and phagocytic capacity of neutrophils in WB at day 2 or day 5 post CLP.
D. Measurement of phagocytic capacity of monocyte in WB and PLF at day 2 or day 5 post CLP.
E. Heatmap on the expression of phenotypic marker, CD206, MHC-II and CD86, on monocytes across various tissues.

WB, whole blood; PLF, peritoneal lavage fluid; LN, lymph node; SP, spleen. For A-D, shading represents the area within the error band (SEM) of each group at day 2 or 5. N=6 sham, n=15 for CLP/vehicle and n=14 CLP/MSCs animals per group, with the data shown as mean ± SEM, $*p<0.05$, $**p<0.01$, $***p<0.005$. #, $p<0.05$ comparing CLP/Vehicle vs sham. A-D, multiple comparison by one-way ANOVA with Dunnett's test. CLP, cecal ligation and puncture. ROS, reactive oxygen species.

4.3.2 Beneficial Myeloid Cell Activation and Function Changes in Human Sepsis Blood by ex vivo Co-culture with MSCs

To evaluate and confirm that MSCs can modulate dysfunctional myeloid cells in sepsis patients, we utilized an *ex vivo* system by co-culturing for 24 hours MSCs with WB collected from ICU sepsis patients (Figure S4.2A, see Table S4.1 for patient characteristics). Cell viability of total leukocytes was assessed first, and no significant change in cell death levels was noted post-coculture with MSCs in this ex vivo model (Figure S4.2B). Mass cytometry (CyTOF) analysis was conducted to deeply profile the changes in immune cell populations with or without exposure to MSCs. The t-distributed stochastic neighbour embedding (tSNE) algorithm was conducted on CD45+ gated leukocytes from sepsis blood samples alone (Sepsis) or samples co-cultured with MSCs (Sepsis/MSCs). The tSNE map with PhenoGraph clustering algorithm analysis generated visualization of cells grouped by similarities of marker expressions. Altered phenotypes of total leukocytes in sepsis WB was observed, comparing to healthy WB cells (Figure S4.2C). PhenoGraph identified 11 clusters with concatenated cells from sepsis blood samples alone (Sepsis) and co-cultured with MSCs (Sepsis/MSCs) (Figure 4.2A, left panel). When combining the phenotype marker with the tSNE visualization map, neutrophil populations represented the largest clusters, which were identified by positive expression of CD66b (Figure 4.2A, right panel and Figure S4.2C). Distinct phenotypic shifts in neutrophil populations were observed after co-culturing MSCs with septic patients' whole blood (clusters 2 and 3 in particular) (Figure 4.2B).

To reveal the phenotypic difference amongst 5 neutrophil clusters (clusters 1, 2, 3, 4 and 7) in sepsis, we extracted the median intensities of neutrophil-relevant markers and generated a dot plot (Figure 4.2C). The distinct decrease in CD66b, CD11b and CD16 expression in clusters 1, 2, 3, 4 and 7 compared to neutrophils isolated from health donors (HD), suggest the presence of neutrophils at various levels of maturity (Figure 4.2C). Furthermore, cluster 2 neutrophils showed a non-activated and modulatory neutrophil phenotype ($CD15^{high}CD33^{high}$ and $CD64^{-}$), while cluster 3 cells represented an activated population ($CD15^{low}CD33^{low}CD64^{+}$) (Figure 4.2C). Elevated CD64 biomarker expression on neutrophil[107]. and monocyte[108] correlated with inflammation, infectious diseases, and tissue damage in sepsis patients. Compared to neutrophils in Sepsis WB, the presence of MSCs (Sepsis/MSC WB) enriched cluster 2 modulatory neutrophils and reduced cluster 3 inflammatory neutrophils (Figure 4.2D). Neutrophil clusters 1, 4 and 7 did not show significant alterations after MSCs co-culture (Figure S4.2D).

Monocytes from sepsis whole blood were identified as cluster 5 (CD11b+CD14+) (Figure 4.2A and S4.2C). Cluster 5 percentage was not altered by co-culture with MSCs (Figure 4.2E). However, MSCs shifted the population towards M2-like phenotypes (higher CD206 and lower CD64 expression) and a less immunotolerant phenotype (higher HLA-DR and CD86, and lower PD-L1 expression) (Figure 4.2F, Sepsis vc Sepsis/WB), consistent with what we observed in the experiments with CLP-induced septic animals receiving MSCs (Figure 4.1E).

We next investigated how these phenotypic changes in neutrophils and monocytes translated to biological functions. Neutrophils (CD66b+ cells) from sepsis patients showed impairment in ROS-production and phagocytic capacities, compared to neutrophils from healthy donors (HD) (grey: range measured from HD, Figure 4.2G). Co-culture with MSCs significantly rescued these functions in sepsis neutrophils closer to healthy levels (Figure 4.2G). Similarly, co-culture with MSCs improved the phagocytic activity of CD14+ monocytes, which was markedly reduced in Sepsis (Figure 4.2H).

Finally, we measured neutrophil functional biomarkers (myeloperoxidase [MPO], neutrophil elastase [NE], cell-free DNA [cfDNA]; Figure S4.2E) from the archived patient plasma samples collected from a phase 1 clinical trial that administered allogeneic MSCs intravenously to septic shock patients (NCT02421484)[109]. Acknowledging the small patient cohort for phase I trial, a time course analysis was conducted for exploration. In the dose-stratified principal component analysis (PCA) analysis, we observed recovery of neutrophil functions in both observational (patients who did not receive MSCs) and interventional cohorts (patients who received 0.3 million MSCs/kg or 1 million MSCs/kg), as evidence by the convergency of all groups towards neutrophil biomarker profile in HD. As time course trajectory presented in Figure 4.2I, neutrophil functions in MSC-treated group, particularly in patients treated with 1 million MSCs/kg, progressively moved away from the study baseline (at time of enrollment, of which patients had not received MSCs in interventional groups) and closer (than non-treated patients in observational cohort) towards functions seen in healthy volunteer (Figure 4.2I).

These data suggested that MSCs in a septic environment conferred immunomodulatory activities on neutrophils and monocytes by phenotypic modulation and effective functional enhancement, consistent with our findings in an *in vivo* CLP animal model with MSC treatment.

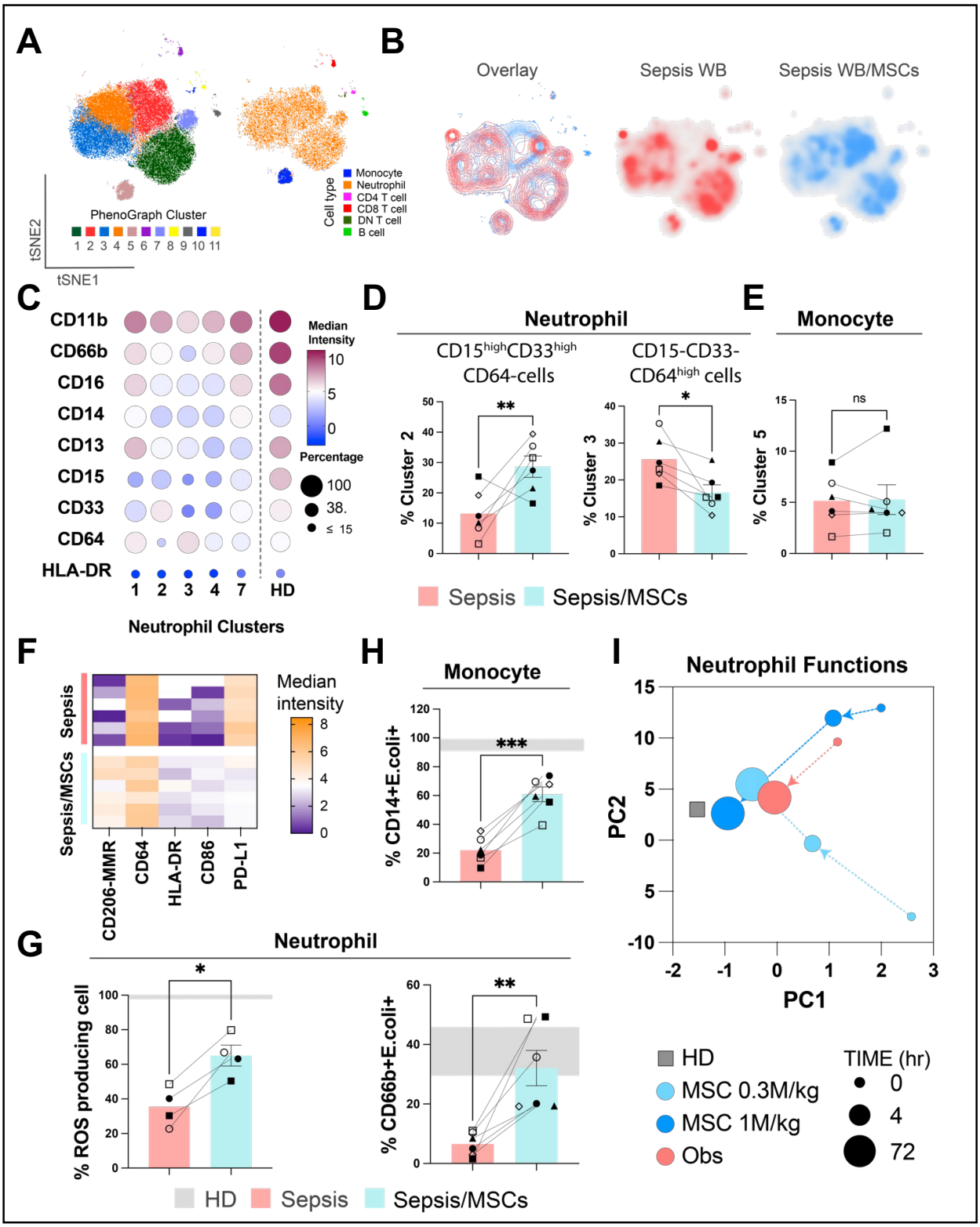
A
PhenoGraph Cluster
1 2 3 4 5 6 7 8 9 10 11
tSNE2
tSNE1
Cell type
Monocyte
Neutrophil
CD4 T cell
CD8 T cell
DN T cell
B cell
B
Overlay
Sepsis WB
Sepsis WB/MSCs
C
CD11b
CD66b
CD16
CD14
CD13
CD15
CD33
CD64
HLA-DR
1 2 3 4 7 HD
Median Intensity
10
5
0
Percentage
100
38.
≤ 15
D
Neutrophil
CD15highCD33high CD64-cells
CD15-CD33- CD64high cells
% Cluster 2
% Cluster 3
**
*
E
Monocyte
% Cluster 5
ns
Sepsis
Sepsis/MSCs
F
Neutrophil Clusters
Sepsis
Sepsis/MSCs
CD206-MMR
CD64
HLA-DR
CD86
PD-L1
Median intensity
8
6
4
2
0
H
Monocyte
% CD14+E.coli+
***
I
Neutrophil Functions
PC2
PC1
HD
MSC 0.3M/kg
MSC 1M/kg
Obs
TIME (hr)
0
4
72
G
Neutrophil
% ROS producing cell
% CD66b+E.coli+
*
**
HD
Sepsis
Sepsis/MSCs

Figure 4.2 MSCs Modulate Dysfunctional neutrophils and monocytes in Sepsis Patient Whole Blood

A. After co-culturing with MSCs, density analysis of t-SNE maps demonstrated distinct phenotypic shift of whole blood immune cell clusters of sepsis patient samples Immune cell subsets were identified from CyTOF data by unsupervised clustering with the PhenoGraph algorithm. Each dot represents one cell (100,000 cells total). The t-SNE plot overlayed with PhenoGraph clusters and lineage markers was shown.
B. Density analysis to visualize population depletion and enrichment between sepsis and sepsis/MSC.
C. Dot plot showed median fluorescent level of neutrophil related markers in clusters 1, 2, 3, 4, and 7; with the size of dot representing percentage of positive cells (size scale shown either as ≤0.25, 5, or 100%). Color of dot representing median intensity of corresponding markers (color scale shown as log expression).
D. Quantification of number of neutrophils expressing markers specified in (C) with selected clusters of myeloid cells (cluster 2 and 3).
E. Quantification of number of monocytes cluster (cluster 5).
F. Heatmap of marker showing CD206-MMR, CD86, CD64, HLA-DR and PD-L1 expression levels of CD14+ monocytes in Cluster 6 of Fig. 5B from mass cytometry data (fluorescent intensity scale shown on the right).
G. Flow cytometry analysis of ROS production (DHR123) and pHrodo *E.coli* phagocytosis by neutrophils, showing improved functions after MSC co-culture.
H. Flow cytometry analysis showed the improved phagocytosis capacity of CD14+ monocyte and CD66b+ neutrophils after MSC co-culture (compared to non-MSC treated).
I. Principal component analysis (PCA) plot on the time course trajectory of healthy donors vs. sepsis patient cohorts, stratified by cell dose received (MSC 0.3M/kg or MSC 1M/kg; or not received for observational cohort [Obs]). Data represent median value of each group of subjects (by treatment and time after normalization to corresponding 0hr baseline). For healthy donor (HD), blood samples were collected at 0hr timepoint to the represent baseline level.

For A-H, n=3 healthy donor (HD), n=6 sepsis patients per group, with each patient represented by different symbol with the data shown as bar graph as mean ± SEM. For I, n=3 healthy donors, n=8 Observational group, n=3 MSC 0.3M/kg, n=3 MSC 1.0M/kg Grey shaded area represents range [min-max] from measured from HD), $*p<0.05$, $**p<0.01$, $***p<0.005$. Comparison done by unpaired two tailed nonparametric tests. For I, n=3 for HD and MSC group and n=5 for observational group. ROS, reactive oxygen species.

4.3.3 Retrieved MSCs from Sepsis Patient Whole Blood Co-culture Display Upregulated Caspase-1 Pathway with Enhanced Myeloid-Related Immune Functionalities

We next aimed to delineate the molecular changes of MSCs in response to the host septic microenvironment and define the mechanisms underlying any changes in the capacities of MSCs to modulate myeloid phenotypes and functions. After co-culture with whole blood from human healthy donors (HD-MSCs) or sepsis patients (Sepsis-MSCs), MSCs were retrieved by cell sorting using negative expression of CD45 and positivity of CD90. MSCs that had not been cultured with whole blood but had undergone a sorting process were used as baseline control (Ctrl-MSCs). Cells demonstrated high viabilities immediately post sorting and normal MSC morphology after 24-hour culture (Figure S4.3A and B). Changes in MSC transcriptomic profiles in response to exposure to the sepsis microenvironment were assessed using a focused PCR immune-response array (Figure S4.3C). Using unsupervised multivariate analysis, PCA revealed that while transcripts from HD-MSCs and Ctrl-MSCs clustered closely together, there was a clear sepadration in immune-related gene expression profile between Sepsis-MSCs and HD-MSCs (or Ctrl-MSCs) (Figure 4.3A). Significantly upregulated genes (fold change greater than 2 compared to Ctrl-MSCs, FDR<0.05) for Sepsis-MSCs or HD-MSCs were plotted on a snail plot in Figure 4.3B. Amongst these, we identified the upregulation of multiple upstream and downstream targets in the caspase pathway, including *CASP1*, *NLRP3*, *NFKB1*, and *IL1B* as well as genes of myeloid regulatory cytokines (*CSF2, CXCL8, CXCL10* and *IL6*) (Figure 4.3B). Two genes, *CD4 and IFNA1*, were found to be downregulated in HD-MSCs, which further reduced in Sepsis-MSCs (compared to Ctrl-MSCs, Figure S4.3D). Retrieved MSCs were also plated

down on cell culture plates to collect conditioned media for cytokine analysis. We observed increased production of a wide range of cytokines (heatmap of Figure 4.3C). Of particular, cytokines upregulated transcriptomic expression shown in Figure 3B, including IL-8 (CXCL8), G-CSF, GM-CSF, IL-1β, IL-6, and IP-10 (CXCL10), were confirmed with significantly increased secretion in retrieved Sepsis-MSCs (compared to HD-MSCs or Ctrl-MSCs), while secretion of FGF and VEGF were unaltered (Figure 4.3C, and Figure S4.3E). To further investigate the functional properties of MSCs after encountering a sepsis environment, we tested the ability of the retrieved MSCs to enhance bacterial phagocytosis of CD14+ monocytes after lipopolysaccharide (LPS) injury (Figure S4.3F). Whereas LPS injury caused marked reduced phagocytic capacity of CD14+ monocytes, MSCs pre-exposed to sepsis microenvironment (patient blood) showed significantly superior ability to rescue monocyte phagocytosis, compared to MSCs pre-exposed to healthy donor blood (HD-MSCs, Figure 4.3D). Altogether, we confirmed that MSCs after exposure to whole blood from sepsis patients led to the activation of immune response-related genes, including caspase-1 pathway, increased secretion of myeloid-related cytokines, and augmented functional attributes of MSCs to rescue monocyte functions after LPS injury.

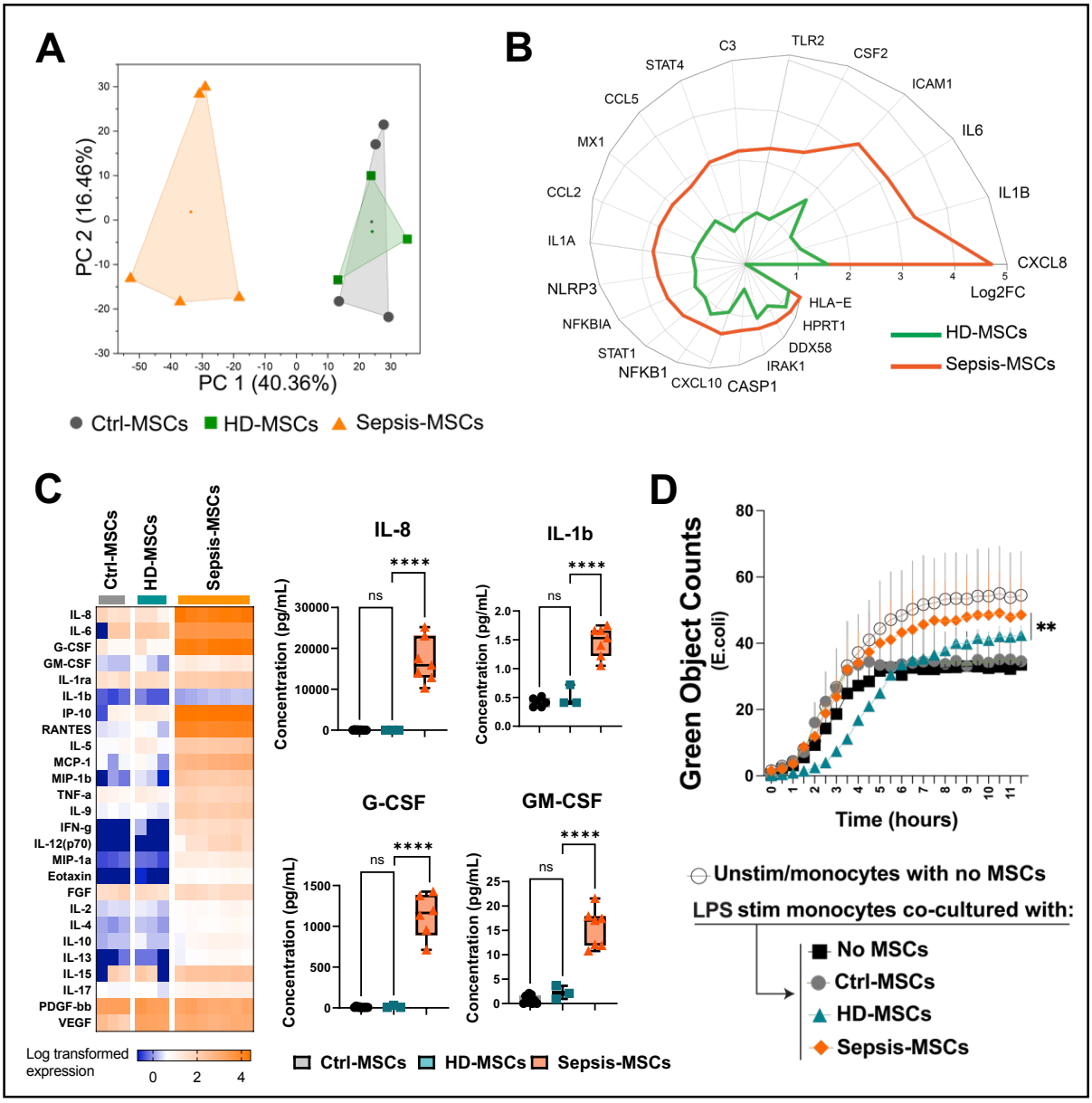
A
PC 2 (16.46%)
PC 1 (40.36%)
Ctrl-MSCs
HD-MSCs
Sepsis-MSCs
B
C3
TLR2
CSF2
ICAM1
IL6
IL1B
CXCL8
Log2FC
HLA-E
HPRT1
DDX58
IRAK1
CASP1
CXCL10
NFKB1
STAT1
NFKBIA
NLRP3
IL1A
CCL2
MX1
CCL5
STAT4
HD-MSCs
Sepsis-MSCs
C
Ctrl-MSCs
HD-MSCs
Sepsis-MSCs
IL-8
IL-6
G-CSF
GM-CSF
IL-1ra
IL-1b
IP-10
RANTES
IL-5
MCP-1
MIP-1b
TNF-a
IL-9
IFN-g
IL-12(p70)
MIP-1a
Eotaxin
FGF
IL-2
IL-4
IL-10
IL-13
IL-15
IL-17
PDGF-bb
VEGF
Log transformed expression
IL-8
IL-1b
G-CSF
GM-CSF
Concentration (pg/mL)
ns
****
D
Green Object Counts (E.coli)
Time (hours)
**
Unstim/monocytes with no MSCs
LPS stim monocytes co-cultured with:
No MSCs
Ctrl-MSCs
HD-MSCs
Sepsis-MSCs

Figure 4.3 MSCs Retrieved after Coculture with Human Sepsis Whole Blood Displayed Upregulated Caspase-1 Pathway and Enhanced Ability to Modulate Monocyte Functions.

A. PCA plot with convex hull on the data from innate and adaptive immune responses PCR array, conducted on the MSCs retrieved from co-culture with control (Ctrl-), healthy donor (HD-) and Sepsis-whole blood.
B. Snail plots showed top significantly altered genes comparing HD- or Sepsis-MSCs over Ctrl-MSCs, with threshold of fold change (FC) > 2 and $p<0.05$.
C. Cytokine analysis of Ctrl-, HD- and Sepsis-MSCs that showed increase secretion by Sepsis-MSCs.
D. *In vitro* phagocytosis assay was used to evaluate the potency of the retrieved MSCs, with Sepsis-MSCs exhibited the most enhanced ability to rescue monocyte phagocytosis.

N=4 experiments, Ctrl-MSCs=MSCs without whole blood co-culture but undergone FACS sorting. N=3 healthy donor, HD-MSCs = MSCs sorted after co-cultured with healthy volunteer whole blood. N=5 sepsis patients, Sepsis-MSCs=MSCs sorted after co-cultured with sepsis whole blood. (C-D) the data shown as mean ± SEM. $*p<0.05$, $**p<0.01$, $***p<0.005$, $****p<0.001$. Comparison done by one way ANOVA with Dunnett's comparison.

4.3.4 Sepsis-Environment Stimuli Mimic Enhances Modulatory Effects of MSCs

In light of recent studies demonstrating that caspase-3-mediated apoptosis may play a role in MSC-mediated immunosuppression[110,111], it was notable to us that retrieved Sepsis-MSCs exhibited significantly increased expression within caspase-1 pathway, including CASP1, NLRP3, NFKB1, and IL1B, without affecting cell viability (Figure 4.3B and S4.3A). We next examined whether the specific caspase-1 activation in MSCs could enhance the therapeutic activity of MSCs. However, the traditional caspase-1 activation (LPS plus nigericin) resulted in significant cell death (Figure S4.4A), which does not reproduce the high viability of MSCs retrieved from incubation with sepsis patient blood (Figure S4.3A). We then stimulated MSCs using a combination of three cytokines (IFN-γ, TNF-α, and IL-1β) in physiologically relevant dose[112,113] to recapitulate the sepsis environment (Cytomix-MSCs). Cytomix-MSCs, derived from 3 different donors, showed consistent transcriptomic profile (via RNA sequencing) that was consistent with that of retrieved Sepsis-MSCs, with upregulation of genes in the caspase-1 pathway, including *CASP1, NLRP3, NFKB1*, and *IL1B* and myeloid regulatory cytokines (*CSF2, CXCL8, CXCL10,* and *IL6*) (Figure S4.4B). We further confirmed a marked increase in caspase-1, nlrp3, and gasdermin D protein expressions after MSCs were exposed to cytomix (Figure 4.4A and S4.4C). This was further associated with increased secretion of IL-8 (CXCL8), G-CSF, IL-1b and G-CSF by multiplex analysis (Figure 4.4B) at 24h after cytomix treatment compared to unstimulated cells (Unstim-MSCs). The activation of caspase-1 in MSCs under a sepsis environment was further confirmed using caspase-1 FAM-FLICA (labeled the cleaved and active enzyme in living cells), which showed significant increases in FLICA+ cells (Figure 4.4C). It is of note

that the cytomix stimulation employed here specifically activated caspase-1 but not caspase-3 in MSCs (Figure S4.4D), while maintaining high viability (Figure S4.4E).

We further evaluated the effects of cytomix on MSC immunomodulatory activity by first employing co-culture of MSCs and purified monocyte in culture media. We confirmed that Cytomix-MSCs exhibited enhanced potency to rescue LPS-induced phagocytic impairment in monocytes (Figure S4.4F), similar to functional improvement from retrieved MSCs after sepsis patient blood co-culture (Figure 4.3D). Having established that activation of caspase-1 pathway was achieved by cytomix stimulation (Cytomix-MSCs), these cells (or Unstim-MSCs as control) were then co-cultured with LPS-stimulated whole blood (from a healthy donor) to create a controlled and reproducible sepsis environment further. We followed up with CyTOF analysis to profile the global population changes of neutrophils and monocytes. Following a similar analytic workflow for septic blood samples, a tSNE analysis was first conducted, followed by Phenograph clustering algorithm (Figure S4.5A). Neutrophils (CD66+) formed the four large clusters (1, 2, 3 and 4) (Figure 4.4D and S4.5A and B). Notably, density analysis of tSNE map showed distinct shifts (shown by density intensity) in neutrophil clusters amongst LPS-stimulated WB, and ones co-cultured with Unstim-MSCs or Cytomix-MSCs (Figure 4.4D). Neutrophil-related markers revealed that cluster 2 exhibited elevated expression of CD14 and CD64 (heatmap in Figure S4.5C), which represents an activated and inflammatory phenotype. By quantifying the shifts of clusters between LPS-stimulated WB co-cultured with Unstim-MSCs vs. Cytomix-MSCs, Cytomix-MSCs demonstrated a greater ability to suppress neutrophils activation as evidenced by less of cluster 2 (activated profile) and the enriched cluster 4 (resting state,

with higher CD33 expression) neutrophils (Figure 4.4E, right panel). There were no significant alterations of clusters 1 and 3 when co-cultured with Cytomix-MSCs compared to the unstimulated MSCs group (Figure S4.5D).

To further test whether the activation of caspase-1 pathway in MSCs could be harnessed for a better therapeutic effect, Cytomix-MSCs were administered into the CLP-induced septic mice. Cytomix-MSCs treatment resulted in a significantly improved 5-day survival in septic mice by 42% ($p<0.05$ vs. CLP/Vehicle), which was higher than using non-Cytomix treated-MSCs alone (21% improvement in survival vs. CLP/vehicle). We also harvested whole blood and phenotyped neutrophil and monocyte cellular responses in these animals. In accordance with our previous finding (Figure 4.1), circulating neutrophil was higher in both Unstim-MSCs and Cytomix-MSCs treated septic compared to the CLP/vehicle group (Figure 4.4G). However, interestingly, mild elevated CXCR2 expression (vs CLP/Vehicle) was observed in neutrophils of the Unstim-MSCs treated group, but it was further significantly increased in animals of Cytomix-MSC treatment to the level similar to sham (Figure 4.4H). Being a key regulator in neutrophil release and migration, CXCR2 were reported to be downregulated by 50% on neutrophils from septic patients compared with normal donors, impairing neutrophil mobilization[114-116]. Our data suggested that MSCs with activated caspase-1 by Cytomix-priming could more greatly restore neutrophil mobilizing capacity in sepsis for more extended host benefits. CD86 expression, a co-stimulatory molecule for antigen presentation, on neutrophils was unaltered amongst treatment groups. Furthermore, Unstim-MSCs and Cytomix-MSCs elevated monocyte percentage at a similar

extent in WB (Figure 4.4I). As observed previously (Figure 4.1), Unstim-MSCs induced changes in monocytic profiles (increase of CD206 and I-A/I-E [MHC-II] and decrease of CD64); however, they were further potentiated with Cytomix-MSC treatment ($p<0.05$, vs. CLP/vehicle, Figure 4.4J). All in all, these data show that activation of caspase-1 by sepsis-like stimuli in MSCs led to the improvement in septic mice survival and enhanced the ability of MSCs to modulate neutrophil and monocyte phenotypes and functions.

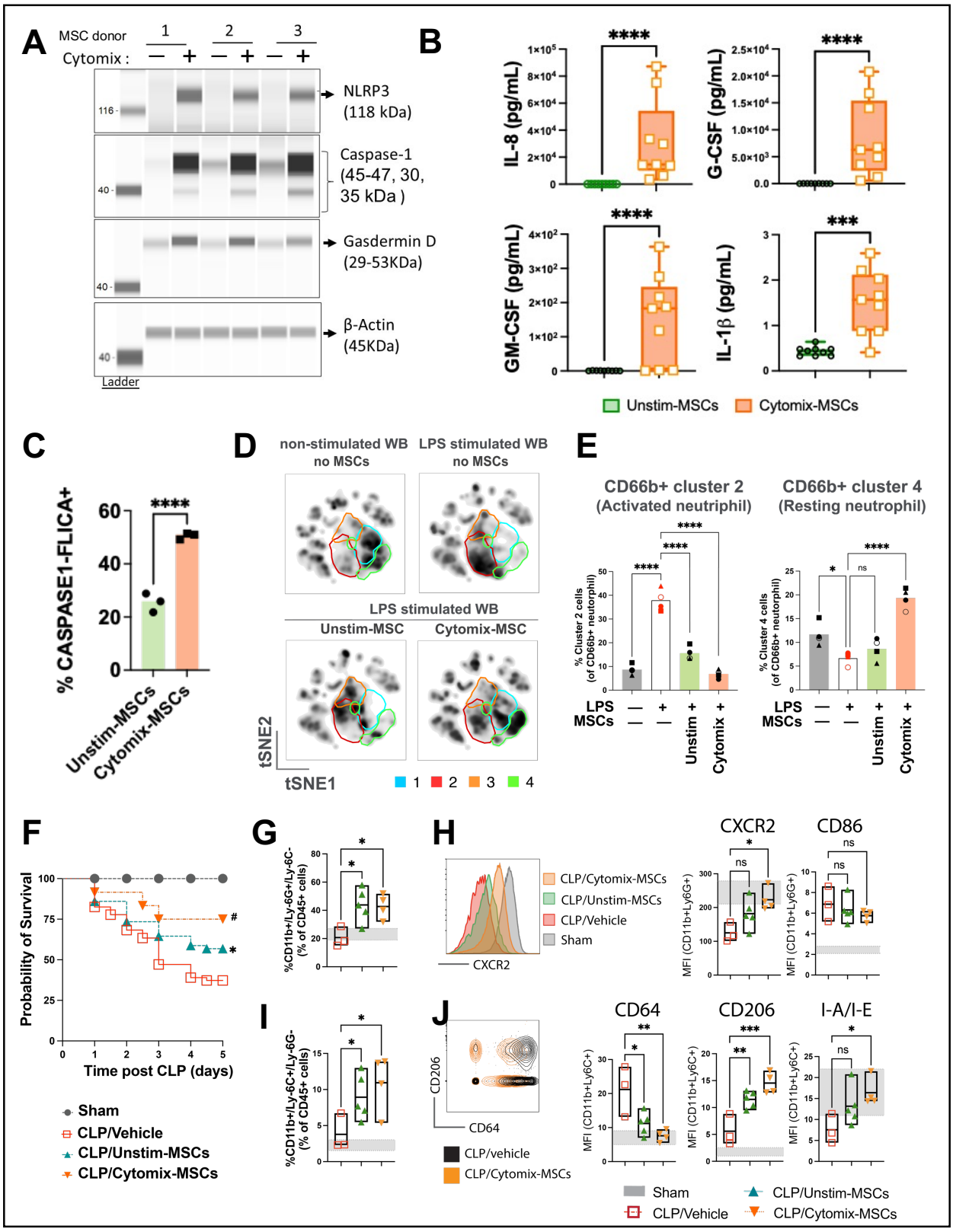
A
MSC donor
1
2
3
Cytomix :
— + — + — +
116 -
40 -
40 -
40 -
Ladder
NLRP3
(118 kDa)
Caspase-1
(45-47, 30,
35 kDa)
Gasdermin D
(29-53KDa)
β-Actin
(45KDa)
B
IL-8 (pg/mL)
G-CSF (pg/mL)
GM-CSF (pg/mL)
IL-1β (pg/mL)
****
***
Unstim-MSCs
Cytomix-MSCs
C
% CASPASE1-FLICA+
Unstim-MSCs
Cytomix-MSCs
D
non-stimulated WB
no MSCs
LPS stimulated WB
no MSCs
LPS stimulated WB
Unstim-MSC
Cytomix-MSC
tSNE2
tSNE1
1 2 3 4
E
CD66b+ cluster 2
(Activated neutriphil)
CD66b+ cluster 4
(Resting neutrophil)
% Cluster 2 cells
(of CD66b+ neutorphil)
% Cluster 4 cells
(of CD66b+ neutorphil)
LPS
MSCs
Unstim
Cytomix
F
Probability of Survival
Time post CLP (days)
Sham
CLP/Vehicle
CLP/Unstim-MSCs
CLP/Cytomix-MSCs
G
%CD11b+/Ly-6G+/Ly-6C-
(% of CD45+ cells)
H
CLP/Cytomix-MSCs
CLP/Unstim-MSCs
CLP/Vehicle
Sham
CXCR2
CXCR2
CD86
MFI (CD11b+Ly6G+)
I
%CD11b+/Ly-6C+/Ly-6G-
(% of CD45+ cells)
J
CD206
CD64
CLP/vehicle
CLP/Cytomix-MSCs
CD64
CD206
I-A/I-E
MFI (CD11b+Ly6C+)
Sham
CLP/Vehicle
CLP/Unstim-MSCs
CLP/Cytomix-MSCs

Figure 4.4 MSCs Trained with Sepsis-Like Mimics (Cytomix) Exhibited Activated Molecular Profile for Enhanced Myeloid Modulation.

A. Western blot analysis revealed the increase protein expression of NLRP3, caspase-1 and Gasdermin D in MSCs following sepsis-like mimic stimulation.
B. Cytokine analysis of unstimulated (Unstim-) and cytomix-stimulated (Cytomix)-MSCs revealed increased IL-8, G-CSF, GM-CSF and IL-1b secretion from Cytomix-MSCs.
C. Quantification of FLICA analysis showing the activation of caspase-1 in Cytomix-MSCs compared to Ctrl-MSCs
D. Density analysis of t-SNE maps demonstrated distinct phenotypic shift of neutrophil clusters after co-culturing of Ctrl- or Cytomix-MSCs with LPS-stimulated healthy whole blood (WB), compared to WB without MSCs co-culture.
E. Quantification of cluster 2 (marked in red in D) and 4 (marked in green in D) neutrophil clusters from D.
F. 5-day survival curve of CLP sepsis mice after vehicle-, Unstim-, or Cytomix-MSCs treatment.
G. Quantification of neutrophil (CD11bLy6G+Ly6C-) percentage of total CD45+ leukocytes.
H. Representative flow plot and quantification of CXCR2 and CD86 expression (Mean fluorescent intensity) of the neutrophils.
I. Quantification of monocyte (CD11bLy6G-Ly6C+) percentage of total CD45+ leukocytes.
J. Representative flow plot and quantification of CD64, CD206 and I-A/I-E expression (Mean fluorescent intensity) of the monocytes.

For A-C, n=3 experiments. For D and E, n=3 healthy donors. The data is shown as bar plot as mean ± SEM, with each symbol represents one MSC donor. Multiple comparison was done by one way ANOVA with Dunnett's comparison. For F, Sham=16, CLP/Vehicle=54, CLP/Unstim-MSCs=48, CLP/Cytomix-MSCs =12 with Log-rank test *, $p<0.05$ comparing CLP/Unstim-MSCs vs CLP/Vehicle, #, $p<0.05$ comparing CLP/Cytomix-MSCs vs CLP/Vehicle. For G-J, n=3 CLP/vehicle, n=5 CLP/Ctrl-MSCs, n=4 CLP/Cytomix-MSCs. $*p<0.05$, $**p<0.01$, $***p<0.005$, $****p<0.001$. Multiple comparison done by one way ANOVA with Dunnett's comparison. CLP, cecal ligation and puncture.

4.3.5 *Knockdown of Caspase-1 in MSCs Led to the Loss of Ability to Modulate Myeloid Cells in Sepsis*

Finally, to confirm that caspase-1 pathway is essential for MSCs to facilitate myeloid modulation in sepsis, we used a caspase-1 specific inhibitor and siRNA knockdown of caspase-1 ($MSCs^{CASP1\ KD}$) and confirmed the level of knockdown. Both caspase-1 specific inhibitor YVAD treatment and siRNA knock down approaches led to the inhibition of caspase-1 activity in Cytomix-MSCs, as shown by the reduction of FLICA-positive cells (Figure S4.6A). Silencing of caspase-1, via siRNA, resulted in the selective attenuation of Cytomix-induced IL-1β and IL-8 secretions by MSCs (Figure S4.6B) and abrogated the enhanced ability of Cytomix-MSCs to restore of phagocytic functions of LPS-injured monocytes ($MSCs^{CASP1\ KD}$ vs scramble control [MSC^{SC}] group, $p<0.05$) (Figure S4.6C). Cytokines, such as IL-6 and IP-10, were not impacted by caspase-1 knockdown (Figure S4.6B).

Next, we tested $MSCs^{CASP1\ KD}$ in an *ex vivo* co-culture system using WB from human sepsis patients, followed by CyTOF single-cell analysis of protein expression. UMAP and flowSOM (Self-Organizing Maps) algorithms were used to generate cell clusters and examine the cluster shifts among conditions. Myeloid populations were identified using lineage markers over the total leukocyte population, identifying 17 cell lineages (Figure S4.6D and E). We further highlighted the 4 central cell populations with the signal strength of key phenotypic markers defining cellular lineages merged on UMAP with a color scale (Figure S4.6F). Within myeloid cells, sepsis WB co-cultured with scramble control transfected MSCs ($MSCs^{SC}$)

consistently induced phenotypic changes in the myeloid population when compared to Sepsis WB alone, which was markedly blunted by caspase-1 siRNA knockdown (Figure 4.5A).

Consistent with Figure 2, MSCs^{SC} were able to reduce the proportion of activated neutrophils (clusters 6 and 15, high CD64 and CD14 expression) and enrich modulatory neutrophil (clusters 12, 16 and 17, elevated CD33 and CD15, surface marked expression levels of neutrophil clusters shown in Figure 4.5B). These modulatory effects were largely abolished by caspase-1 knockdown (vs. MSCs^{SC}, Figure 4.5C and S4.6G). Importantly, the loss of caspase-1 expression further diminished the capacity of MSCs to enhance neutrophil phagocytic ability (Sepsis/MSCs^{SC} vs. Sepsis/MSCs$^{CASP1\ KD}$, Figure 4.5D). For monocytes (clusters 1 and 2), deficiency in caspase-1 (MSC$^{CASP1\ KD}$) abrogated the ability of MSCs to increase cluster 1 (M2-like modulatory with higher expression of CD206 and high HLA-DR) and to decrease immune tolerant cluster 2 (low CD206 and HLA-DR expression; Figure 4.5E). Similarly, MSC$^{CASP1\ KD}$ showed a diminished ability to rescue monocytic phagocytosis (vs MSCs^{SC}, Figure 4.5F). These results confirmed that caspase-1 plays a critical role in the myeloid modulatory activity of MSCs in a sepsis environment.

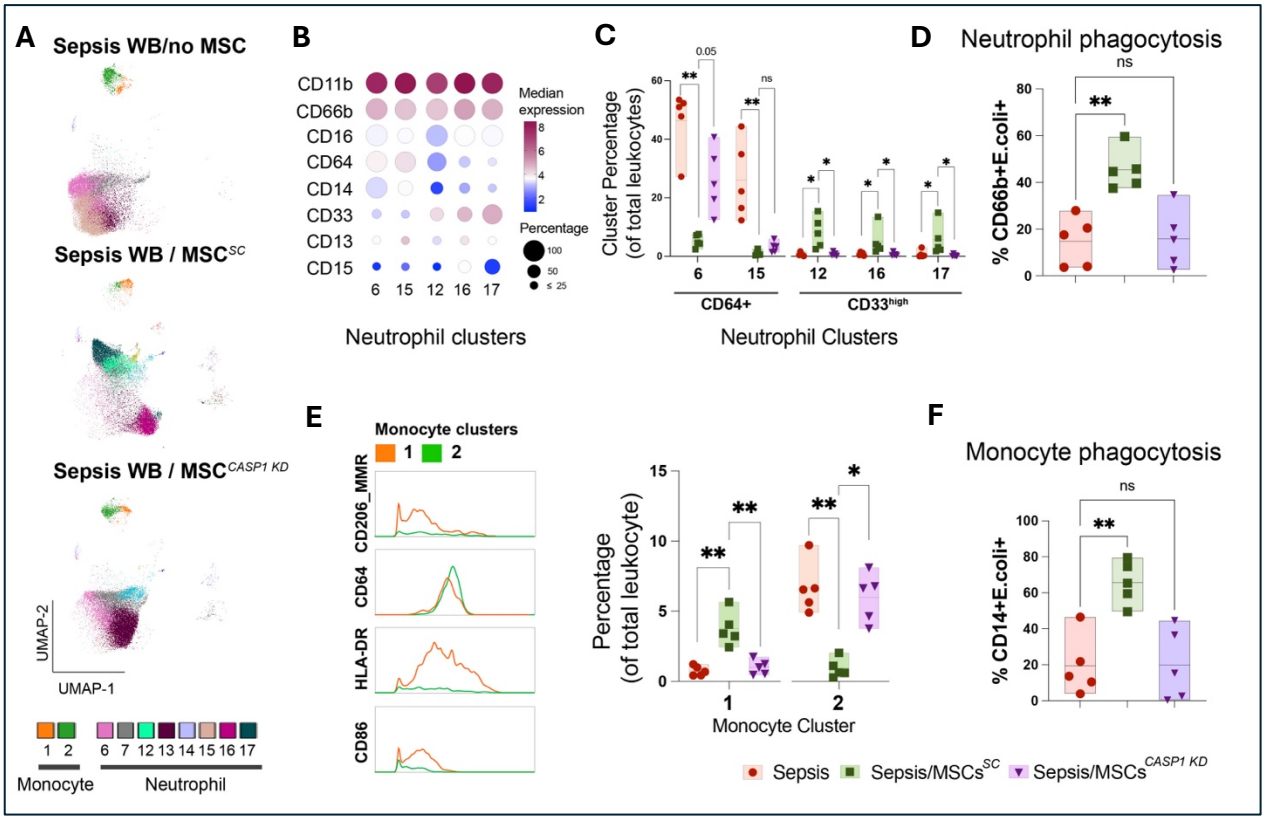
A
Sepsis WB/no MSC
Sepsis WB / MSC^SC
Sepsis WB / MSC^CASP1 KD
UMAP-2
UMAP-1
1 2
6 7 12 13 14 15 16 17
Monocyte
Neutrophil
B
CD11b
CD66b
CD16
CD64
CD14
CD33
CD13
CD15
6 15 12 16 17
Median expression
Percentage
Neutrophil clusters
C
Cluster Percentage (of total leukocytes)
0.05
ns
CD64+
CD33high
6 15 12 16 17
Neutrophil Clusters
D
Neutrophil phagocytosis
% CD66b+E.coli+
ns
E
Monocyte clusters
1 2
CD206_MMR
CD64
HLA-DR
CD86
Percentage (of total leukocyte)
Monocyte Cluster
F
Monocyte phagocytosis
% CD14+E.coli+
ns
Sepsis
Sepsis/MSCs^SC
Sepsis/MSCs^CASP1 KD

Figure 4.5 Knockdown of Caspase-1 Pathway in MSCs Abrogates Cell's Abilities to Modulate Neutrophils and Monocyte in Human Sepsis.

A. UMAP of CD11b+ myeloid cell subsets were identified from CyTOF data by unsupervised clustering overlaid with flowSOM clustering algorithm. Each dot represents one cell (100,000 cells total).
B. Heatmap of neutrophil relevant markers on significantly altered neutrophil clusters.
C. Quantification of significantly altered neutrophil clusters.
D. Assessment of phagocytosis abilities of neutrophils.
E. Representative plot and quantification of monocyte clusters.
F. Assessment of phagocytosis abilities of monocytes.

n=5 septic patients' whole blood (WB), graphed as bar plot in mean ± SEM, each symbol represents one blood donor, $*p<0.05$, $**p<0.01$. Multiple comparison done by one way ANOVA with Dunnett's comparison. $MSCs^{SC}$, MSCs with scramble control RNA. $MSCs^{CASP1KD}$, MSCs with siRNA specifically targeting *CASP1*.

4.4 Discussion

Sepsis is a multifaceted disease involving a complex regulation of the immune system. The current study explored the role of the sepsis microenvironment in the adaptive reprogramming of MSCs to enhance their ability to modulate host immune cells. Using clinically relevant human sepsis patient samples and a polymicrobial sepsis animal model, we demonstrated that MSCs rebalanced the innate immune cell landscape during sepsis by dampening activation of phenotype on myeloid population (neutrophils and monocytes) and improving pathogen clearance capacity of innate immune cells. Additionally, this study provided the first evidence that MSCs in a sepsis environment can adopt a uniquely altered transcriptome by a mechanism involving the upregulation of caspase-1 pathway and secretion of cytokines tailored towards modulating myeloid population. The novel role of caspase-1 activation in MSCs is essential for the induction of MSCs-mediated modulations of neutrophil and monocyte phenotypes and functions was further implicated by selective inhibition of this pathway. We now provide important mechanistic insights into adaptive reprogramming of MSCs by the sepsis milieu mediated by caspase-1 activation, that could be used to enhance the therapeutic benefit of this cell product for the treatment of sepsis and other acute inflammatory disorders

Neutrophils and monocytes are key players in the pathogenesis and resolution of sepsis. Elucidation of the functional status of neutrophils in patients with sepsis has been hampered by conflicting data[93]. For instance, while some studies reported that the release of ROS and pro-inflammatory cytokines by neutrophils contribute to organ damage and subsequent multiple organ dysfunction[93,117], others suggested that oxidant activity and phagocytosis capacity of neutrophils were impaired during sepsis[118,119], potentially leading

to reduced pathogen killing and clearance. Given the inherent challenges in the isolation and culture of neutrophils from patients, there has been only a limited number of studies that thoroughly evaluated potential changes in neutrophil phenotype and functional behavior in sepsis patients. Not only is the study of neutrophils difficult due to their short half-life in circulation and after isolation, but also little is known on whether and how MSCs, when infused to patients, can modulate dysfunctional neutrophils in sepsis. To date, existing research has used *in vitro* assay system of co-culturing MSCs with purified neutrophils, which provided some evidence that under *in vitro* experimental conditions, MSCs could preserve neutrophil viability[120] while reducing respiratory burst[121,122], nitric oxide production[120] and elastase activity[123]. We utilized both a clinically relevant sepsis animal and a human *ex vivo* whole blood model to delineate how MSCs shift phenotypes and restore functions of neutrophils in sepsis under physiological setting. Both models allow us to capture the reciprocal responses of MSCs activated by host environment on neutrophils. Our data showed MSCs shifted activation states of neutrophils towards a modulatory profile and significantly rescued defective cellular functions (improved ROS production and phagocytosis). Furthermore, clinical studies have shown that the level of neutrophil-derived circulating cfDNA and MPO-DNA complex levels directly correlated with severity of organ dysfunction and 28-day mortality rates[124,125]. Having measured in the current study, serial plasma samples archived from septic shock patients who had been treated with MSCs reflected better longitudinal neutrophil functional responses, showing trends in reducing MPO, NE and cfDNA levels over time, potentially implying better neutrophil functional recovery in these patients.

While circulating monocytes are believed to be the source of immediate cytokine release in sepsis at the initial early response to infection, an altered monocyte response is regularly reported in sepsis patients[126,127]. This includes downregulation of major histocompatibility (MHC) class II and CD86 as well as failure to secrete cytokines by monocytes[128]. Several *in vitro* and animal studies have shown that MSCs can promote the polarization of monocytes toward an anti-inflammatory/immune-regulatory (type 2 or M2) phenotype[23,129]. In the current study, we further demonstrated that even when being placed within sepsis environment, MSCs enhanced their ability to drive monocyte towards type 2 polarization. More importantly, we reported here that after co-culture with MSCs, monocytes from sepsis patients exhibited better antigen-presenting capacity (increased HLA-DR and CD86 expression) and strengthened antimicrobial functions (phagocytosis). Taken together with our findings from animal models and with human samples, we demonstrated that MSCs can facilitate pleotropic modulation of multiple immune cell populations in a global setting, towards improving immune resolution in sepsis.

How MSCs react to changing host environmental cues with distinct adaptive responses is currently under active investigation. A recent study has shown that, during localized injection at the wound site, MSCs could sense low environmental TGF-β1 levels, with a compensatory release TGF-β1 to enhance wound healing process[130]. In another study, Liotta and colleagues showed that functional TLR3 and TLR4, which respond to environmental pattern associated molecular patterns (PAMPs), were necessary for human

MSCs lost their abilities to suppress T cell proliferation[131]. To harness effects of environmental cues on MSCs, combinations of a variety of cytokines were proposed to pre-activate MSCs in order to improve their immunosuppressive properties[132]. However, many of these studies employed strategies either used a unphysiologically high concentrations of cytokines or just with IFN-□ alone (i.e.,10-200 ng/ml), which failed to represent the disease environment that MSCs would typically experience in sepsis patients.

In our human *ex vivo* model, we retrieved MSCs after incubation with physiologically relevant, human sepsis whole blood and discovered these retrieved MSCs displayed a unique activation profile, specifically activation of caspase-1. Caspase-1 is an enzyme primarily involved in the innate immune response and plays an important role in immune activation[133]. Unlike the apoptotic caspases that can be classified into initiators (e.g., caspase-2) and executioners (e.g., caspase-3), caspase-1 could act as both initiator and executioner, thus contributing to the immune response in a versatile manner[134]. While caspase-1 is commonly regarded as a potent pro-inflammatory regulator that directly cleaves GSDMD (pore formation), pro-IL-1b, and pro-IL-18, promoting pyroptotic cell death and cytokine secretion[135], caspase-1 also has been reported to exert a regulatory effect, such as the inhibition of NLRP3 functions in allergic airway inflammation model[136]. Studies of caspase-1 in sepsis revealed a complexed role and generated several controversies. First, Sarkar et al. showed caspase-1 knockout, but not IL-1 or IL-18, in animal was protective against *E.coli*-induced sepsis[137]. However, a work by Vandenabeele and co-workers showed caspase-1 alone did not confer protection in CLP-induced sepsis[138].

Further studies revealed downregulation of caspase-1 and defective IL-1β production in septic patients, and this represented an important immunological feature in sepsis[139].

Little has been reported on the role of caspase-1 pathway in regulating MSC functionalities, and none has reported caspase-1 involvement in MSC-mediated myeloid modulation. In osteoporosis, Wang and colleague reported that caspase-1 can be activated in MSCs, which led to the inhibition of osteogenic differentiation potential of MSCs[140]. Chen et al. demonstrated that endogenous bone-associated MSCs, from mice with Inflammatory bowel disease, secreted IL-1β/18 and underwent pyroptosis mediated by activation of NLRP3 inflammasome. However, they failed to activate caspase-1 and induce pyroptosis in adipose tissue-derived human MSCs via LPS with nigericin stimulation *in vitro*[141]. Ahn et al. demonstrated that NLPR3 activation in umbilical cord-derived MSCs suppressed osteoblast differentiation but improved immunosuppression on T cells *in vitro*[142]. Our current study revealed, for the first time, that under the influence of sepsis environment, caspase-1 is activated in MSCs, and this caspase-1 activation drives immunomodulatory functions of MSCs on dysregulated neutrophils and monocytes. It is also noteworthy to mention that the activation of caspase-1 in MSCs can take place in the absence of inducing cell death in MSCs. Our observation contrasts with the recent data that report caspase-3 induced MSC apoptosis plays a role in MSC-induced immunosuppression[110,111]. We demonstrated that sepsis environment drives MSCs into cytokine-predominant caspase-1 signaling, which allows MSCs to prolong cytokine production without going through cell death. While we report here for the first time in MSCs, this caspase-1 induced state

(increased cytokine secretion without cell death) was observed in immune cells[134]. We confirmed that this caspase-1 mediated activation of MSCs, induced by exposure to a sepsis-like conditional mimics, can indeed contribute to the cell's enhanced ability to modulate the neutrophil and monocyte immune responses. Assessment of cytokine secretion profile of MSCs suggested that caspase-1 activation is highly associated with a paracrine secretion profile of MSCs, and caspase-1 inhibition induced a secondary loss of functions (reduced IL-8 and IL1b secretion) of MSCs. All in all, we report here that caspase-1 activation is essential for MSCs-mediated myeloid modulation in sepsis. This is consistent with an essential role for caspase-1 activation in MSCs-mediated myeloid modulation and suggests novel opportunities to target this pathway to enhance the therapeutic potential of MSCs for the treatment of sepsis.

4.5 Limitation of Study

In the current study, we utilized bone marrow-derived MSCs to investigate how sepsis environment affects immunomodulation functions of MSCs. Varying molecular profiles have been reported among MSCs isolated from different tissue sources. As the majority of clinical trials source MSCs from bone marrow[3], knowledge from our current study still has broad implications for clinical translation and can be leveraged for future comparative analysis of effects of MSCs from different tissue sources for treating immune diseases. Furthermore, we acknowledge that due to the small sample size of interventional cohort of septic shock patients who received MSCs for the clinical trial, the robustness of statistical power is limited. Our study focused only on MSCs in the context of sepsis, therefore,

functionalities of MSCs in other immune disorders warrant further studies in a disease-specific manner.

4.6 Acknowledgments

The work was supported by Emergent Ventures, Thistledown Foundation (Fast Grant), The Ottawa Hospital Foundation COVID-19 Emergency Response Fund, and Ontario Institute of Regenerative Medicine (OIRM) Disease Team Grant. The authors gratefully acknowledge the support of Drs. Gareth Palidwor and Christopher Porter of Bioinformatics Core Facility of the University of Ottawa and the OHRI for the generation of count matrix and technical support; Dr. Damian Carragher, mass cytometry proteomic core of OHRI, for providing technical assistance in CyTOF data analysis; Rebecca Porteous of The Ottawa Hospital for supporting participant recruitment; Jose Champagne for her contribution for grant application.

4.7 Author Contributions

Y.T and L.S.M: Conceptualization, Data curation, Methodology, Investigation, Visualization, Formal analysis, and Writing – original draft; P.M, Y.W., and G.H.: Investigation, Methodology, and Validation; A.M, M.S, J.V and M.F: Resources; J.H. and I.W.: Resource - participants recruitment; L.M.: Clinical Supervision, and Writing – review & editing; D.J.S: Supervision, Funding acquisition, and Writing – review & editing; S.H.J.M: Conceptualization, Funding acquisition, Project administration, Supervision, Writing – review & editing.

4.8 Declaration of Interests

The funding institution had no role in the conception, design or conduct of the study, data collection or analysis, interpretation or presentation of the data, or preparation, review or approval of the manuscript. We also like to declare the following conflicts of interest: D.J.S. holds a patent for Cell-based therapy for the pulmonary system, and S.H.J.M. have received personal fees from Northern Therapeutics that are outside of this submitted work. The remaining authors have disclosed that they do not have any conflicts of interest.

4.9 Materials and Methods

Healthy Volunteer and Sepsis Cohorts

The Ottawa Health Sciences Network Research Ethics Board (REB) approved protocols for recruiting 3 health donors and 16 sepsis patients for *ex vivo* studies (Table S1). Archived patients samples were used from the Cellular Immunotherapy for Septic Shock trial, as reported previously.[109] Serial plasma from 8 participants in the observational cohort (not receiving MSCs), and three patients from 2 dose escelation cohorts receiving 0.3 or 1 million MSCs/kg, were included in the neutrophil biomarker analysis (Myeloperoxidase (MPO) kit (ProteinSimple), cell-free DNA (Thermofisher) and Neutrophil-Elastase kit (Biotechne), according to manufacturer's instruction).

MSC Culture and Ex vivo Models

Human bone marrow-derived MSCs (3 donors) were cultured and characterized as described previously [61,109]. For cytomix treatment, MSCs were incubated with or without cytomix (1ng/mL IFNγ, IL-1β and TNFα). For RNA silencing, MSCs were transfected with negative or *CASP1* siRNAs using RNAiMAX. For *ex vivo* assay, MSCs was co-cultured with whole blood ([WB] from health volunteer stimulated with LPS, or sepsis patients) for 24hr. MSCs (CD90+CD45-) were sorted for further analysis after sepsis WB co-culture, and WB were collected for CyTOF, flow cytometry analysis or functional assays.

Cecal Ligation and Puncture (CLP) Animal Model

Animal experiments were approved by the University of Ottawa Animal Care Committee. Eight-week-old C57BL/6N female mice were obtained, cecum was isolated and ligated below the ileocecal valve followed by double-side puncture of the cecum using a 20G needle. Six hours post-CLP or sham operation, animals were randomized for infusion with vehicle (Sham, CLP/vehicle) or MSCs (CLP/MSCs, 2.5×10^5 cells, 100 µL total volume) intravenously 6h post CLP operation. Two or five days after the procedure, animals were euthanized to collect samples.

RNA and Protein Expression Analysis

MSCs incubated with or without cytomix were analyzed at 6hr for transcriptome changes (RNA sequencing) and at 24hr for protein expression. Target intracellular protein expression was measured by an automated capillary western blotting system, and cytokine production were measured by Immunoassay kit (Bio-Rad). mRNA expression using qPCR were performed in MSC retrieved after 24hr co-culture with WB. RNA sequence is stored in

Sequence Read Archive (SRA). Assays were conducted by personnel blinded to the identities of samples.

Mass cytometry (CyTOF) processing and analysis

Three to four individual WB samples were barcoded for CyTOF. Cells were washed and pooled for surface staining. Files were processed following Fluidigm recommendation, including randomization and normalization. Then files were concatenated, debarcoded and randomized according to Fluidigm's instructions using the CyTOF Software.

Statistical Analysis

Statistical analysis was performed using GraphPad PrismV10.0 software, with multiple groups comparison analyzed by one-way ANOVA followed by Dunnett's post hoc test unless stated otherwise. Cytokine data was logarithmic transformed before analysis. Statistical significance was set at $p<0.05$.

Detailed Methods are included in the Supplementary (see Chapter 4 supplementary, page 139).

Chapter 5 General Discussion

In my current thesis, I delineated the crosstalk of MSCs and host environment in three infectious disease settings: severe COVID-19, H1N1 IAV induced ALI, and sepsis. I first showed that, after exposure to the viral mimic (polyI:C), MSCs upregulated the genes and proteins associated with antiviral and immunomodulatory responses. Together with increased expression of antiviral proteins, these changes translated to greater effector functions in regulating monocytes and granulocytes, and in inhibiting SARS-CoV-2 pseudovirus entry into epithelial cells. I further demonstrated that the addition of pIC-MSCs to COVID-19 patient whole blood significantly reduced inflammatory neutrophils and increased M2 monocytes while enhancing their phagocytic effector functions and rebalancing the dysregulated immune responses seen in severe SARS-CoV-2 infection. Next, in a severe H1N1 IAV induced ALI model, I provided *in vivo* evidence that MSCs promoted the selective recruitment of immune cells to the site of infection during H1N1 infection, with reductions in proinflammatory phenotypes. However, MSCs offered no survival benefit in IAV-infected animals, possibly due to MSCs' H1N1 IAV susceptibility and subsequent significant cell death. Lastly, by utilizing an *ex vivo* human and *in vivo* animal model, I investigated neutrophil and monocyte modulation by MSCs in sepsis. I provided evidence that MSCs altered the phenotypes and improved the functions of myeloid cells. Transcriptomic and cytokine analyses revealed activation of caspase-1 pathway in MSCs after exposure to sepsis, which was identified as an essential molecular mechanism mediating immunomodulatory effects of MSCs on dysfunctional myeloid cells. In conclusion, my results demonstrate an interplay between MSCs and host immune

environment in COVID-19, H1N1 induced ALI and sepsis. I showed that the pathogens and host immune responses could differentially limit or enhance the therapeutic activity of MSCs in a disease dependent manner. These novel insights can be used to refine MSC-based therapies.

5.1 Host Factors Affecting the Therapeutic Activity of MSCs

Variations in the host responses, inflammation status, and tissue microenvironment (e.g. hypoxia) are considered as important factors affecting the efficacy of MSCs after administration[143]. Yet, as discussed in Chapter 1, there are limited studies exploring how MSCs respond to host environments. A study by Galleu et al. showed that intravenously administered MSCs underwent perforin-dependent apoptosis induced by the recipient immune system in graft-versus-host disease (GvHD) model, and that subsequent phagocytosis of apoptotic MSCs by recipient macrophages was an important mechanism contributing to immunosuppressive efficacy of MSCs[111]. Also, MSCs were shown to be more potent in suppressing GvHD when host inflammation was more severe[144]. Abreu et al. further demonstrated differential disease-specific MSC responses when they were exposed to BALF of ARDS versus cystic fibrosis patients with fungal infections[145]. This is consistent with my data which confirmed pathogen-specific effects of two types of viral infections (Sars-Cov-2 and H1N1 IAV). In addition to the immune responses, other host factors related to the stage of disease progression and disease microenvironment may also impact MSC functions. For example, it has been reported that exposure of MSCs to hypoxic conditions stimulated an increased expression of soluble bioactive factors, enhancing the

angiogenic potential of MSCs[39]. The present study was focused on systemic administration of MSCs, which is the most common delivery method in clinical trials[146], with a detailed analysis of interactions between MSCs and host whole blood. However, in the context of local tissue delivery, there are a range of other potential tissue specific factors (e.g. matrix stiffness and tissue specific cell types) that need be taken into consideration in future research to explore the interaction between MSCs and a local tissue microenvironment.

The intricate crosstalk between MSCs and their surrounding environment is crucial in determining their responsiveness in disease contexts. In tumor microenvironment, the interaction between MSCs, immune cells and tumor cells can either promote or inhibit tumor development[147]. Elevated levels of cytokines such as fibroblast growth factor-2 (FGF-2), monocyte chemotactic protein-1 (MCP-1/CCL2), and the pro-inflammatory IL-6 have been shown to enhance MSC recruitment to the tumor site[148]. Furthermore, presence of pro-inflammatory cytokines, such as TNFα, within the tumor microenvironment promotes MSC recruitment and facilitates the migration and invasiveness of breast and ovarian tumors[149]. MSCs influence T cells within tumors by secreting immune modulators such as NO, prostaglandin E2 (PGE2), IL-6, IL-10, IDO metabolites, and HLA-G. These factors promote immune tolerance and drive a shift from a Th1 to a Th2 immune response[150]. Regarding tumor associated macrophages, MSCs reprogram M1 macrophages to M2 polarization in response to tumor environment. The resulting increase in M2 macrophage supports tumor progression by promoting angiogenesis and ECM remodeling[151]. These

findings indicate the importance of specific tumor microenvironmental signals in activating MSCs and their ability to modulate immune cell activity.

5.2 Next Generation MSC Therapy

In recent decades, MSCs have held promise as a cell-based therapy for a wide variety of diseases supported by considerable preclinical and clinical research worldwide. Not only does the new data provided in my thesis reveal the plasticity of MSCs to adapt to their surrounding environments, but also uncovers novel mechanisms underlying the interplay between MSCs and host in severe viral infection and sepsis. These new insights combined with breakthroughs in engineering MSCs will enable optimization of therapeutic potential of MSCs.

5.2.1 Modification of MSCs

Preconditioning or genetic engineering of MSCs are being explored to improve the immunomodulatory and therapeutic effect of MSC therapies [152]. First, a range of preconditioning strategies are being explored to enhance the therapeutic capacity of MSCs in preclinical models of ARDS and sepsis. Preconditioning MSCs with IFNγ enhanced their immunomodulatory effects by improving cell–cell interactions and increasing the secretion of immunosuppressive soluble factors[152,153]. Hypoxic conditioning of MSCs could upregulate the secretion of bioactive molecules, including vascular endothelial growth factor and angiopoietin-1[154]. Hypoxia-primed MSCs showed more prolonged engraftment in vivo, which consequently improved respiratory function and reduced inflammatory and pro-

fibrotic factor production in pulmonary fibrosis[155]. Pre-activation of MSCs with ARDS patient serum also enhanced their anti-inflammatory capacity, as evidenced by an increase in the secretion of IL-10, and these preconditioned MSCs were also more effective in reducing lung injury scores, inflammatory cell counts, and pulmonary edema[156]. Altogether, there is a large body of preclinical work supports functional enhancement of MSCs by various preconditioning strategies. Several preconditioned MSC products have reached clinical investigation, including IFNγ-preconditioned MSCs for asthma (NCT05035862) and acute GvHD (NCT04328714), and hypoxia-MSCs for severe COVID-19 (NCT04753476) and critical limb ischemia (NCT02336646). In this study, I revealed that the exposure of MSCs to a viral and sepsis host environment induced selective functional enhancements. I first demonstrated that priming MSCs by exposure to a viral mimic could be an effective therapeutic approach to improve the immunomodulatory and antiviral effectiveness of MSCs to treat COVID-19. It is worth mentioning that polyI:C-primed MSCs exhibited an enhanced antiviral protein expression and modulated secretome profile, which ultimately stimulated greater host defense, contributing to the inhibition of SARS-CoV-2 virus entry to epithelial cells. I also provided important mechanistic insights that, when exposed to sepsis milieu, MSCs underwent transcriptional, secretomic and functional adjustments, via caspase-1 activation, to enhance myeloid modulations and therefore more potent therapeutic effects.

Genetic engineering is also used to further enhance the inherent anti-inflammatory functions of MSCs. MSCs with overexpressing decoy IL-1 receptors exhibited the enhanced

effects in reducing neutrophil infiltration in the lung airspace, along with a significant decrease of TNF-α and IL-6 detected in the BAL of ALI animals[157]. Moreover, our group also previously demonstrated that MSCs with angiopoietin-1 overexpression was significantly more effective in a murine model of LPS-induced ALI, providing additive benefits in both pulmonary vascular permeability and alveolar inflammation[81]. We further continued a first-in-human clinical investigation of a genetic enhanced MSC therapy in adult septic shock patients (NCT04961658). Last, my thesis provides an improved understanding of the role of the host environment in MSC function, which can be used to guide novel approaches for MSC engineering. More insights into the crosstalk between MSCs and the host environments will translate into modification strategies towards a specific mechanism of action for therapeutic enhancement of MSCs dependent on the types of infections.

5.2.2 MSC-free Therapy

MSC-derived extracellular vesicles (EVs) are promising cell-free therapeutics for inflammatory diseases, primarily due to their ability to transfer of mRNAs, proteins, and miRNAs. In respiratory disorders, MSC-derived microvesicles have demonstrated efficacy in treating severe bacterial pneumonia[158]. Notably, MSC-EVs have shown significant benefits in ALI, including reducing inflammation, enhancing alveolar epithelial regeneration, and improving pulmonary endothelial repair[159]. The miRNAs, proteins, mRNAs and mitochondria within MSC-EVs play pivotal roles in modulating immune responses and promoting lung repair[160]. MSC-EVs transfer miR-27a-3p to alveolar macrophages, drives M2 polarization and thereby alleviating ALI[161]. Furthermore, MSC-EVs

interact with immune cells to stimulate TGF-β production and increase Tregs [162], which have been beneficial in influenza infection by increasing viral elimination[163]. A study by Akbari et al. further highlighted the potential of MSCs and MSC-derived EVs in treating COVID-19 patients[164]. In 2020, clinical trials have been initiated to evaluate the safety and efficacy of MSC-EVs for COVID-19 (e.g. NCT05216562, NCT04493242, NCT05116761, NCT05125562). In animal models of sepsis, MSC-EVs have improved survival and reduced inflammation, largely attributed to miRNAs, such as miR-233[165], miR-21[166], and miRNA-146a[167] etc. Despite these promising findings, further research is essential to elucidate the immunomodulatory mechanisms and identify the specific MSC-EV cargo responsible for the observed therapeutic effects. Moreover, tailoring MSC-EV modifications for specific diseases should be explored to enhance their efficacy as cell-free therapeutics.

5.3 Conclusion

In conclusion, my work shows the remarkable plasticity of MSCs, with the ability to adjust their activity and therapeutic efficacy depending on the specific pathogens and the host microenvironment. Through studying the intricate interplay of MSCs in three infectious settings, I identified three differential mechanisms responsible for this plasticity in MSC function. First, the level of MSCs' susceptibility to the pathogens may limit or enhance their functions. When treating COVID-19 with a causative pathogen to which MSCs were nonpermissive, using a viral mimic priming strategy enhanced both antiviral and immune functions of MSCs. However, H1N1 IAV had contrary effects on MSCs. Being highly susceptible to H1N1, therapeutic efficacy of MSCs was limited. I further confirmed that the adaptive reprograming of MSCs by sepsis environment was functionally linked to caspase-1

activation. The findings presented in this thesis, which emerged from a thorough analysis of MSCs in three infectious contexts, unravel the adaptability of MSCs to microenvironment that underpins the response to the cells and identify new approaches to better enhance the efficacy of MSCs. Further research of the specific mechanisms of different microenvironments on MSCs will have an important guiding role for subsequent improvement in MSC clinical benefits.

Appendix

Chapter 2 Supplementary Materials

2.1 Supplementary Figure

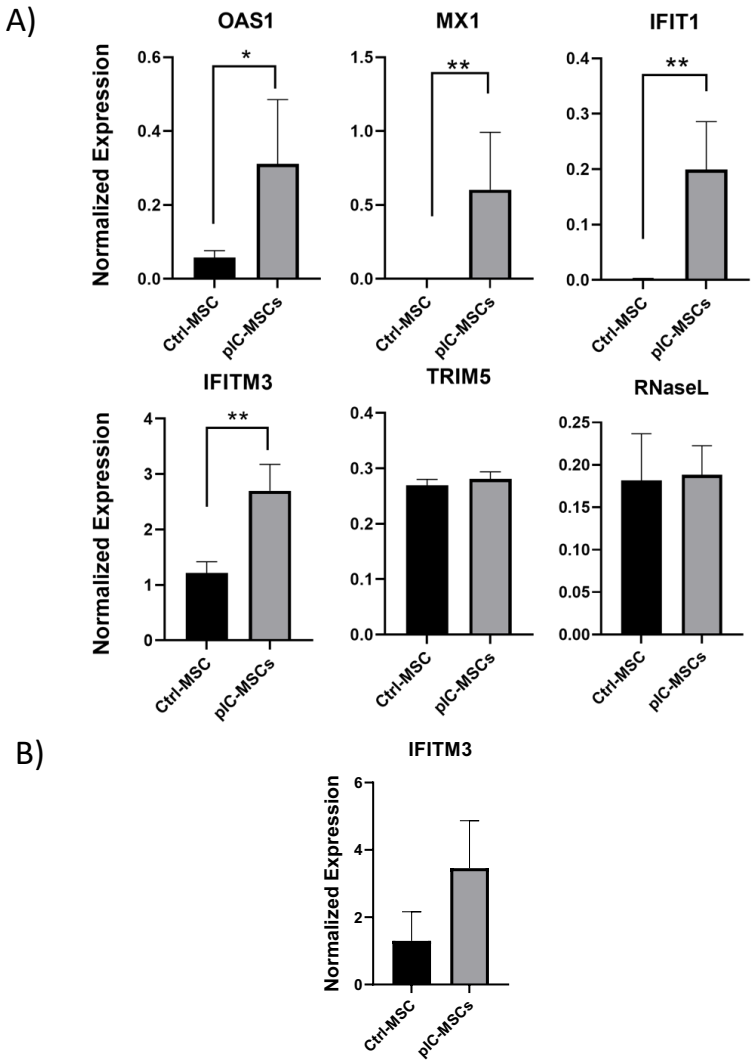

Supplementary Figure 2. 1 pIC Priming Enhances Antiviral Protein of MSCs. Related to Figure 2.2

A) Summary of western blot analysis showing increased intracellular antiviral proteins in MSC lysate after 24 hours of pIC priming (compared to non-pIC primed). B) Summary of western blot analysis showing expression of secreted antiviral protein IFITM3 found in supernatant of MSCs. Data were normalized using housekeeping protein from stain-free blot (total protein) using ImageLab software (Bi-Rad). n=3-5 of independent experiments with the data shown as mean ± SEM. ∗p<0.05, ∗∗p<0.01.

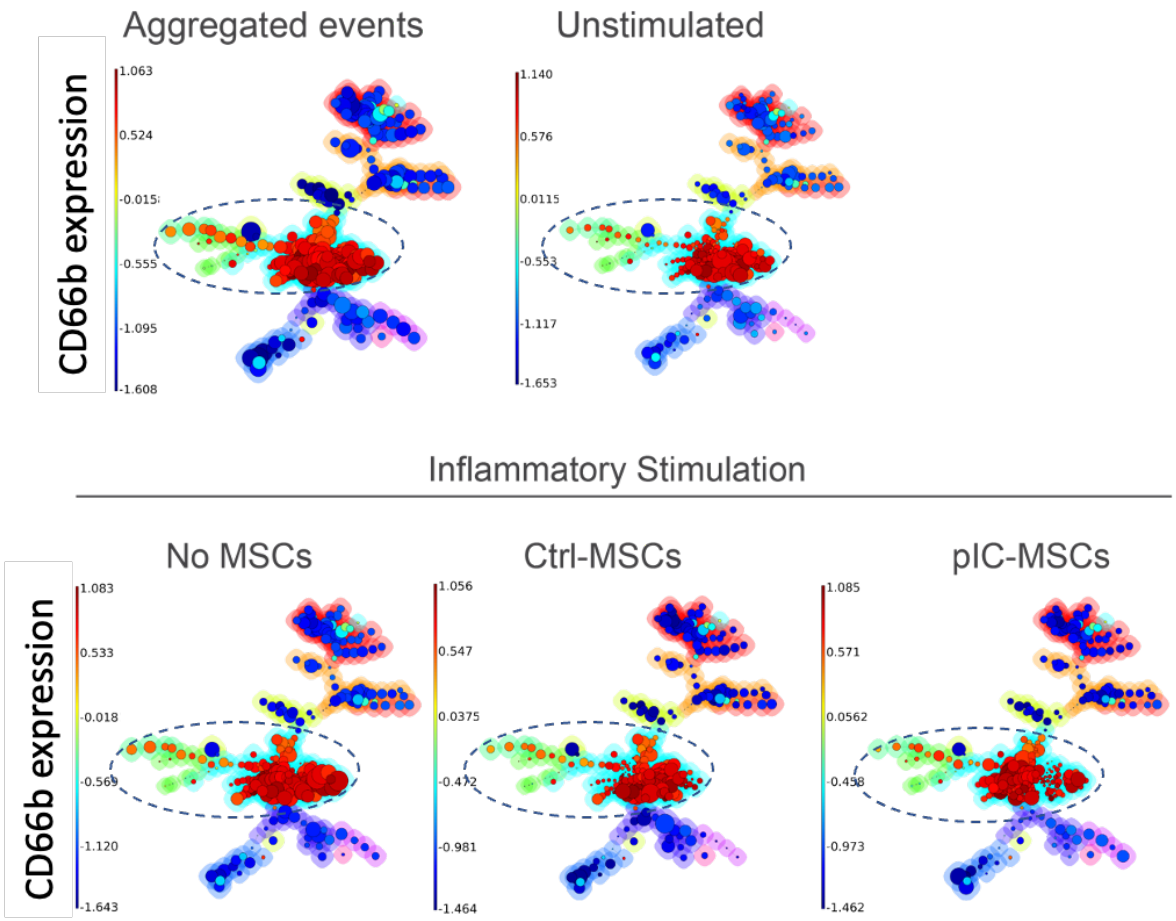

Supplementary Figure 2. 2 Ability of MSCs Upon Viral Stimuli Exposure to Modulate Immune Cell Responses Ex Vivo. Related to Figure 2.3.

Cell subsets from mass cytometry data was identified by unsupervised clustering with FlowSOM algorithm in whole blood samples. Minimal spanning tree (MST) was shown for total aggregated events (100,000), and different treatment conditions (unstimulated or stimulated whole blood with or without MSC co-culture). Color indicates level of CD66b expression (within dash circle), with color scale listing at the left side of the panel.

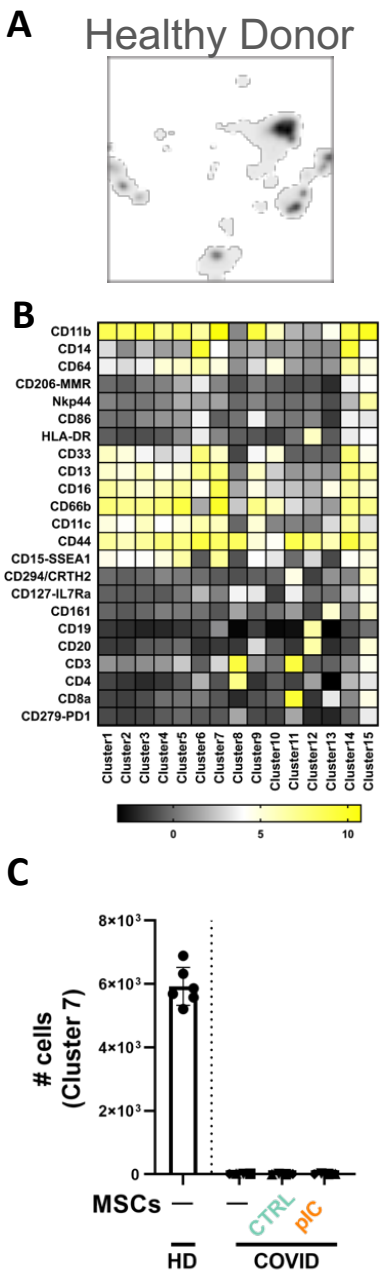

Supplementary Figure 2. 3 MSCs Were Not Permissive to SARS-CoV-2 and pIC-MSCs Modulates Immune Responses in Severe COVID-19. Related to Figure 2.5.

A) t-SNE of healthy donor was shown. B) Heatmap of 23-marker expression was shown for 15 identified clusters of mass cytometry data in Fig. 2.4B. C) Quantification of cluster 7 cell number of mass cytometry data in Fig. 2.4B. n=4 of independent experiments with the data shown as mean ± SD.

2.2 Supplementary Table

Supplementary Table 2. 1 Summary of Healthy Donors and COVID-19 Patient Characteristics (related to Figure 2.5).

	Healthy donors (n=4)	ICU COVID-19 patients (n=4)
Age, yr, median	38 (31 to 57)	73.5 (65 to 88)
Sex, female, n (%)	3 (75)	3 (75)
APACHE II score, median (range)		15.5 (13 to 22)
Mortality, n (%)		3 (75)
Hematology		
White blood cell, $x10^9$/L, (range)		6.6 (3.5 to 9.9)
Red Blood Cell, $x10^{12}$/L /L, (range)		3.3 (2.8-4.17)
Platelet, $x10^9$/L, (range)		91.5 (70 to 388)
Neutrophil, $x10^9$/L, (range)		6.0 (3.2 to 7.2)
Lymphocyte, $x10^9$/L, (range)		0.4 (0.1 to 2)
Monocyte, $x10^9$/L, (range)		0.2 (0.1 to 0.7)
Biochemistry organ disfunction markers		
Renal, Creatine Kinase, U/L		47 (n/a to 221)
Hepatic, bilirubin, umol/L		9 (6 to 33)
Lactate, umol/L		1.3 (0.9 to 3)
Biomarkers associated with severe COVID-19		
D-Dimer, ug/L		2543.5 (1131 to 8932)
Ferritin, ug/L		1806.5 (292 to 7266)
Lactate Dehydrogenase, U/L		477 (214 to 864)

Chapter 3 Supplementary Materials

3.1 Supplementary Figure

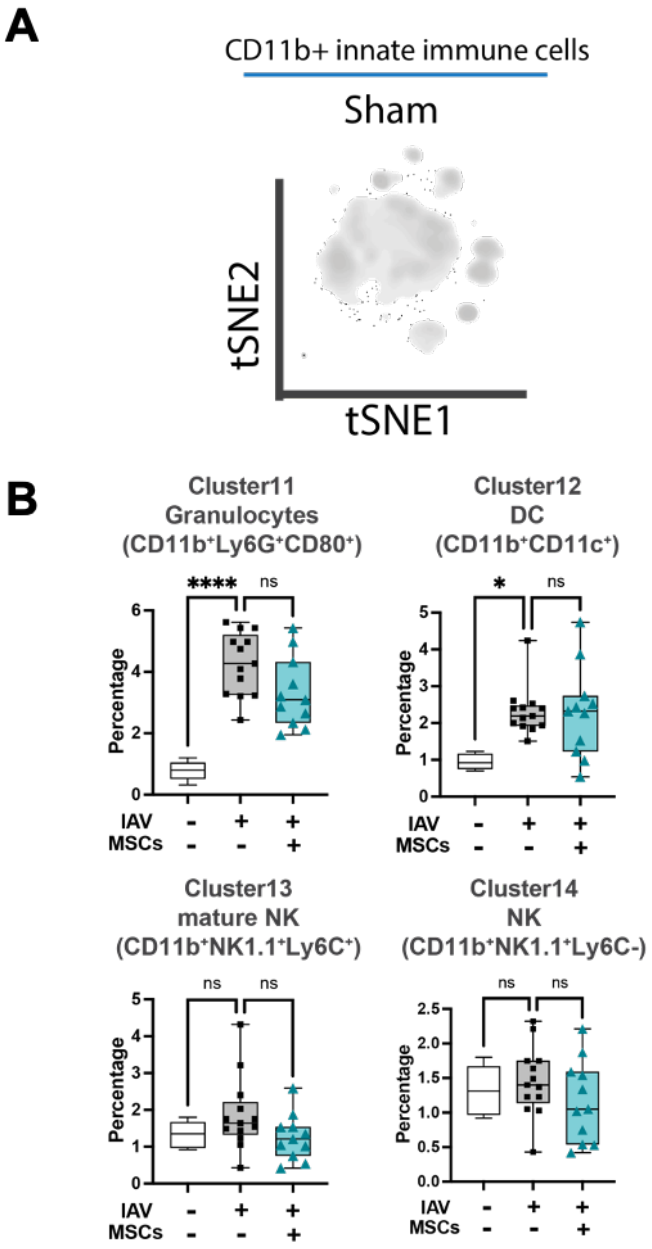

Supplementary Figure 3. 1 Mass Cytometry Analysis of circulating innate immune cells in H1N1-induced ALI. Related to Figure 3.1

(A). t-SNE plot of sham group.
(B). Quantification of cell subpopulation.
n = 6 of sham, n=13 of IAV/vehicle- and n=11 of IAV/MSC-treated animals with the data shown as Dunnett's box-and-whisker plots. ∗p < 0.05, ∗∗p < 0.01, ∗∗∗p < 0.005, ∗∗∗∗p < 0.001.

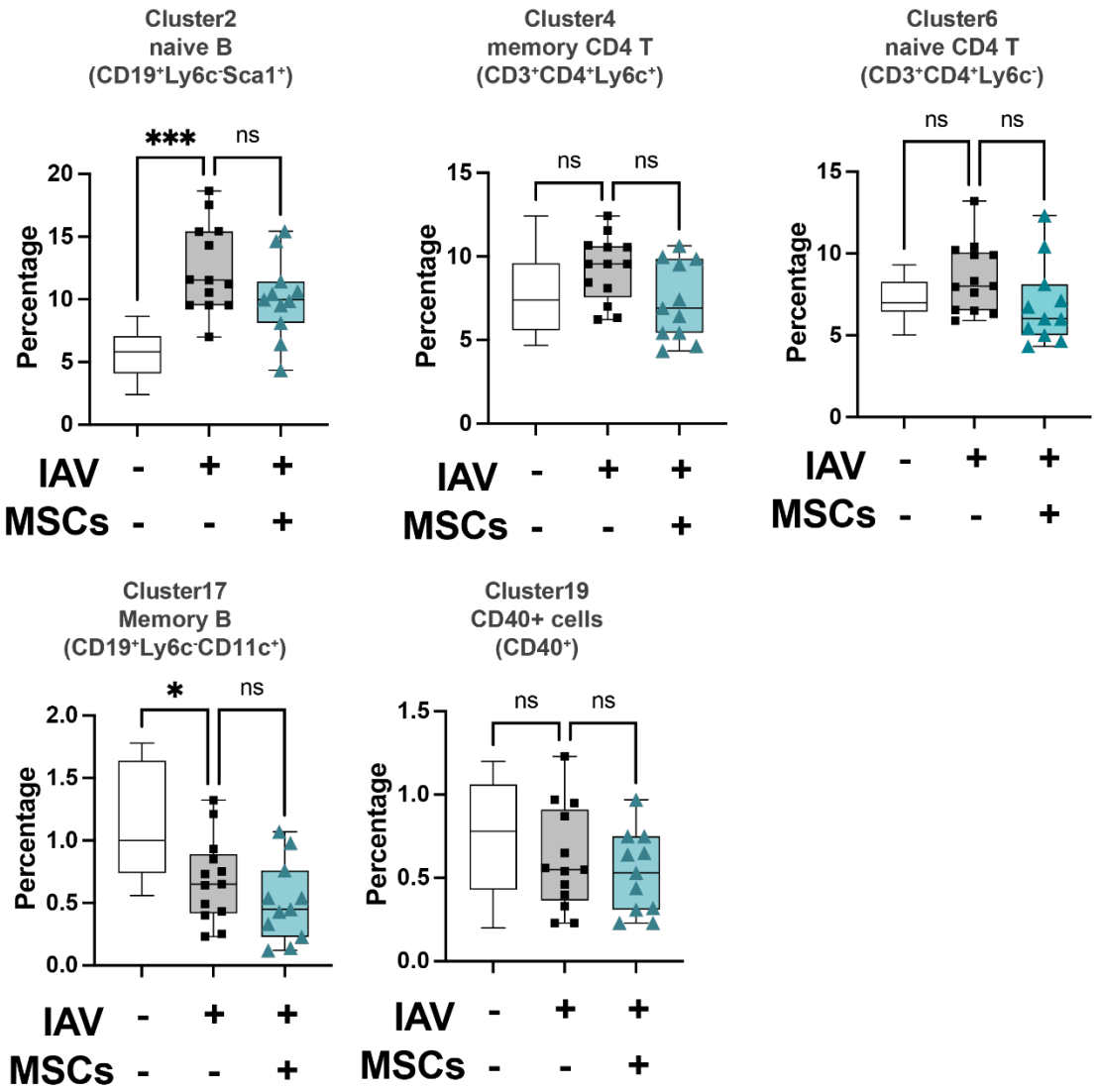

Supplementary Figure 3. 2 Mass Cytometry Analysis of circulating adaptive immune cell in H1N1-induced ALI. Related to Figure 3.2

Quantification of cell subpopulation.
n = 6 of sham, n=13 of IAV/vehicle- and n=11 of IAV/MSC-treated animals with the data shown as Dunnett's box-and-whisker plots. ∗p<0.05, ∗∗p < 0.01, ∗∗∗p < 0.005, ∗∗∗∗p <0.001.

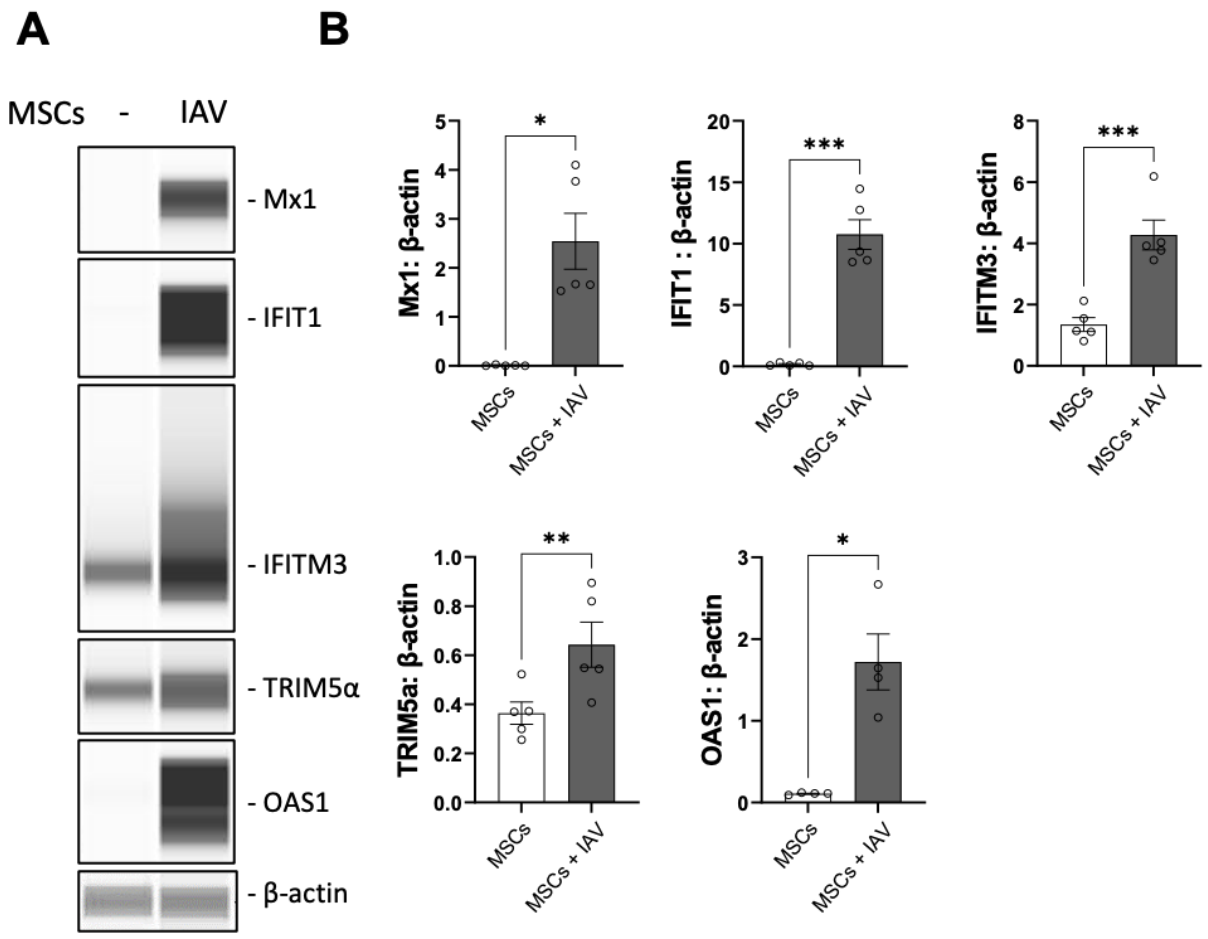

Supplementary Figure 3. Upregulation of antiviral protein expression in MSCs when infected by H1N1 IAV.

(A) Western blot analysis showed increased antiviral protein expressions in MSCs after in vitro exposure to H1N1 (MOI 0.1, 24h exposure).

(B) Densitometry analysis of protein expression detected using automated western blot. n = 5 with the data shown as mean ± SEM, ∗p <0.05, ∗∗p <0.01, *** p <0.005.

3.2 Supplementary Table

Supplementary Table 3. 1 List of Antibodies

ANTIBODY - HUMAN	**Supplier**	**Catalogue #**	**RRID**
RNase L (D4B4J) Rabbit mAb	Cell Signaling Technology	27281	AB_2798941
OAS1 (D1W3A) Rabbit mAb	Cell Signaling Technology	14498	AB_2798498
MX1 (D3W7I) Rabbit mAb	Cell Signaling Technology	37849	AB_2799122
IFITM3 (D8E8G) XP® Rabbit mAb	Cell Signaling Technology	59212	AB_2799561
TRIM5α (D6Z8L) Rabbit mAb	Cell Signaling Technology	14326	AB_2798451
IFIT1 (D2X9Z) Rabbit mAb	Cell Signaling Technology	14769	AB_2783869
Monoclonal Anti-β-Actin, mouse, clone AC-15, ascites fluid	Sigma-Aldrich	A5441	AB_476744
ANTIBODY - MOUSE	Supplier	Catalogue #	RRID
Anti-Mouse CD3e (145-2C11)-152Sm	Fluidigm	3152004C	N/A
Anti-Mouse CD4 (RM4-5)-145Nd	Fluidigm	3145002C	N/A
Anti-Mouse CD8a (53-6.7)-168Er	Fluidigm	3168003C	N/A
Anti-Mouse CD279 (RMP1-30)-159Tb	Fluidigm	3159006C	N/A
Anti-Mouse CD11b (M1/70)-148Nd	Fluidigm	3148003C	N/A
Anti-Mouse CD11c (N418)-209Bi	Fluidigm	3209005C	N/A
Anti-Mouse I-A/IE (M5/114.15.2)-174Yb	Fluidigm	3174003C	N/A
Anti-Mouse/Rat CD40 (HM40-3)-161Dy	Fluidigm	3161020C	N/A
Anti-Mouse CD80 (16-10A1)-171Yb	Fluidigm	3171008C	N/A
Anti-Mouse CD86 (GL1)-172Yb	Fluidigm	3172016C	N/A

Anti-Mouse Ly-6C (HK1.4)-162D	Fluidigm	3162014C	N/A
Anti-Mouse Ly-6G (1A8)-141Pr	Fluidigm	3141008C	N/A
Anti-Mouse CD206/ MMR (C068C2)-169Tm	Fluidigm	3169021C	N/A
Anti-Mouse CD64 (X54-5/7.1)-151Eu	Fluidigm	3151012C	N/A
Anti-Human/Mouse CD27 (LG.3A10)-150Nd	Fluidigm	3150017C	N/A
Anti-Mouse Ly-6A/E (Sca-1) (D7)-164Dy	Fluidigm	3164005C	N/A
Anti-Mouse CD45 (30-F11)-89Y	Fluidigm	3089005C	N/A
Anti-Mouse CD274/ PD-L1 (10F.9G2)-153Eu	Fluidigm	3153016C	N/A
Anti-Mouse F4/80 (BM8)-146Nd	Fluidigm	3146008C	N/A
Anti-Mouse NK1.1 (PK136)-170Er	Fluidigm	3170002C	N/A
Anti-Mouse CD19 (6D5)-166Er	Fluidigm	3166015C	N/A
Anti-Mouse CD69 (H1.2F3)-143Nd	Fluidigm	3143004C	N/A
Anti-Mouse CD45 (30-F11)-89Y	Fluidigm	3089005C	N/A

Chapter 4 Supplementary Materials

Method details

Healthy Volunteer and Sepsis Cohort

This study was approved by the Research Ethics Board (REB) (Ottawa Health Science Network REB, REB ID: 20200312-01H and #20190401-01H). After providing written informed consent, 3 health donors and 16 sepsis patients were included in the study. Information on age, sex and blood analysis of Sepsis patients were listed in Table S1. It is noted a wider age range for sepsis patient, compared to healthy donors. Sepsis patients were recruited in the intensive care unit of the Ottawa Hospital between June 2020 and February 2023. Sepsis patients treated with MSCs were obtained from patients enrolled in the Cellular Immunotherapy for septic shock (CISS) trial. The trial was approved by Health Canada and Ottawa Health Sciences Network Research Ethics Board (OHSN-REB ID: 20140809-01H). Trial design, recruitment, MSCs preparation and clinical outcome were reported previously19. In summary, 8 septic shock participants in observational cohort (did not receive MSCs) were included the neutrophil markers analysis. The interventional cohort included three dose-escalation cohorts of nine septic shock patients, with three patients in each cohort received 0.3, 1, or 3 million cells per kg body weight of MSCs. The cohort of patients who received 3 million cells/kg was excluded from the PCA analysis due to missing samples at baseline (0hr) and 4hr timepoint.

Bone Marrow aspirates and MSCs Culture

Bone marrow aspirates were obtained from commercial vendor (Lonza) or at The Ottawa Hospital (with informed written consent and ethical approval granted by the Ottawa Health Science Network Research Ethics Board, REB ID: 20120929-01 H). Human bone marrow derived MSC (n=3 different donors; 2 females and 1 male) were cultured, characterized, and cryopreserved as described previously20,21. MSCs have been characterized to meet all the criteria (plastic adherence, differentiation potential, and cell surface antigen expression) that proposed by the International Society for Cellular Therapy (ISCT)22 as previously described20,21,23. Cryopreserved MSCs were thawed and plated overnight in the Nutristem complete media (Sartorius) for in vitro or ex vivo assays. For in vivo studies, cryopreserved MSCs were thawed and diluted to targeted concentration in plasmalyte A supplemented with 5% human albumin. MSCs were maintained at 37 °C in a humidified incubator containing 5% CO2. All experiments used cells between passages 3 to 5.

For ex vivo human sepsis model, MSCs were directly co-culture with whole blood collected from sepsis patients for 24hr. After incubation, sepsis whole blood was harvested for mass cytometry (CyTOF) analysis and MSCs were washed and sorted. In sepsis-like environment priming, MSCs were incubated with or without 1ng/mL cytomix (IFN□, IL-1□ and TNF□) for 6h for sample collection for RNAseq analysis, or 24 hours for protein expression (total cell lysate and secreted protein in the supernatant).

Cecal ligation and puncture (CLP) animal model

All animal experiments were conducted under the protocol approved by the University of Ottawa Animal Care Committee (ACC, institutional animal protocol #3483). Animals were allowed to acclimate in the animal care facility for one week prior to the experiment date. Animals were housed according to Canadian Council on Animal Care (CCAC) guidelines. All animals were housed in either groups of 3 or 4, in conventional breeding cages within the animal care facility. A standard chow diet was provided within the hopper of the cage to avoid soiling, and water was provided ad libitum. All cage bedding was changed on a weekly cycle. Animals were housed in a 20°C-23°C temperature-controlled room with a 12-hour light, 12-hour dark cycle, and 40%-60% humidity.

For the experimental model, 8-week old healthy C57BL/6N female mice were obtained from Charles River Laboratories (Kingston, ON). After receiving either CLP or sham procedure, animals were randomly assigned (random.org; Randomness and Integrity Services Ltd.) for the infusion of vehicle control or MSCs. On Day 0 of the study, the cecum was isolated and ligated directly below the ileocecal valve followed by double side puncture of the cecum by a 20 G needle. The cecum was then gently compress to extrude a droplet of fecal matter from each hole and the ligated/punctured section of the cecum carefully returned to the abdomen. Sham operation was performed by isolation of the cecum without ligation and puncture. The incision was closed using 5-0 silk sutures and skin was closed using AutoClips. Six hours post-CLP or sham operation, animals were anesthetized with 2% isoflurane gas (in 100% oxygen) and were infused with vehicle (Sham, CLP/vehicle) or MSCs (CLP/MSCs, 2.5 × 105 cells, 100 µL total volume) via the jugular vein. Mice were allowed to

recover from anesthesia and were monitored daily by trained laboratory personnel, as well as the veterinary technicians on site, until the end of study. Two or five days after the sham or CLP procedure, the animals were euthanized using standard lab protocol. Bone marrow, whole blood, mesenteric lymph nodes, or peritoneal lavage was harvested, and plasma samples were also collected. Cell infusion, animal wellness, and sample analyses were performed in a blinded fashion, with independent operators blinded for the group assignment. Any correlation between treatment name and nature of the treatment was only revealed following the data collection and analysis period.

Blood collection and processing

For immune profile studies, mice were sacrificed 2 or 5 days after CLP surgery to evaluate the therapeutic efficacy by collecting samples for analysis. Whole blood was drawn from inferior vene cava, plasma was subsequently processed by centrifugation at 1,700g for 10 minutes followed by 10,000g spin for 5 minutes.

MSCs sorting from sepsis whole blood.

After 24hr co-culture with sepsis whole blood, whole blood was harvested, fixed and stored for downstream CyTOF analysis. MSCs were washed twice thoroughly with PBS and dissociated using TrypLE select (Gibco). After another two washes with PBS (Gibco), Human FC block (BDbioscience) was added in cell solution. CD90-PE (BDbioscience) and CD45-FITC (BDbioscience), listed in Table S2, were added for 30-minute incubation at 4C.

MSCs were sorted using CD90+ and CD45- gating by Sony MA900 Cell Sorting instrument (Sony) or Beckman Coulter MoFlo XDP (Beckman Coulter). After sorting, a portion of cells were pelleted and stored for PCR array analysis, while another set of cells was plated overnight to collect conditioned media and conduct functional assay.

Myeloperoxidase and neutrophil elastase ELISA

Serial plasma samples from CISS trial were thawed and centrifuged at 10,000g for 5 minutes. Myeloperoxidase (MPO) neutrophil elastase, cellfree DNA were measured using Simple plex cartridge (Protein simple, Biotechne), together with Ella instrument (Protein simple, Biotechne) under 1:100 dilution and Human Neutrophil Elastase/ELA2 DuoSet ELISA kit (Biotechne), Sytox DNA staining (Thermo Fisher Scientific) with 1:100 dilution, with Omega plate reader (BMG labtech) under 1:500 dilution, according to manufacturer's instruction.

RNA silencing

MSCs were plated at 0.5 × 105 cells/well in a 24-well plate and transfected the next day according to the manufacturer's instructions (Thermo Fisher Scientific). Briefly, 1 µL siRNA (CASP1 CASP1P2 Silencer Select and Silencer Select Negative Control; Thermo Fisher Scientific) were diluted in 50 µl, Opti-MEM and mixed with 3 µL RNAiMAX (Thermo Fisher Scientific) transfection reagent by vortex. The samples were then incubated for 5 min at room temperature to allow the formation of transfection complexes before adding onto

MSCs. MSCs were stimulated with Cytomix and caspase-1 activity was assessed by FAM-FLICA assay (BioRad).

Quantitative Real-time Polymerase Chain Reaction (qRT-PCR)

Total RNA was extracted from cells using miRNeasy Mini Kit (Qiagen). The double-stranded cDNA was prepared using the RT^2 First Strand Kit (Qiagen) and PCR was performed using RT^2 Profiler™ PCR Array Human Innate & Adaptive Immune Responses (Qiagen), according to the manufacturer's instructions. Real-time PCR was performed on CFX384 machine (Bio-Rad) using the following conditions: initial activation step of 10min at 95 °C, followed by 40 cycles of amplification (94 °C for 15 sec, 60 °C for 1min). Data analysis was performed using GeneGlobe (Qiagen), setting CT (cycle threshold) cut-off at 35. The normalization was performed using automatic selection, software algorithm selection of optimum reference set of gene in the array panel. The reference genes automatically selected were NOD1, TRAF6, MAPK1, IFNAR1 and TYK2.

RNAseq Library Preparation and Sequencing & Data Analysis

MSCs (n= 3 different donors) were incubated with or without cytomix for 6 hours, then cell lysates were collected and sent to Qiagen NextGeneration Service for RNA isolation and library preparation. In summary, the libraries' size distribution was validated and quality inspected on a Bioanalyzer 2100 or BioAnalyzer 4200 TapeStation (Agilent Technologies). Sequencing was performed on an Illumina NextSeq500 instrument (76 cycles) generating

single end reads; Qiagen service reported an average 38.2 million reads were obtained for each sample. Raw counts were compiled into FASTQ format, and the reads containing adapter sequences or qualified as low-quality reads were filtered out from the dataset. All samples passed the FASTQC Quality Scores (i.e. per sequence quality scores, sequence quality histograms and adapter content). Quality controlled FASTQ files were aligned to human reference genome GRCh38.p13 using HISAT2 aligner software 24 to obtain the raw counts matrix. Data was mapped and count matrix were generated by Bioinformatics Department at the OHRI. The R programming language (R version 3.6.3 and RStudio version 1.2.5033) was used to perform the gene expression analysis of the reads. Differential expression analysis was performed using the default parameters of R DEseq2 package version 1.2625. Heatmaps were generated via Graph Pad Prism using normalized count value from the DEseq analysis 26 and illustrates the variation of selected genes (each row), with each column represents MSC derived from 1 bone marrow donor (n=3 donor).

Data and Code Availability

The RNA-seq sequence data will be stored in Sequence Read Archive (SRA). Datasets will be accessible upon publication. The STAR Methods details the analysis procedures conducted. This paper does not report original code. The public available scripts used to generate the figures reported in this paper. Any further questions or request for additional information to reproduce this work can be directed to the Lead Contact.

Cytokine measurement

The conditioned media were collected from cultured cells, and cell debris were eliminated by spun down at 1,000g for 15 min at 4oC. Supernatant was collected and stored at -80°C. Plasma was collected by 1,700g centrifugation at 10 minutes followed by one 10,000g spin for 5 minutes. Cytokines and growth factors contents in the supernatant were detected using multiplex immunoassay kit (Bio-Rad) following manufacturers' instruction. Assays were conducted by personnel blinded to the identities of samples.

Immunomodulatory assays to assess MSCs potency and functions

For ex vivo assay, whole blood (sodium citrate as anticoagulant) from healthy volunteer purchased from commercial vendor (StemCell Technologies) or obtained from healthy volunteer at OHRI or sepsis patient was directly co-cultured with MSCs (primed with or without sepsis like stimuli) for 24 hours. For ex vivo acute inflammation system, whole blood, obtained from health volunteers, were co-cultured with or without MSCSs in the presence of lipopolysaccharide (10 ng/mL). After co-cultured, part of whole blood was saved for CyTOF analysis (details bellow), while the rest underwent RBC lysis (Thermo Fisher Scientific) to obtain total white blood cells. Cells were washed with flow cytometry washing buffer (PBS supplemented with 2% fetal bovine serum). For apoptosis staining, cells were incubated with AnnexinV (BD Biosciences) and PI (Thermo Fisher Scientific) for 15min at room temperature followed by flow cytometry analysis (Attune NxT acoustic focusing cytometer, Thermo Fisher Scientific). For phagocytosis analysis, pHrodo E.coli

bioparticle (Thermo Fisher Scientific) was added to whole blood culture system and incubated for 15 min at 37ºC. Cells were then washed and stained with anti-human CD14 and anti-human CD66b (BD Biosciences), listed in Table S2, for 30 min at 4ºC. After staining, washed cells were analyzed by flow cytometry (LSRFortessa cytometer, BD Biosciences).

Flow cytometry

Cells were first treated with Fc-block (BDbiosence) before staining with the antibodies listed in resource table for cell differential analysis.

For fluorescent labeled inhibitor of caspase activity (FLICA) assays, cell suspensions were incubated with the FAM-FLICA reagent according to the manufacturer's protocol (Bio-Rad). Cells were stained with 5uL Annexin-V-V450 (BDbioscience) and 1:1000 dilution of propidium iodide (PI) (Thermo Fisher Scientific). Gating of positive populations was based on Fluorescence minus one control (FMO) samples.

Sample processing and antigen staining of mass cytometry-based immune cell profiling (CyTOF)

For CyTOF sample processing, 250 µL of human whole blood (collected with sodium citrate) or mouse whole blood (EDTA) via caudal (inferior) vena cava was lysed in 350 µL of

stable-lyse V2 and then fixed in 1 mL of stable-store V2 (Smart Tube Inc., San Carlos, US), as described in the user's manual and stored at -80ºC until further processing. Further, whole blood samples were thawed and washed, followed by barcoding using Cell-ID 20-Plex Pd Barcoding Kit (Fluidigm). Up to 4 individual samples were barcoded for 30 min at room temperature. Cells were then washed and pooled for surface staining. For surface staining, cells were resuspended in diluted human Fc-block (BDbioscience) for 10 minutes and incubated with antibody staining cocktails, listed in Table S2, for 30 min at room temperature. After incubation, cells were washed with staining buffer and fixed overnight in MaxPar Fix-I buffer with iridium intercalator (Fluidigm). Immediately prior to data acquisition, samples were washed once with each of Cell Staining Buffer (Fluidigm) and Cell Acquisition Solution (Fluidigm). Samples were then resuspended at a concentration of 5x105 cells per mL in Cell Acquisition Solution containing EQ Four Element Calibration Beads (5:1 Ratio) (Fluidigm). The samples were acquired on a Helios Mass Cytometer equipped with a wide-bore sample injector at a rate of 300-500 events per second. After acquisition, repeat acquisitions of the same sample were concatenated as necessary and normalized using the Fluidigm software. Normalized fcs files were gated to exclude debris, doublets and dead cells using Cytobank software.

Mass cytometry data analyses

Files were processed following Fluidigm recommendation, including randomization and normalization using EQ Beads signal. Then files were concatenated, debarcoded and

randomized according to Fluidigm's instructions using the CyTOF Software. Gating to identify and export single cells was done in Cytobank27. Clustering analysis was done with either FlowSOM (Cytobank)28 or PhenoGraph 29 as stated as part of the R Bioconductor package Cytofkit 30 and Flowjo X using the markers listed in Key Resource Table with up to 50,000 cells per sample. The transformation method used was cytofAsinh, and the visualization method was t-SNE or UMAP. The t-SNE or UMAP map overlaid with PhenoGraph-defined cell populations were generated using ggplot2 package in RStudio and FlowJo.

Western blot analysis

MSCs were seeded into 24-well plates (100,000 cell/well) and treated the day after with Cytomix. After 24h, cell lysate was collected with a cell scraper after adding sample lysis buffer cocktail containing proteinase inhibitor cocktail (Sigma-Millipore). Protein quantification was performed using Bradford reagent (Bio-Rad). Target protein signal was measured by automated capillary electrophoresis-based western blotting system (Jess, ProteinSimple, San Jose, CA, USA). Samples were diluted to 1ug/uL total protein in simple western sample buffers from the 12-230 kDa Jess Separation Module cartridge kit (cat# SM-W004), heated at 95ºC for 5 minutes, then loaded to the plate. All Jess simple western system experiments were conducted according to the manufacturer's instructions. Compass for SW software (ProteinSimple) was used to analyze and quantify protein band intensities.

Quantification and Statistical Analysis

Statistical analysis was performed using GraphPad PrismV10.0 software (GraphPad Software). Numerical data are presented as mean ± SEM unless otherwise stated. Multiple groups were analyzed by one-way ANOVA followed by Dunnett's multiple comparisons test unless stated otherwise. For the analysis of cytokine data, logarithmic transformation was performed to normalize the cytokines. Statistical significance was set at $p < 0.05$.

4.1 Supplementary Figure

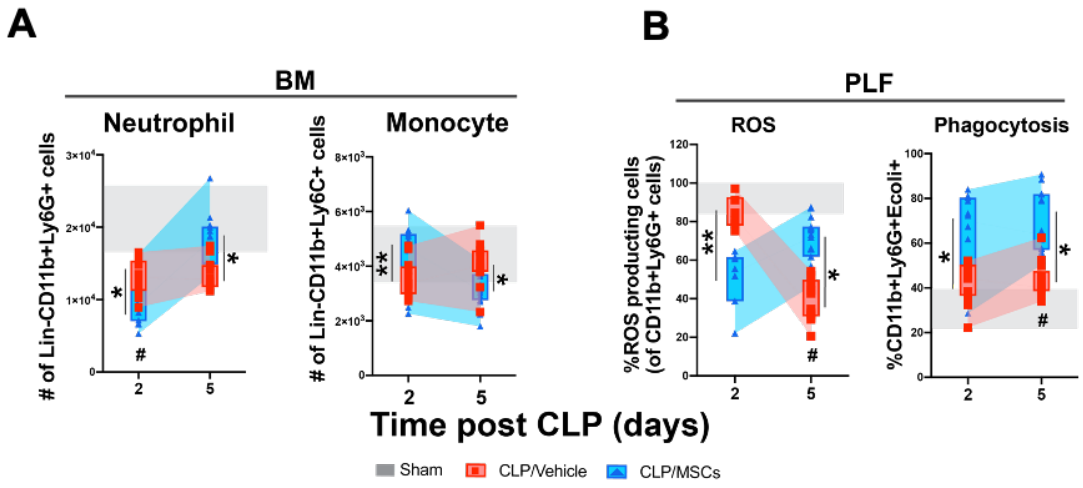

Supplementary Figure 4. 1 Compositional and functional changes of neutrophils and monocytes in Different Tissues of CLP Induce

A. Quantification of neutrophil (CD11b+Ly6G+) population in BM and LN at day 2 or day 5 post CLP.
B. Measurement of ROS production and phagocytic capacity of neutrophils in PLF at day 2 or day 5 post CLP.
C. Quantification of monocyte (CD11b+Ly6C+) population in BM and LN at day 2 or day 5 post CLP.

BM, bone marrow; PLF, peritoneal lavage fluid; LN, lymph node. n=6 sham n=15 for CLP/vehicle and n=14 CLP/MSCs animals per group, with the data shown as bar graph as mean ± SEM, ∗p<0.05, ∗∗p<0.01, ∗∗∗p<0.005, ∗∗∗∗p<0.001. Comparison done by unpaired two tailed t-test.

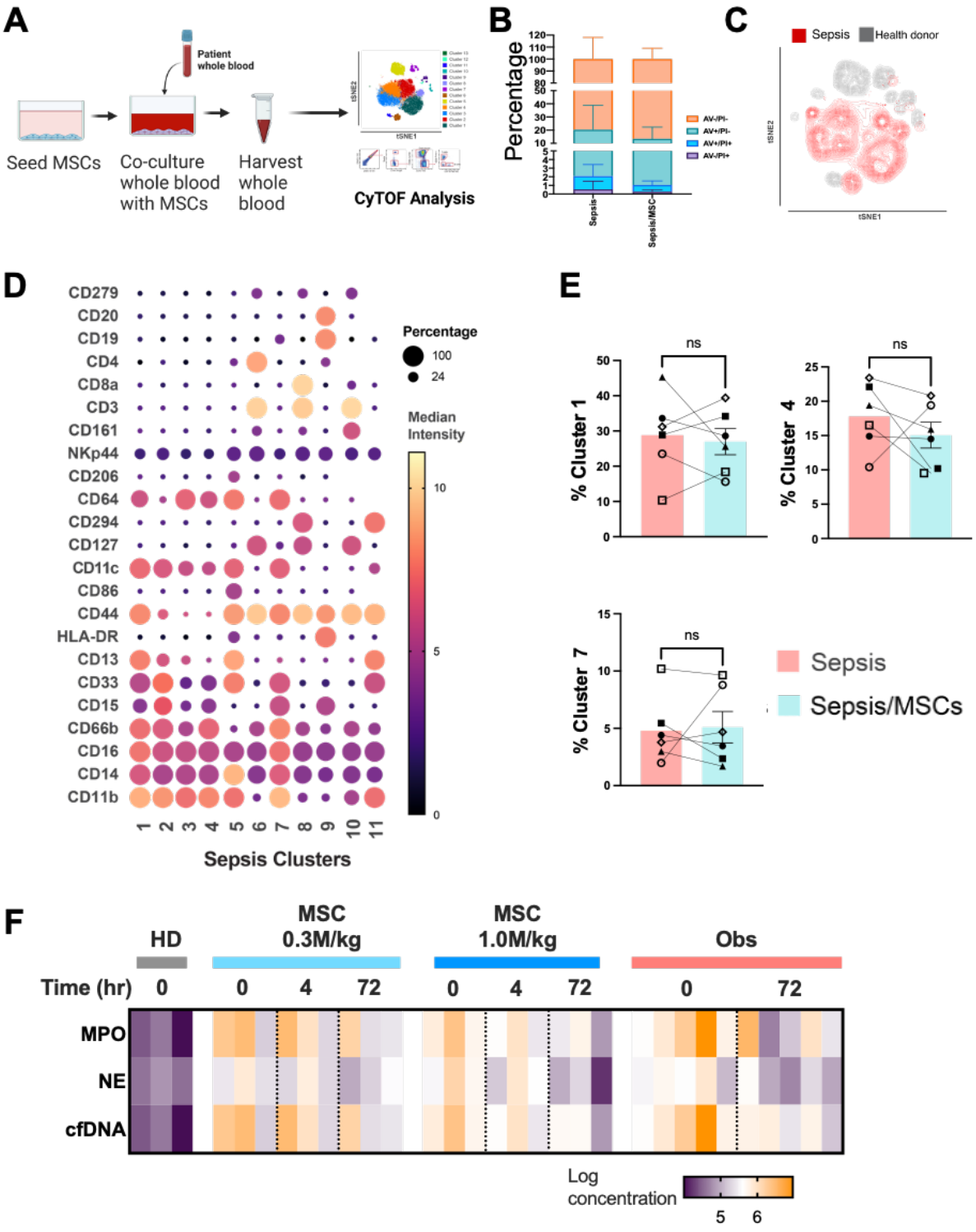
A
Patient whole blood
Seed MSCs
Co-culture whole blood with MSCs
Harvest whole blood
CyTOF Analysis
B
Percentage
AV-/PI-
AV+/PI-
AV+/PI+
AV-/PI+
Sepsis
Sepsis/MSC
C
Sepsis
Health donor
tSNE2
tSNE1
D
CD279
CD20
CD19
CD4
CD8a
CD3
CD161
NKp44
CD206
CD64
CD294
CD127
CD11c
CD86
CD44
HLA-DR
CD13
CD33
CD15
CD66b
CD16
CD14
CD11b
Percentage
100
24
Median Intensity
10
5
0
1 2 3 4 5 6 7 8 9 10 11
Sepsis Clusters
E
% Cluster 1
% Cluster 4
% Cluster 7
ns
Sepsis
Sepsis/MSCs
F
HD
MSC 0.3M/kg
MSC 1.0M/kg
Obs
Time (hr)
0
0 4 72
0 4 72
0 72
MPO
NE
cfDNA
Log concentration
5 6

Supplementary Figure 4. 2 Analysis of effects of MSCs on myeloid responses in human sepsis ex vivo. Related to Figure 4.2.

A. Schematic diagram of ex vivo human sepsis model system.
B. Measurement of viability of totally leukocytes by Annexin V/PI staining
C. Dot plot showing expression of all 23 surface markers of each clusters.
D. Quantification of clusters 1, 4, and 7.
E. Fold change (Fc) of neutrophil function related analytes from plasma of observation or MSC cohort.

For B-D experiments, n=3 healthy donor (HD), n=6 sepsis patients per group, with each patient represented by different symbol with the data shown as bar graph as mean ± SEM (grey shaded area: range from measured from HD), $*p<0.05$, $**p<0.01$, $***p<0.005$, $****p<0.001$. Comparison done by unpaired two tailed t-test. For E, n=5 for observational cohort, n=3 for each of MSC cohorts

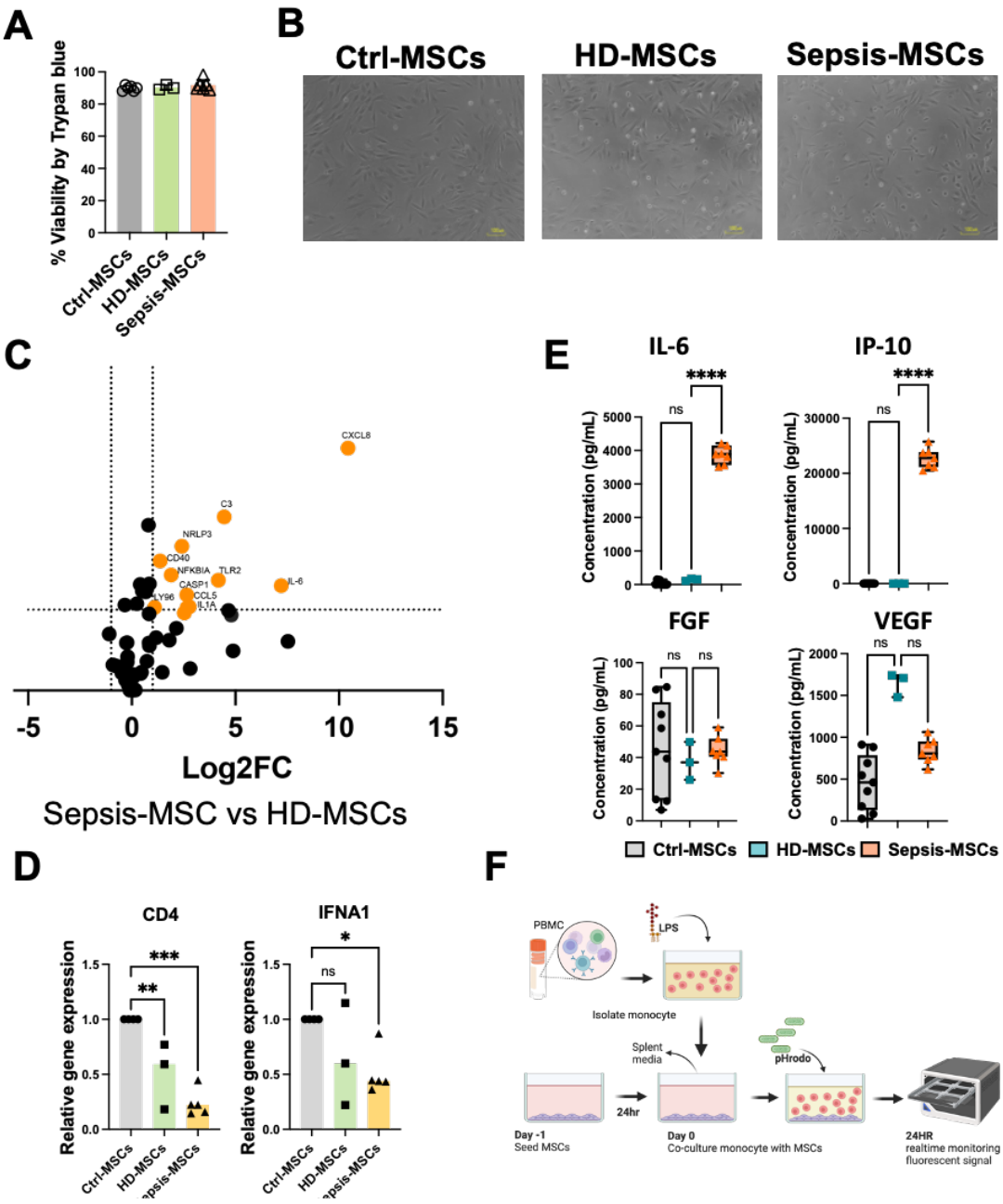
A
% Viability by Trypan blue
100
80
60
40
20
0
Ctrl-MSCs
HD-MSCs
Sepsis-MSCs
B
Ctrl-MSCs
HD-MSCs
Sepsis-MSCs
C
CXCL8
C3
NRLP3
CD40
NFKBIA
TLR2
CASP1
IL-6
LY96
CCL5
IL1A
-5
0
5
10
15
Log2FC
Sepsis-MSC vs HD-MSCs
D
CD4
IFNA1
Relative gene expression
***
**
*
ns
1.5
1.0
0.5
0.0
Ctrl-MSCs
HD-MSCs
E
IL-6
IP-10
FGF
VEGF
Concentration (pg/mL)
****
ns
5000
4000
3000
2000
1000
0
30000
20000
10000
100
80
60
40
20
2000
1500
1000
500
Ctrl-MSCs
HD-MSCs
Sepsis-MSCs
F
PBMC
LPS
Isolate monocyte
Splent media
pHrodo
24hr
Day -1
Seed MSCs
Day 0
Co-culture monocyte with MSCs
24HR
realtime monitoring of fluorescent signal

Supplementary Figure 4. 3 Analysis of retrieved MSCs from sepsis whole blood. Related to Figure 4.3.

A. Representative picture of MSCs after overnight attachment showing normal MSCs morphology.
B. Volcano plot of PCR array comparing Sepsis-MSCs vs HD-MSCs
C. Two downregulated genes with $p<0.05$ and fold change over 2.
D. Increase of IL-6 and IP-10 secretion after MSCs exposed to sepsis environment.
E. Schematic of secondary coculture system to measure retrieved Sepsis-MSCs functionality.

N=3 healthy donors and n=5 septic patients, the data shown as mean ± SEM. $*p<0.05$, $**p<0.01$, $***p<0.005$, $****p<0.001$. Comparison done by one way ANOVA with Dunnett's comparison.

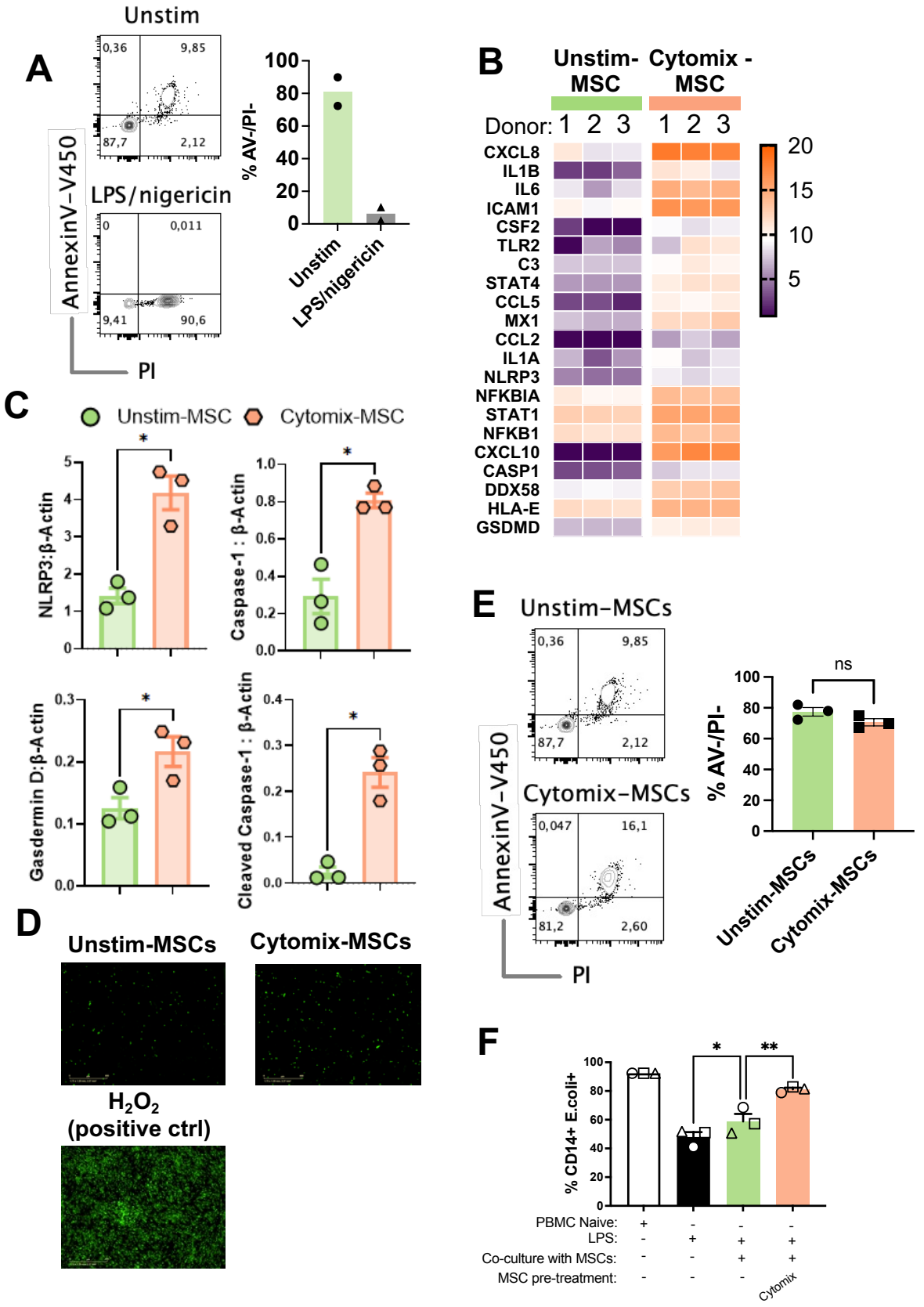
A
Unstim
0,36
9,85
87,7
2,12
LPS/nigericin
0
0,011
9,41
90,6
AnnexinV-V450
PI
% AV-/PI-
100
80
60
40
20
0
Unstim
LPS/nigericin
B
Unstim-MSC
Cytomix-MSC
Donor: 1 2 3 1 2 3
CXCL8
IL1B
IL6
ICAM1
CSF2
TLR2
C3
STAT4
CCL5
MX1
CCL2
IL1A
NLRP3
NFKBIA
STAT1
NFKB1
CXCL10
CASP1
DDX58
HLA-E
GSDMD
20
15
10
5
C
Unstim-MSC
Cytomix-MSC
NLRP3:β-Actin
Caspase-1 : β-Actin
Gasdermin D:β-Actin
Cleaved Caspase-1 : β-Actin
*
D
Unstim-MSCs
Cytomix-MSCs
H2O2
(positive ctrl)
E
Unstim-MSCs
0,36
9,85
87,7
2,12
Cytomix-MSCs
0,047
16,1
81,2
2,60
AnnexinV-V450
PI
% AV-/PI-
ns
Unstim-MSCs
Cytomix-MSCs
F
% CD14+ E.coli+
*
**
PBMC Naive:
LPS:
Co-culture with MSCs:
MSC pre-treatment:
Cytomix

Supplementary Figure 4. 4 Analysis of MSCs activated by sepsis-like stimuli. Related to Figure 4.4

A. Measurement of viability by Trypan blue of MSCs after stimulation by LPS and nigericin.
B. Heatmap of altered genes showing similar upregulation of transcriptomic profile of Cytomix-MSCs to Sepsis-MSCs.
C. Densitometry analysis of protein of Figure 4.4A.
D. Sepsis-like stimulation did not include caspase-3 activation.
E. Measurement of viability by Annexin V and PI staining of Unstim- and Cytomix-MSCs.
F. Qualification of phagocytic activity of monocyte post LPS after coculturing with Unstim- or Cytomix-MSCs derived from three donors.

n=3-6. The data shown as bar plot as mean ± SEM. comparison done by two tailed t-test. $*p<0.05$, $**p<0.01$, $***p<0.005$, $****p<0.001$

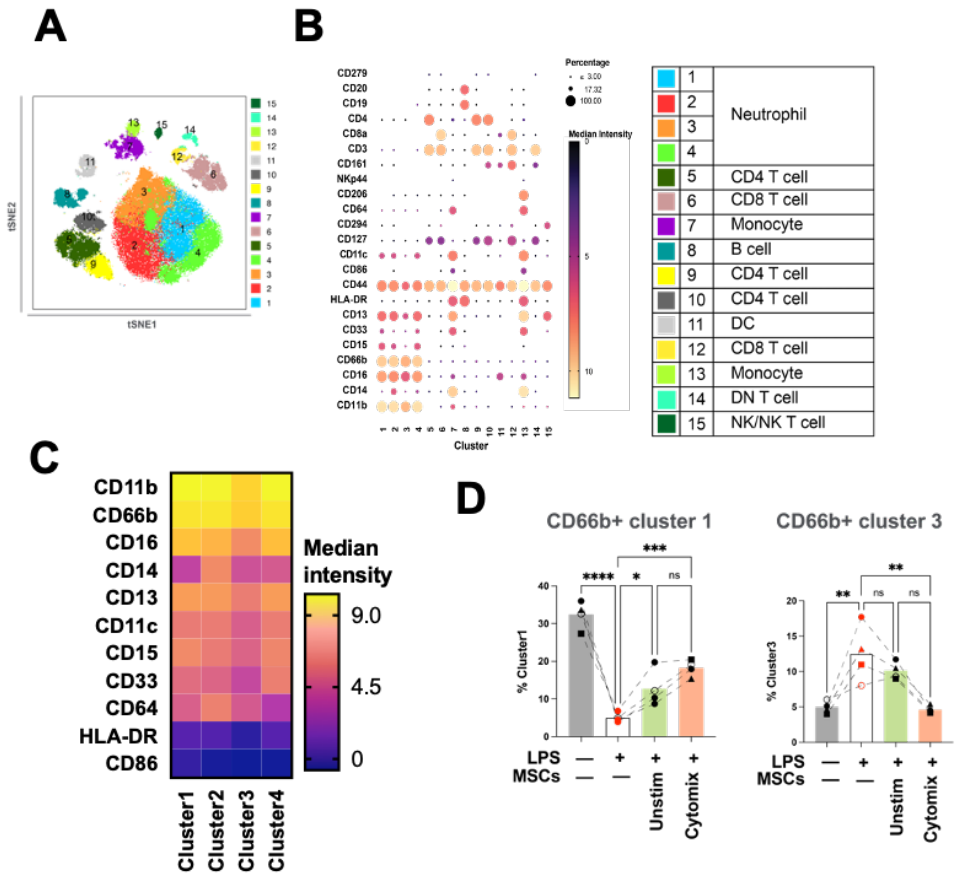

Supplementary Figure 4. 5 Dimensionality reduction analysis of effects of MSCs in acute inflammation model. Related to Figure 4.4.

A. tSNE map of totally leukocyte overlaid with clusters identified by Phenograph.
B. Dot plot showing expression of all 23 surface markers of each cluster.
C. Heatmap of neutrophil relevant marker expression in cluster 1, 2, 3 and 4.
D. Quantification of clusters 1 and 3.

For all experiments, n=3 healthy donor, with each patient represented by different symbol with the data shown as bar graph as mean ± SEM, ∗p<0.05, ∗∗p<0.01, ∗∗∗p<0.005, ∗∗∗∗p<0.001. Comparison done by one way ANOVA with Dunnett's comparison.

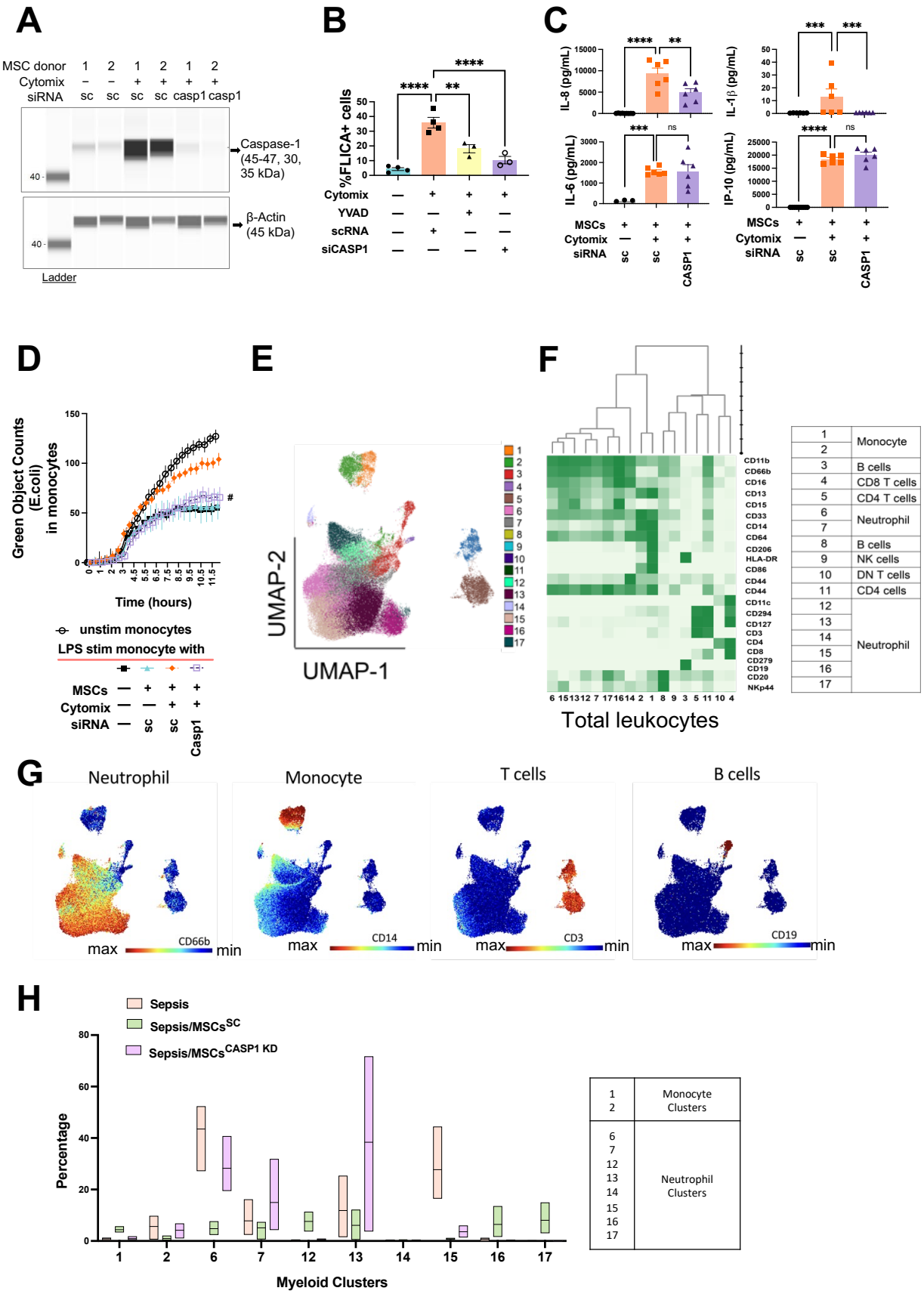
A
MSC donor 1 2 1 2 1 2
Cytomix – – + + + +
siRNA sc sc sc sc casp1 casp1
Caspase-1 (45-47, 30, 35 kDa)
β-Actin (45 kDa)
40
Ladder
B
%FLICA+ cells
Cytomix
YVAD
scRNA
siCASP1
C
IL-8 (pg/mL)
IL-1β (pg/mL)
IL-6 (pg/mL)
IP-10 (pg/mL)
MSCs
Cytomix
siRNA
sc
CASP1
D
Green Object Counts (E.coli) in monocytes
Time (hours)
unstim monocytes
LPS stim monocyte with
MSCs
Cytomix
siRNA
Casp1
E
UMAP-2
UMAP-1
F
CD11b
CD66b
CD16
CD13
CD15
CD33
CD14
CD64
CD206
HLA-DR
CD86
CD44
CD44
CD11c
CD294
CD127
CD3
CD4
CD8
CD279
CD19
CD20
NKp44
Total leukocytes
1 Monocyte
2
3 B cells
4 CD8 T cells
5 CD4 T cells
6 Neutrophil
7
8 B cells
9 NK cells
10 DN T cells
11 CD4 cells
12 Neutrophil
13
14
15
16
17
G
Neutrophil
Monocyte
T cells
B cells
CD66b
CD14
CD3
CD19
max
min
H
Sepsis
Sepsis/MSCs^SC
Sepsis/MSCs^CASP1 KD
Percentage
Myeloid Clusters
1 2 Monocyte Clusters
6 7 12 13 14 15 16 17 Neutrophil Clusters

Supplementary Figure 4. 6 Knockdown of caspase-1 rendered loss of MSC induced myeloid modulations. Related to Figure 4.5

A. Quantification of caspase-1 FLICA activity of $MSCs^{SC}$ and $MSCs^{CASP1}$
B. After caspase-1 silencing, Cytomix-MSCs lost the ability to secret IL-1 and IL-8 after sepsis like stimulation.
C. MSCs with siCASP1 knockdown were tested in in vitro phagocytosis assay and showed loss of ability to modulate monocyte phagocytosis. #, $p<0.05$ comparing Cytomix-MSCs vs Ctrl-MSCs.
D. UMAP map of totally leukocyte overlaid with clusters identified by FlowSOM.
E. Heatmap showing expression of all 23 surface markers of each cluster.
F. Color map of expression of lineage markers on UMAP.
G. Quantification of all myeloid clusters.

For A-C, n=4-6. The data shown as bar plot or dot plot as mean ± SEM. Multiple comparison done by one way ANOVA with Dunnett's comparison. $*p<0.05$, $**p<0.01$, $***p<0.005$, $****p<0.001$.# $p<0.05$ comparing $MSCs^{SC}$ vs $MSCs^{CASP1}$. For D-H, n=3 healthy donor, with each patient represented by different symbol with the data shown as bar graph as mean ± SEM. Comparison done by one way ANOVA with Dunnett's comparison.

4.2 Supplementary Table

Supplementary Table 4. 1 Patient Characteristics

	Healthy donor (n=6)	Septic patients (n=16)
Age, yr, median	38 (31 to 57)	73.5 (43 to 86)
Sex, female, n (%)	4 (67)	6 (38)
APACHE II score, median (range)		19.5 (10 to 31)
Mortality, n (%)		7 (44)
Infection source		
Bacteria		13
Unknown		3
Hematology		
White blood cell, $x10^9$/L, (range)		17.3 (6.3 to 100.7)
Red Blood Cell, $x10^{12}$/L /L, (range)		3.74 (2.05 to 4.42)
Platelet, $x10^9$/L, (range)		212.5 (27 to 667)
Neutrophil, $x10^9$/L, (range)		15.1 (0 to 78.0)
Lymphocyte, $x10^9$/L, (range)		0.45 (0.15 to 6)
Monocyte, $x10^9$/L, (range)		0.5 (0.2 to 1.5)
Biochemistry organ disfunction markers		
Renal, Creatine, U/L		127 (55 to 775)
Hepatic, bilirubin, umol/L		10 (4 to 28)
Lactate, umol/L		2.3 (0.8 to 12.3)

APACHE = Acute Physiology and Chronic Health Evaluation

Supplementary Table 4. 2 Key resource table

REAGENT or RESOURCE	SOURCE	IDENTIFIER
Antibodies		
Anti-human CD3- BUV395	BD Biosciences	564000, RRID:AB_2744382;
Anti-human CD19- BUV395	BD Biosciences	563551,RRID:AB_2738274
Anti-human CD11b-PerCP-eFluor710	e-Bioscience	563168, RRID:AB_2716860
Anti-human CD14-BV421	BD Biosciences	563743, RRID:AB_2744289
Anti-human CD15-Alexa647	BD Biosciences	562369, RRID:AB_11153125
Anti-human CD33-BB515	BD Biosciences	564588, RRID:AB_2738856
Anti-human HLA-DR-PE	BD Biosciences	555812 RRID:AB_477415 or RRID:AB_10899213
Anti-human CD66		
Anti-human CD69		
Anti-human CD15 (SSEA-1)	Fluidigm	3172021C
Anti-human CD294 (CRTH2)	Fluidigm	3163003C
Anti-human CD3	Fluidigm	3154003C
Anti-human CD279 (PD-1)	Fluidigm	3155009C
Anti-human CD14	Fluidigm	3148010C
Anti-human CD16	Fluidigm	3145008C
Anti-human CD19	Fluidigm	3169011C
Anti-human CD127 (IL-7Ra)	Fluidigm	3165008C
Anti-human CD13	Fluidigm	3160014C
Anti-human CD11b (Mac-1)	Fluidigm	3209003C
Anti-human CD44	Fluidigm	3150018C
Anti-human CD45	Fluidigm	3089003C
Anti-human CD66b	Fluidigm	3152011C
Anti-human CD33	Fluidigm	3158001C
Anti-human CD64	Fluidigm	3146006C
Anti-human CD206 (MMR)	Fluidigm	3168008C
Anti-human HLA-DR	Fluidigm	3173005C
Anti-human CD161	Fluidigm	3159004C
Anti-human CD20	Fluidigm	3171012C
Anti-human CD11c	Fluidigm	3147008C
Anti-human CD86	Fluidigm	3156008C
Anti-human Nkp44	R&D System	MAB22491, RRID:AB_2149423
Anti-human CD4	Fluidigm	3174004C
Anti-human CD8a	Fluidigm	3162015C
Anti-mouse antibodies:		
Anti-mouse CD3e	Fluidigm	3152004C
Anti-mouse CD4	Fluidigm	3145002C
Anti-mouse CD8a	Fluidigm	3168003C

Anti-mouse CD279 (PD-1)	Fluidigm	3159006C
Anti-mouse CD11b (Mac-1)	Fluidigm	3148003C
Anti-mouse CD11c	Fluidigm	3209005C
Anti-mouse I-A/I-E	Fluidigm	3174003C
Anti-mouse CD40	Fluidigm	3161020C
Anti-mouse CD80 (B7-1)	Fluidigm	3171008C
Anti-mouse CD86	Fluidigm	3172016C
Anti-mouse Ly-6C	Fluidigm	3162014C
Anti-mouse Ly-6G	Fluidigm	3141008C
Anti-mouse CD206 (MMR)	Fluidigm	3169021C
Anti-mouse CD64	Fluidigm	3151012C
Anti-mouse Siglec-F		
Anti-mouse CD27	Fluidigm	3150017C
Anti-mouse Ly-6A/E (Sca-1)	Fluidigm	3164005C
Anti-mouse CD45	Fluidigm	3089005C
Anti-mouse CD274 (PD-L1)	Fluidigm	3153016C
Anti-mouse F4/80	Fluidigm	3146008C
Anti-mouse CXCR2	R&D System	MAB2164, RRID:AB_358062
Anti-mouse CD161 (NK1.1)	Fluidigm	3170002C
Anti-mouse CD19	Fluidigm	3166015C
Anti-mouse CD25	R&D System	MAB9164-100
Anti-mouse CD69	Fluidigm	3143004C
Anti-Mouse CD3e BV 510	BD Biosciences	563024
Anti-Mouse CD45.2 PerCP-Cy™5.5	BD Biosciences	561096
Anti-Mouse CD4 BUV395	BD Biosciences	563790
Anti-Mouse CD8 BV421	BD Biosciences	563898
Anti-Mouse CD19 APC-R700	BD Biosciences	565473
Anti-mouse CD11b BV711	BD Biosciences	563168
Anti-Mouse Ly6G FITC	BD Biosciences	561105
Anti-Mouse Ly6C PE-CF594	BD Biosciences	562728
Anti-Mouse CD25 BV786	BD Biosciences	564023
NLRP3 Polyclonal antibody	Proteintech Group Inc	19771-1-AP, RRID:AB_10646484
Gasdermin D (L60) antibody	Cell Signaling Technology	93709, RRID:AB_2800210
Caspase 1/p20/p10 Polyclonal antibody	Proteintech Group Inc	22915-1-AP, RRID:AB_2876874
beta -Actin Antibody	R&D Systems, Inc. a Bio-Techne Brand	MAB8929
Bacterial and Virus Strains		
Biological Samples		
Healthy Whole Blood	STEMCELL Technologies & OHRI	REB ID: 20200312-01H

Bone Marrow Aspirates	Lonza, OHRI	REB ID: 20120929-01 H
Patient Blood Samples	The Ottawa Hospital	REB ID: #20190401-01H
Chemicals, Peptides, and Recombinant Proteins		
Polyinosinic–polycytidylic acid potassium salt	Sigma	P9582
BD Cytofix Fixation Buffer	BD Biosciences	554655
MSC NutriStem® XF Medium (Basal Medium + Supplement)	Biological Industries	05-200-1A-KT
Alveolar Epithelial Medium-phenol red free	ScienceCell	3201-PRF
Protease Inhibitor Cocktail	Sigma-Aldrich	535140-1ML
RIPA Lysis and Extraction Buffer	Thermo-Fisher	89901
Cell Signaling Lysis buffer	Sigma-Millipore	43-040
Criterion TGX Stain Free, 4-20%	Bio-Rad	5678095
Precision Plus Protein All Blue Standards	Bio-Rad	1610373
Clarity Max Western ECL Substrate,	Bio-Rad	1705062
Low Fluorescence PVDF membrane	Bio-Rad	1704275
pHrodo E.coli bioparticle	ThermoFisher	P35366
Dynabeads Human T-Activator CD3/CD28	GibCo	11161D
Annexin V	BD Biosciences	
Propidium iodide	ThermoFisher	
Stable-lyse V2	Smart Tube/Fisher	501351694
Stable-store V2	Smart Tube/Fisher	501351693
SARS-CoV-2 pseudovirus	Montana Molecular	C1110G
Critical Commercial Assays		
miRNeasy Mini Kit	Qiagen	217004
QuantiTect® Reverse Transcription Kit	Qiagen	205311
Bio-Plex Pro Mouse Cytokine 23-plex	Bio-Rad	M60009RDPD
ExoQuick-TC	SBI	EXOTC50A-1
Cell-ID 20-Plex Pd Barcoding Kit	Fluidigm	201060
MaxPar Fix-I buffer with iridium intercalator	Fluidigm	
EQ Four Element Calibration Beads	Fluidigm	
UltraComp eBeads™ Compensation Beads	Thermofisher	01-2222-41
MaxPar X8 labeling kit	Fluidigm	
Deposited Data		
Human reference genome GRCh38.13	NCBI Genome Reference	https://www.ncbi.nlm.nih.gov/assembly/GCF_000001405.39/
Experimental Models: Cell Lines		
Experimental Models: Organisms/Strains		

8-9 week old female mice	Charles River Laboratories	C57BL/6N
Oligonucleotides		
Recombinant DNA		
Software and Algorithms		
R software	r-project.org	https://www.r-project.org/
RStudio	RStudio Server Open-Source	https://www.rstudio.com/products/rstudio/#rstudio-desktop
FASTAQC	Babraham Institute	https://www.bioinformatics.babraham.ac.uk/projects/fastqc/
HISAT2	Kim, Paggi et al. 2019	https://daehwankimlab.github.io/hisat2/
Prism 9.0	Graphpad	https://www.graphpad.com/scientific-software/prism/
FlowJo X software	FlowJo, LLC	https://www.flowjo.com/
Bio-Plex Manager	Bio-Rad	https://www.bio-rad.com/en-ca/product/bio-plex-manager-software-standard-edition?ID=5846e84e-03a7-4599-a8ae-7ba5dd2c7684
QIAGEN Ingenuity Pathway Analysis	Qiagen	https://digitalinsights.qiagen.com/products-overview/discovery-insights-portfolio/analysis-and-visualization/qiagen-ipa/
DESeq2	Love, Huber et al. 2014	https://bioconductor.org/packages/release/bioc/html/DESeq2.html
g:GOSt (g:Profiler)	ELIXIR infrastructure	https://biit.cs.ut.ee/gprofiler/gost
ggplot2		https://ggplot2.tidyverse.org/

Complex Heatmap	Gu, Eils et al. 2016	http://bioconductor.org/packages/release/bioc/html/ComplexHeatmap.html
Cytofkit	Chen, Lau et al. 2016	https://github.com/JinmiaoChenLab/cytofkit
cytofAsinh		
Cytobank	[168]	https://cytobank.org/
FlowSOM	(Van Gassen, Callebaut et al. 2015	https://support.cytobank.org/hc/en-us/articles/360018965212-Introduction-to-FlowSOM-in-Cytobank
PhenoGraph	(Levine, Simonds et al. 2015	
String-db	Snel, Lehmann et al. 2000	https://string-db.org/
Omiq		
Other		
Bio-Plex 200	Bio-Rad	https://www.bio-rad.com/en-ca/product/bio-plex-200-systems?ID=715b85f1-6a4e-41b3-b5d9-80202d779e13
LSRFortessa cytometer	BD Bioscience	https://www.bdbiosciences.com/en-in/instruments/research-instruments/research-cell-analyzers/lsrfortessa
Attune NxT acoustic focusing cytometer	ThermoFisher	https://www.thermofisher.com/ca/en/home/life-science/cell-analysis/flow-cytometry/flow-cytometers/attune-nxt-flow-cytometer.html
Helios mass cytometer	Fluidigm	https://www.fluidigm.com/products/helios

Reference

1. Singer, M., Deutschman, C.S., Seymour, C.W., Shankar-Hari, M., Annane, D., Bauer, M., Bellomo, R., Bernard, G.R., Chiche, J.-D., Coopersmith, C.M., et al. (2016). The Third International Consensus Definitions for Sepsis and Septic Shock (Sepsis-3). JAMA *315*, 801-810. 10.1001/jama.2016.0287.

2. Genga, K.R., and Russell, J.A. (2017). Update of Sepsis in the Intensive Care Unit. Journal of Innate Immunity *9*, 441-455. 10.1159/000477419.

3. Thompson, M., Mei, S.H.J., Wolfe, D., Champagne, J., Fergusson, D., Stewart, D.J., Sullivan, K.J., Doxtator, E., Lalu, M., English, S.W., et al. (2020). Cell therapy with intravascular administration of mesenchymal stromal cells continues to appear safe: An updated systematic review and meta-analysis. EClinicalMedicine *19*, 100249. 10.1016/j.eclinm.2019.100249.

4. Gong, H., Chen, Y., Chen, M., Li, J., Zhang, H., Yan, S., and Lv, C. (2022). Advanced development and mechanism of sepsis-related acute respiratory distress syndrome. Frontiers in Medicine *9*. 10.3389/fmed.2022.1043859.

5. Thompson, B.T., Chambers, R.C., and Liu, K.D. (2017). Acute Respiratory Distress Syndrome. N Engl J Med *377*, 562. 10.1056/NEJMra1608077.

6. Ranieri, V.M., Rubenfeld, G.D., Thompson, B.T., Ferguson, N.D., Caldwell, E., Fan, E., Camporota, L., and Slutsky, A.S. (2012). Acute Respiratory Distress Syndrome: The Berlin Definition. JAMA *307*, 2526-2533. 10.1001/jama.2012.5669.

7. Ashbaugh, D.G., Bigelow, D.B., Petty, T.L., and Levine, B.E. (2005). Ashbaugh DG, Bigelow DB, Petty TL, Levine BE. Acute respiratory distress in adults. The Lancet, Saturday 12 August 1967. Critical care and resuscitation *7*, 60-61. 10.1016/S1441-2772(23)01574-0.

8. Luyt, C.-É., Combes, A., Trouillet, J.-L., Nieszkowska, A., and Chastre, J. (2011). Virus-induced acute respiratory distress syndrome: Epidemiology, management and outcome. La Presse Médicale *40*, e561-e568. 10.1016/j.lpm.2011.05.027.

9. The Acute Respiratory Distress Syndrome. (2004). Annals of Internal Medicine *141*, 460-470. 10.7326/0003-4819-141-6-200409210-00012 %m 15381520.

10. Diaz, A., Barria, P., Niederman, M., Restrepo, M.I., Dreyse, J., Fuentes, G., Couble, B., and Saldias, F. (2007). Etiology of community-acquired pneumonia in hospitalized patients in Chile : The increasing prevalence of respiratory viruses among classic pathogens. Chest *131*, 779-787. 10.1378/chest.06-1800.

11. Moine, P., Vercken, J.B., Chevret, S., Chastang, C., and Gajdos, P. (1994). Severe community-acquired pneumonia. Etiology, epidemiology, and prognosis factors.

French Study Group for Community-Acquired Pneumonia in the Intensive Care Unit. Chest *105*, 1487-1495.

12. Jennings, L.C., Anderson, T.P., Beynon, K.A., Chua, A., Laing, R.T.R., Werno, A.M., Young, S.A., Chambers, S.T., and Murdoch, D.R. (2008). Incidence and characteristics of viral community-acquired pneumonia in adults. Thorax *63*, 42-48. 10.1136/thx.2006.075077.

13. Johnstone, J., Majumdar, S.R., Fox, J.D., and Marrie, T.J. (2008). Human Metapneumovirus Pneumonia in Adults: Results of a Prospective Study. Clinical infectious diseases *46*, 571-574. 10.1086/526776.

14. Peiris, J.S.M., Yuen, K.Y., Osterhaus, A.D.M.E., and Stöhr, K. (2003). The Severe Acute Respiratory Syndrome. New England Journal of Medicine *349*, 2431-2441. 10.1056/nejmra032498.

15. Yang, X., Yu, Y., Xu, J., Shu, H., Xia, J., Liu, H., Wu, Y., Zhang, L., Yu, Z., Fang, M., et al. (2020). Clinical course and outcomes of critically ill patients with SARS-CoV-2 pneumonia in Wuhan, China: a single-centered, retrospective, observational study. Lancet Respir Med *8*, 475-481. 10.1016/S2213-2600(20)30079-5.

16. Claas, E.C.J., Osterhaus, A.D.M.E., van Beek, R., De Jong, J.C., Rimmelzwaan, G.F., Senne, D.A., Krauss, S., Shortridge, K.F., and Webster, R.G. (1998). Human influenza A H5N1 virus related to a highly pathogenic avian influenza virus. The Lancet (British edition) *351*, 472-477. 10.1016/S0140-6736(97)11212-0.

17. Domínguez-Cherit, G., Lapinsky, S.E., Macias, A.E., Pinto, R., Espinosa-Perez, L., de la Torre, A., Poblano-Morales, M., Baltazar-Torres, J.A., Bautista, E., Martinez, A., et al. (2009). Critically Ill Patients With 2009 Influenza A(H1N1) in Mexico. JAMA : the journal of the American Medical Association *302*, 1880-1887. 10.1001/jama.2009.1536.

18. Kumar, A., Zarychanski, R., Pinto, R., Cook, D.J., Marshall, J., Lacroix, J., Stelfox, T., Bagshaw, S., Choong, K., Lamontagne, F., et al. (2009). Critically Ill Patients With 2009 Influenza A(H1N1) Infection in Canada. JAMA : the journal of the American Medical Association *302*, 1872-1879. 10.1001/jama.2009.1496.

19. Presanis, A.M., Angelis, D.D., Hagy, A., Reed, C., Riley, S., Cooper, B.S., Finelli, L., Biedrzycki, P., Lipsitch, M., and Team3¶, S.F. (2009). The Severity of Pandemic H1N1 Influenza in the United States, from April to July 2009: A Bayesian Analysis: e1000207. PLoS medicine *6*. 10.1371/journal.pmed.1000207.

20. Wu, F., Zhao, S., Yu, B., Chen, Y.-M., Wang, W., Song, Z.-G., Hu, Y., Tao, Z.-W., Tian, J.-H., Pei, Y.-Y., et al. (2020). A new coronavirus associated with human respiratory disease in China. Nature *579*, 265-269. 10.1038/s41586-020-2008-3.

21. Arraes, S.M.A., Freitas, M.S., Da Silva, S.V., De Paula Neto, H.A., Alves-Filho, J.C., Martins, M.A., Basile-Filho, A., Tavares-Murta, B.M., Barja-Fidalgo, C., and Cunha, F.Q. (2006). Impaired neutrophil chemotaxis in sepsis associates with GRK expression and inhibition of actin assembly and tyrosine phosphorylation. Blood *108*, 2906-2913. 10.1182/blood-2006-05-024638.

22. Bone, R.C., Grodzin, C.J., and Balk, R.A. (1997). Sepsis: A New Hypothesis for Pathogenesis of the Disease Process. Chest *112*, 235-243. 10.1378/chest.112.1.235.

23. Deng, Y., Zhang, Y., Ye, L., Zhang, T., Cheng, J., Chen, G., Zhang, Q., and Yang, Y. (2016). Umbilical Cord-derived Mesenchymal Stem Cells Instruct Monocytes Towards an IL10-producing Phenotype by Secreting IL6 and HGF. Scientific Reports *6*, 37566. 10.1038/srep37566.

24. Souza-Moreira, L., Tan, Y., Wang, Y., Wang, J.-P., Salkhordeh, M., Virgo, J., Florian, M., Murray, A.B.P., Watpool, I., McIntyre, L., et al. (2022). Poly(I:C) enhances mesenchymal stem cell control of myeloid cells from COVID-19 patients. iScience *25*. 10.1016/j.isci.2022.104188.

25. Bruzzesi, E., Ranzenigo, M., Castagna, A., and Spagnuolo, V. (2021). Neutralizing monoclonal antibodies for the treatment and prophylaxis of SARS-CoV-2 infection. New Microbiol *44*, 135-144.

26. Leng, Z., Zhu, R., Hou, W., Feng, Y., Yang, Y., Han, Q., Shan, G., Meng, F., Du, D., Wang, S., et al. (2020). Transplantation of ACE2. Aging Dis *11*, 216-228. 10.14336/AD.2020.0228.

27. Metcalfe, S.M. (2020). Mesenchymal stem cells and management of COVID-19 pneumonia. Med Drug Discov *5*, 100019. 10.1016/j.medidd.2020.100019.

28. McIntyre, L.A., Stewart, D.J., Mei, S.H.J., Courtman, D., Watpool, I., Granton, J., Marshall, J., Dos Santos, C., Walley, K.R., Winston, B.W., et al. (2018). Cellular Immunotherapy for Septic Shock. A Phase I Clinical Trial. Am J Respir Crit Care Med *197*, 337-347. 10.1164/rccm.201705-1006OC.

29. Squillaro, T., Peluso, G., and Galderisi, U. (2016). Clinical Trials With Mesenchymal Stem Cells: An Update. Cell Transplant *25*, 829-848. 10.3727/096368915X689622.

30. Ringdén, O., Uzunel, M., Rasmusson, I., Remberger, M., Sundberg, B., Lönnies, H., Marschall, H.U., Dlugosz, A., Szakos, A., Hassan, Z., et al. (2006). Mesenchymal stem cells for treatment of therapy-resistant graft-versus-host disease. Transplantation *81*, 1390-1397. 10.1097/01.tp.0000214462.63943.14.

31. Lanzoni, G., Linetsky, E., Correa, D., Messinger Cayetano, S., Alvarez, R.A., Kouroupis, D., Alvarez Gil, A., Poggioli, R., Ruiz, P., Marttos, A.C., et al. (2021).

Umbilical cord mesenchymal stem cells for COVID-19 acute respiratory distress syndrome: A double-blind, phase 1/2a, randomized controlled trial. Stem Cells Transl Med *10*, 660-673. 10.1002/sctm.20-0472.

32. Matthay, M.A., Calfee, C.S., Zhuo, H., Thompson, B.T., Wilson, J.G., Levitt, J.E., Rogers, A.J., Gotts, J.E., Wiener-Kronish, J.P., Bajwa, E.K., et al. (2019). Treatment with allogeneic mesenchymal stromal cells for moderate to severe acute respiratory distress syndrome (START study): a randomised phase 2a safety trial. Lancet Respir Med *7*, 154-162. 10.1016/S2213-2600(18)30418-1.

33. Bellingan, G., Jacono, F., Bannard-Smith, J., Brealey, D., Meyer, N., Thickett, D., Young, D., Bentley, A., McVerry, B.J., Wunderink, R.G., et al. (2022). Safety and efficacy of multipotent adult progenitor cells in acute respiratory distress syndrome (MUST-ARDS): a multicentre, randomised, double-blind, placebo-controlled phase 1/2 trial. Intensive Care Med *48*, 36-44. 10.1007/s00134-021-06570-4.

34. UniProt, C. (2021). UniProt: the universal protein knowledgebase in 2021. Nucleic Acids Res *49*, D480-D489. 10.1093/nar/gkaa1100.

35. Zhu, X., He, Z., Yuan, J., Wen, W., Huang, X., Hu, Y., Lin, C., Pan, J., Li, R., Deng, H., et al. (2015). IFITM3-containing exosome as a novel mediator for anti-viral response in dengue virus infection. Cell Microbiol *17*, 105-118. 10.1111/cmi.12339.

36. Zou, X., Yuan, M., Zhang, T., Zheng, N., and Wu, Z. (2021). EVs Containing Host Restriction Factor IFITM3 Inhibited ZIKV Infection of Fetuses in Pregnant Mice through Trans-placenta Delivery. Mol Ther *29*, 176-190. 10.1016/j.ymthe.2020.09.026.

37. Khatri, M., and Saif, Y.M. (2013). Influenza virus infects bone marrow mesenchymal stromal cells in vitro: implications for bone marrow transplantation. Cell Transplant *22*, 461-468. 10.3727/096368912X656063.

38. Hoffmann, J.J. (2009). Neutrophil CD64: a diagnostic marker for infection and sepsis. Clin Chem Lab Med *47*, 903-916. 10.1515/CCLM.2009.224.

39. Noronha, N.C., Mizukami, A., Caliári-Oliveira, C., Cominal, J.G., Rocha, J.L.M., Covas, D.T., Swiech, K., and Malmegrim, K.C.R. (2019). Priming approaches to improve the efficacy of mesenchymal stromal cell-based therapies. Stem Cell Res Ther *10*, 131. 10.1186/s13287-019-1224-y.

40. Waterman, R.S., Tomchuck, S.L., Henkle, S.L., and Betancourt, A.M. (2010). A New Mesenchymal Stem Cell (MSC) Paradigm: Polarization into a Pro-Inflammatory MSC1 or an Immunosuppressive MSC2 Phenotype. PLoS ONE *5*, e10088. 10.1371/journal.pone.0010088.

41. Zhao, X., Liu, D., Gong, W., Zhao, G., Liu, L., Yang, L., and Hou, Y. (2014). The toll-like receptor 3 ligand, poly(I:C), improves immunosuppressive function and therapeutic effect of mesenchymal stem cells on sepsis via inhibiting MiR-143. Stem Cells *32*, 521-533. 10.1002/stem.1543.

42. Pierce, L.M., and Kurata, W.E. (2021). Priming With Toll-Like Receptor 3 Agonist Poly(I:C) Enhances Content of Innate Immune Defense Proteins but Not MicroRNAs in Human Mesenchymal Stem Cell-Derived Extracellular Vesicles. Front Cell Dev Biol *9*, 676356. 10.3389/fcell.2021.676356.

43. Prelli Bozzo, C., Nchioua, R., Volcic, M., Koepke, L., Kruger, J., Schutz, D., Heller, S., Sturzel, C.M., Kmiec, D., Conzelmann, C., et al. (2021). IFITM proteins promote SARS-CoV-2 infection and are targets for virus inhibition in vitro. Nat Commun *12*, 4584. 10.1038/s41467-021-24817-y.

44. Wu, X., Dao Thi, V.L., Huang, Y., Billerbeck, E., Saha, D., Hoffmann, H.H., Wang, Y., Silva, L.A.V., Sarbanes, S., Sun, T., et al. (2018). Intrinsic Immunity Shapes Viral Resistance of Stem Cells. Cell *172*, 423-438.e425. 10.1016/j.cell.2017.11.018.

45. Rebouillat, D., and Hovanessian, A.G. (1999). The human 2',5'-oligoadenylate synthetase family: interferon-induced proteins with unique enzymatic properties. J Interferon Cytokine Res *19*, 295-308. 10.1089/107999099313992.

46. Zhou, S., Butler-Laporte, G., Nakanishi, T., Morrison, D.R., Afilalo, J., Afilalo, M., Laurent, L., Pietzner, M., Kerrison, N., Zhao, K., et al. (2021). A Neanderthal OAS1 isoform protects individuals of European ancestry against COVID-19 susceptibility and severity. Nature Medicine *27,* 659-667. doi:10.1038/s41591-021-01281-1.

47. Hefti, H.P., Frese, M., Landis, H., Di Paolo, C., Aguzzi, A., Haller, O., and Pavlovic, J. (1999). Human MxA protein protects mice lacking a functional alpha/beta interferon system against La crosse virus and other lethal viral infections. J Virol *73*, 6984-6991. 10.1128/JVI.73.8.6984-6991.1999.

48. Schwemmle, M., Weining, K.C., Richter, M.F., Schumacher, B., and Staeheli, P. (1995). Vesicular stomatitis virus transcription inhibited by purified MxA protein. Virology *206*, 545-554. 10.1016/s0042-6822(95)80071-9.

49. Wrensch, F., Winkler, M., and Pohlmann, S. (2014). IFITM proteins inhibit entry driven by the MERS-coronavirus spike protein: evidence for cholesterol-independent mechanisms. Viruses *6*, 3683-3698. 10.3390/v6093683.

50. Shi, G., Kenney, A.D., Kudryashova, E., Zani, A., Zhang, L., Lai, K.K., Hall-Stoodley, L., Robinson, R.T., Kudryashov, D.S., Compton, A.A., and Yount, J.S. (2021). Opposing activities of IFITM proteins in SARS-CoV-2 infection. EMBO J *40*, e106501. 10.15252/embj.2020106501.

51. Qian, X., Xu, C., Fang, S., Zhao, P., Wang, Y., Liu, H., Yuan, W., and Qi, Z. (2016). Exosomal MicroRNAs Derived From Umbilical Mesenchymal Stem Cells Inhibit Hepatitis C Virus Infection. Stem Cells Transl Med *5*, 1190-1203. 10.5966/sctm.2015-0348.

52. Lauder, S.N., Jones, E., Smart, K., Bloom, A., Williams, A.S., Hindley, J.P., Ondondo, B., Taylor, P.R., Clement, M., Fielding, C., et al. (2013). Interleukin-6 limits influenza-induced inflammation and protects against fatal lung pathology. European Journal of Immunology *43*, 2613-2625. 10.1002/eji.201243018.

53. Yang, R., Masters, A.R., Fortner, K.A., Champagne, D.P., Yanguas-Casás, N., Silberger, D.J., Weaver, C.T., Haynes, L., and Rincon, M. (2016). IL-6 promotes the differentiation of a subset of naive CD8+ T cells into IL-21–producing B helper CD8+ T cells. Journal of Experimental Medicine *213*, 2281-2291. 10.1084/jem.20160417.

54. Trifilo, M.J., Montalto-Morrison, C., Stiles, L.N., Hurst, K.R., Hardison, J.L., Manning, J.E., Masters, P.S., and Lane, T.E. (2004). CXC Chemokine Ligand 10 Controls Viral Infection in the Central Nervous System: Evidence for a Role in Innate Immune Response through Recruitment and Activation of Natural Killer Cells. Journal of Virology *78*, 585-594. 10.1128/jvi.78.2.585-594.2004.

55. Held, K.S., Chen, B.P., Kuziel, W.A., Rollins, B.J., and Lane, T.E. (2004). Differential roles of CCL2 and CCR2 in host defense to coronavirus infection. Virology *329*, 251-260. 10.1016/j.virol.2004.09.006.

56. Vanderbeke, L., Van Mol, P., Van Herck, Y., De Smet, F., Humblet-Baron, S., Martinod, K., Antoranz, A., Arijs, I., Boeckx, B., Bosisio, F.M., et al. (2021). Monocyte-driven atypical cytokine storm and aberrant neutrophil activation as key mediators of COVID-19 disease severity. Nature Communications *12*, 1-15. doi:10.1038/s41467-021-24360-w.

57. Schulte-Schrepping, J., Reusch, N., Paclik, D., Bassler, K., Schlickeiser, S., Zhang, B., Kramer, B., Krammer, T., Brumhard, S., Bonaguro, L., et al. (2020). Severe COVID-19 Is Marked by a Dysregulated Myeloid Cell Compartment. Cell *182*, 1419-1440 e1423. 10.1016/j.cell.2020.08.001.

58. Barnes, B.J., Adrover, J.M., Baxter-Stoltzfus, A., Borczuk, A., Cools-Lartigue, J., Crawford, J.M., Dassler-Plenker, J., Guerci, P., Huynh, C., Knight, J.S., et al. (2020). Targeting potential drivers of COVID-19: Neutrophil extracellular traps. J Exp Med *217*, e20200652. 10.1084/jem.20200652.

59. Chevrier, S., Zurbuchen, Y., Cervia, C., Adamo, S., Raeber, M.E., de Souza, N., Sivapatham, S., Jacobs, A., Bachli, E., Rudiger, A., et al. (2021). A distinct innate immune signature marks progression from mild to severe COVID-19. Cell Rep Med *2*, 100166. 10.1016/j.xcrm.2020.100166.

60. Trombetta, A.C., Farias, G.B., Gomes, A.M.C., Godinho-Santos, A., Rosmaninho, P., Conceição, C.M., Laia, J., Santos, D.F., Almeida, A.R.M., Mota, C., et al. (2021). Severe COVID-19 Recovery Is Associated with Timely Acquisition of a Myeloid Cell Immune-Regulatory Phenotype. Front Immunol *12*, 691725. 10.3389/fimmu.2021.691725.

61. Tan, Y., Salkhordeh, M., Wang, J.P., McRae, A., Souza-Moreira, L., McIntyre, L., Stewart, D.J., and Mei, S.H.J. (2019). Thawed Mesenchymal Stem Cell Product Shows Comparable Immunomodulatory Potency to Cultured Cells In Vitro and in Polymicrobial Septic Animals. Sci Rep *9*, 18078. 10.1038/s41598-019-54462-x.

62. Dominici, M., Le Blanc, K., Mueller, I., Slaper-Cortenbach, I., Marini, F., Krause, D., Deans, R., Keating, A., Prockop, D., and Horwitz, E. (2006). Minimal criteria for defining multipotent mesenchymal stromal cells. The International Society for Cellular Therapy position statement. Cytotherapy *8*, 315-317.

63. Kim, D., Paggi, J.M., Park, C., Bennett, C., and Salzberg, S.L. (2019). Graph-based genome alignment and genotyping with HISAT2 and HISAT-genotype. Nat Biotechnol *37*, 907-915. 10.1038/s41587-019-0201-4.

64. Love, M.I., Huber, W., and Anders, S. (2014). Moderated estimation of fold change and dispersion for RNA-seq data with DESeq2. Genome Biol *15*, 550. 10.1186/s13059-014-0550-8.

65. Gu, Z., Eils, R., and Schlesner, M. (2016). Complex heatmaps reveal patterns and correlations in multidimensional genomic data. Bioinformatics *32*, 2847-2849. 10.1093/bioinformatics/btw313.

66. Snel, B., Lehmann, G., Bork, P., and Huynen, M.A. (2000). STRING: a web-server to retrieve and display the repeatedly occurring neighbourhood of a gene. Nucleic Acids Res *28*, 3442-3444. 10.1093/nar/28.18.3442.

67. Kotecha, N., Krutzik, P.O., and Irish, J.M. (2010). Web-based analysis and publication of flow cytometry experiments. Curr Protoc Cytom *Chapter 10*, Unit10 17. 10.1002/0471142956.cy1017s53.

68. Van Gassen, S., Callebaut, B., Van Helden, M.J., Lambrecht, B.N., Demeester, P., Dhaene, T., and Saeys, Y. (2015). FlowSOM: Using self-organizing maps for visualization and interpretation of cytometry data. Cytometry A *87*, 636-645. 10.1002/cyto.a.22625.

69. Levine, J.H., Simonds, E.F., Bendall, S.C., Davis, K.L., Amir, e.-A., Tadmor, M.D., Litvin, O., Fienberg, H.G., Jager, A., Zunder, E.R., et al. (2015). Data-Driven Phenotypic Dissection of AML Reveals Progenitor-like Cells that Correlate with Prognosis. Cell *162*, 184-197. 10.1016/j.cell.2015.05.047.

70. Chen, H., Lau, M.C., Wong, M.T., Newell, E.W., Poidinger, M., and Chen, J. (2016). Cytofkit: A Bioconductor Package for an Integrated Mass Cytometry Data Analysis Pipeline. PLoS Comput Biol *12*, e1005112. 10.1371/journal.pcbi.1005112.

71. ARDS, D.T.F. (2012). Acute Respiratory Distress Syndrome. JAMA *307*. 10.1001/jama.2012.5669.

72. Matthay, M.A., Zemans, R.L., Zimmerman, G.A., Arabi, Y.M., Beitler, J.R., Mercat, A., Herridge, M., Randolph, A.G., and Calfee, C.S. (2019). Acute respiratory distress syndrome. Nature Reviews Disease Primers *5*. 10.1038/s41572-019-0069-0.

73. Bellani, G., Laffey, J.G., Pham, T., Fan, E., Brochard, L., Esteban, A., Gattinoni, L., Van Haren, F., Larsson, A., Mcauley, D.F., et al. (2016). Epidemiology, Patterns of Care, and Mortality for Patients With Acute Respiratory Distress Syndrome in Intensive Care Units in 50 Countries. JAMA *315*, 788. 10.1001/jama.2016.0291.

74. Flerlage, T., Boyd, D.F., Meliopoulos, V., Thomas, P.G., and Schultz-Cherry, S. (2021). Influenza virus and SARS-CoV-2: pathogenesis and host responses in the respiratory tract. Nature Reviews Microbiology *19*, 425-441. 10.1038/s41579-021-00542-7.

75. Herold, S., Becker, C., Ridge, K.M., and Budinger, G.R.S. (2015). Influenza virus-induced lung injury: pathogenesis and implications for treatment. European Respiratory Journal *45*, 1463-1478. 10.1183/09031936.00186214.

76. Peteranderl, C., Schmoldt, C., and Herold, S. (2016). Human Influenza Virus Infections. Seminars in Respiratory and Critical Care Medicine *37*, 487-500. 10.1055/s-0036-1584801.

77. Skehel, J.J., and Wiley, D.C. (2003). Receptor Binding and Membrane Fusion in Virus Entry: The Influenza Hemagglutinin. https://doi.org/10.1146/annurev.biochem.69.1.531. 10.1146/annurev.biochem.69.1.531.

78. Yang, Z.-Y., Wei, C.-J., Kong, W.-P., Wu, L., Xu, L., Smith, D.F., and Nabel, G.J. (2007). Immunization by Avian H5 Influenza Hemagglutinin Mutants with Altered Receptor Binding Specificity. Science *317*, 825-828. 10.1126/science.1135165.

79. Ventetuolo, C.E., and Muratore, C.S. (2014). Extracorporeal Life Support in Critically Ill Adults. American Journal of Respiratory and Critical Care Medicine *190*, 497-508. 10.1164/rccm.201404-0736ci.

80. Le Blanc, K., and Ringdén, O. (2007). Immunomodulation by mesenchymal stem cells and clinical experience. Journal of Internal Medicine *262*, 509-525. 10.1111/j.1365-2796.2007.01844.x.

81. Mei, S.H.J., Mccarter, S.D., Deng, Y., Parker, C.H., Liles, W.C., and Stewart, D.J. (2007). Prevention of LPS-Induced Acute Lung Injury in Mice by Mesenchymal Stem Cells Overexpressing Angiopoietin 1. PLoS Medicine *4*, e269. 10.1371/journal.pmed.0040269.

82. Mei, S.H., Dos Santos, C.C., and Stewart, D.J. (2016). Advances in Stem Cell and Cell-Based Gene Therapy Approaches for Experimental Acute Lung Injury: A Review of Preclinical Studies. Hum Gene Ther *27*, 802-812. 10.1089/hum.2016.063.

83. Khoury, M., J, C., FF, C., FE, F., PRM, R., and DJ, W. (2020). Current status of cell-based therapies for respiratory virus infections: applicability to COVID-19. The European respiratory journal *55*. 10.1183/13993003.00858-2020.

84. Li, Y., Xu, J., Shi, W., Chen, C., Shao, Y., Zhu, L., Lu, W., and Han, X. (2016). Mesenchymal stromal cell treatment prevents H9N2 avian influenza virus-induced acute lung injury in mice. Stem Cell Research & Therapy *7*, 1-11. doi:10.1186/s13287-016-0395-z.

85. Chan, M.C.W., Kuok, D.I.T., Leung, C.Y.H., Hui, K.P.Y., Valkenburg, S.A., Lau, E.H.Y., Nicholls, J.M., Fang, X., Guan, Y., Lee, J.W., et al. (2016). Human mesenchymal stromal cells reduce influenza A H5N1-associated acute lung injury in vitro and in vivo. Proceedings of the National Academy of Sciences *113*, 3621-3626. 10.1073/pnas.1601911113.

86. Darwish, I., Banner, D., Mubareka, S., Kim, H., Besla, R., Kelvin, D.J., Kain, K.C., and Liles, W.C. (2013). Mesenchymal Stromal (Stem) Cell Therapy Fails to Improve Outcomes in Experimental Severe Influenza. PLoS ONE *8*, e71761. 10.1371/journal.pone.0071761.

87. Gotts, J.E., Abbott, J., and Matthay, M.A. (2014). Influenza causes prolonged disruption of the alveolar-capillary barrier in mice unresponsive to mesenchymal stem cell therapy. https://doi.org/10.1152/ajplung.00110.2014. 10.1152/ajplung.00110.2014.

88. Lam, J.H., and Baumgarth, N. (2019). The Multifaceted B Cell Response to Influenza Virus. J Immunol *202*, 351-359. 10.4049/jimmunol.1801208.

89. La Gruta, N.L., and Turner, S.J. (2014). T cell mediated immunity to influenza: mechanisms of viral control. Trends Immunol *35*, 396-402. 10.1016/j.it.2014.06.004.

90. Singer, M., Deutschman, C.S., Seymour, C.W., Shankar-Hari, M., Annane, D., Bauer, M., Bellomo, R., Bernard, G.R., Chiche, J.-D., Coopersmith, C.M., et al. (2016). The Third International Consensus Definitions for Sepsis and Septic Shock (Sepsis-3). JAMA *315*, 801. 10.1001/jama.2016.0287.

91. Hotchkiss, R.S., Moldawer, L.L., Opal, S.M., Reinhart, K., Turnbull, I.R., and Vincent, J.-L. (2016). Sepsis and septic shock. Nature Reviews Disease Primers *2*, 16045. 10.1038/nrdp.2016.45.

92. Mortaz, E., Alipoor, S.D., Adcock, I.M., Mumby, S., and Koenderman, L. (2018). Update on neutrophil function in severe inflammation. Frontiers in immunology *9*, 2171-2171. 10.3389/fimmu.2018.02171.

93. Brown, K.A., Brain, S.D., Pearson, J.D., Edgeworth, J.D., Lewis, S.M., and Treacher, D.F. (2006). Neutrophils in development of multiple organ failure in sepsis. The Lancet (British edition) *368*, 157-169. 10.1016/S0140-6736(06)69005-3.

94. Sônego, F., Castanheira, F.V.E.S., Ferreira, R.G., Kanashiro, A., Leite, C.A.V.G., Nascimento, D.C., Colón, D.F., Borges, V.d.F., Alves-Filho, J.C., and Cunha, F.Q. (2016). Paradoxical Roles of the Neutrophil in Sepsis: Protective and Deleterious. Frontiers in immunology *7*, 155-155. 10.3389/fimmu.2016.00155.

95. Munoz, C., Carlet, J., Fitting, C., Misset, B., Blériot, J.P., and Cavaillon, J.M. (1991). Dysregulation of in vitro cytokine production by monocytes during sepsis. Journal of Clinical Investigation *88*, 1747-1754. 10.1172/jci115493.

96. Le Blanc, K., and Mougiakakos, D. (2012). Multipotent mesenchymal stromal cells and the innate immune system. Nat Rev Immunol *12*, 383-396. 10.1038/nri3209.

97. Heldring, N., Mäger, I., Wood, M.J., Le Blanc, K., and Andaloussi, S.E. (2015). Therapeutic Potential of Multipotent Mesenchymal Stromal Cells and Their Extracellular Vesicles. Hum Gene Ther *26*, 506-517. 10.1089/hum.2015.072.

98. Souza-Moreira, L., Soares, V.C., Dias, S.D.S.G., and Bozza, P.T. (2019). Adipose-derived Mesenchymal Stromal Cells Modulate Lipid Metabolism and Lipid Droplet Biogenesis via AKT/mTOR -PPARγ Signalling in Macrophages. Sci Rep *9*, 20304. 10.1038/s41598-019-56835-8.

99. Mei, S.H.J., Haitsma, J.J., Santos, C.C.D., Deng, Y., Lai, P.F.H., Slutsky, A.S., Liles, W.C., and Stewart, D.J. (2012). Mesenchymal Stem Cells Reduce Inflammation while Enhancing Bacterial Clearance and Improving Survival in Sepsis. https://doi.org/10.1164/rccm.201001-0010OC. 10.1164/rccm.201001-0010OC.

100. Mei, S.H.J., Haitsma, J.J., Dos Santos, C.C., Deng, Y., Lai, P.F.H., Slutsky, A.S., Liles, W.C., and Stewart, D.J. (2010). Mesenchymal Stem Cells Reduce Inflammation while Enhancing Bacterial Clearance and Improving Survival in Sepsis. American Journal of Respiratory and Critical Care Medicine *182*, 1047-1057. 10.1164/rccm.201001-0010OC.

101. Németh, K., Leelahavanichkul, A., Yuen, P.S.T., Mayer, B., Parmelee, A., Doi, K., Robey, P.G., Leelahavanichkul, K., Koller, B.H., Brown, J.M., et al. (2009). Bone

marrow stromal cells attenuate sepsis via prostaglandin E(2)-dependent reprogramming of host macrophages to increase their interleukin-10 production. Nature Medicine *15*, 42-49. 10.1038/nm.1905.

102. Hall, S.R.R., Tsoyi, K., Ith, B., Padera, R.F., Lederer, J.A., Wang, Z., Liu, X., and Perrella, M.A. (2013). Mesenchymal Stromal Cells Improve Survival During Sepsis in the Absence of Heme Oxygenase-1: The Importance of Neutrophils. Stem Cells *31*, 397-407. 10.1002/stem.1270.

103. Tomchuck, S.L., Department of Microbiology and Immunology, T.U.H.S.C., New Orleans, Louisiana, USA, Zwezdaryk, K.J., Department of Microbiology and Immunology, T.U.H.S.C., New Orleans, Louisiana, USA, Coffelt, S.B., Department of Microbiology and Immunology, T.U.H.S.C., New Orleans, Louisiana, USA, Waterman, R.S., Department of Medicine, T.U.H.S.C., New Orleans, Louisiana, USA, Danka, E.S., Department of Microbiology and Immunology, T.U.H.S.C., New Orleans, Louisiana, USA, et al. (2023). Toll-Like Receptors on Human Mesenchymal Stem Cells Drive Their Migration and Immunomodulating Responses. Stem Cells *26*, 99-107. 10.1634/stemcells.2007-0563.

104. Docheva, D., Popov, C., Mutschler, W., and Schieker, M. (2007). Human mesenchymal stem cells in contact with their environment: surface characteristics and the integrin system. Journal of Cellular and Molecular Medicine *11*, 21-38. 10.1111/j.1582-4934.2007.00001.x.

105. Prockop, D.J., and Youn Oh, J. (2012). Mesenchymal Stem/Stromal Cells (MSCs): Role as Guardians of Inflammation. Molecular Therapy *20*, 14-20. 10.1038/mt.2011.211.

106. Souza-Moreira, L., Tan, Y., Wang, Y., Wang, J.-P., Salkhordeh, M., Virgo, J., Florian, M., Murray, A.B.P., Watpool, I., Mcintyre, L., et al. (2022). Poly(I:C) enhances mesenchymal stem cell control of myeloid cells from COVID-19 patients. iScience *25*, 104188. 10.1016/j.isci.2022.104188.

107. JJ, H. (2009). Neutrophil CD64: a diagnostic marker for infection and sepsis. Clinical chemistry and laboratory medicine *47*. 10.1515/CCLM.2009.224.

108. Barth, E., Fischer, G., Schneider, E.M., Wollmeyer, J., Georgieff, M., and Weiss, M. (2001). DIFFERENCES IN THE EXPRESSION OF CD64 AND mCD14 ON POLYMORPHONUCLEAR CELLS AND ON MONOCYTES IN PATIENTS WITH SEPTIC SHOCK. Cytokine (Philadelphia, Pa.) *14*, 299-302. 10.1006/cyto.2001.0880.

109. McIntyre, L.A., Stewart, D.J., Mei, S.H.J., Courtman, D., Watpool, I., Granton, J., Marshall, J., Santos, C.d., Walley, K.R., Winston, B.W., et al. (2018). Cellular Immunotherapy for Septic Shock. A Phase I Clinical Trial. https://doi.org/10.1164/rccm.201705-1006OC. 10.1164/rccm.201705-1006OC.

110. Pang, S.H.M., D'Rozario, J., Mendonca, S., Bhuvan, T., Payne, N.L., Zheng, D., Hisana, A., Wallis, G., Barugahare, A., Powell, D., et al. (2021). Mesenchymal stromal cell apoptosis is required for their therapeutic function. Nature Communications *12*. 10.1038/s41467-021-26834-3.

111. Galleu, A., Riffo-Vasquez, Y., Trento, C., Lomas, C., Dolcetti, L., Cheung, T.S., von Bonin, M., Barbieri, L., Halai, K., Ward, S., et al. (2017). Apoptosis in mesenchymal stromal cells induces in vivo recipient-mediated immunomodulation. Science translational medicine *9*. 10.1126/scitranslmed.aam7828.

112. K, S., JP, W., C, D.S., KR, W., J, M., DA, F., BW, W., J, G., I, W., DJ, S., et al. (2019). Effects of Mesenchymal Stem Cell Treatment on Systemic Cytokine Levels in a Phase 1 Dose Escalation Safety Trial of Septic Shock Patients. Critical care medicine *47*. 10.1097/CCM.0000000000003657.

113. Bozza, F.A., Salluh, J.I., Japiassu, A.M., Soares, M., Assis, E.F., Gomes, R.N., Bozza, M.T., Castro-Faria-Neto, H.C., and Bozza, P.T. (2007). Cytokine profiles as markers of disease severity in sepsis: a multiplex analysis. Critical Care *11*, R49. 10.1186/cc5783.

114. Cummings, C.J., Martin, T.R., Frevert, C.W., Quan, J.M., Wong, V.A., Mongovin, S.M., Hagen, T.R., Steinberg, K.P., and Goodman, R.B. (1999). Expression and function of the chemokine receptors CXCR1 and CXCR2 in sepsis. J Immunol *162*, 2341-2346.

115. Ness, T.L., Hogaboam, C.M., Strieter, R.M., and Kunkel, S.L. (2003). Immunomodulatory Role of CXCR2 During Experimental Septic Peritonitis. The Journal of Immunology *171*, 3775-3784. 10.4049/jimmunol.171.7.3775.

116. Adams, J.M., Hauser, C.J., Jawa, Livingston, D.H., Lavery, R.F., Fekete, Z., Deitch, E.A., Croce, M.A., Cone, J.B., Simpkins, C., II, and Benoit, R.S. Early trauma polymorphonuclear neutrophil responses to chemokines are associated with development of sepsis, pneumonia, and organ failure. Discussion. held in Hagerstown, MD, 2001. (Lippincott Williams & Wilkins), pp. 452-457.

117. Hoesel, L.M., Neff, T.A., Neff, S.B., Younger, J.G., Olle, E.W., Hongwei, G.A.O., Pianko, M.J., Bernacki, K.D., Sarma, J.V., and Ward, P.A. (2005). Harmful and protective roles of neutrophils in sepsis. Shock (Augusta, Ga.) *24*, 40-47. 10.1097/01.shk.0000170353.80318.d5.

118. Demaret, J., Venet, F., Friggeri, A., Cazalis, M.-A., Plassais, J., Jallades, L., Malcus, C., Poitevin-Later, F., Textoris, J., Lepape, A., and Monneret, G. (2015). Marked alterations of neutrophil functions during sepsis-induced immunosuppression. Journal of Leukocyte Biology *98*, 1081-1090. 10.1189/jlb.4a0415-168rr.

119. Hoogendijk, A.J., Van Vught, L.A., Wiewel, M.A., Fuhler, G.M., Belkasim-Bohoudi, H., Horn, J., Schultz, M.J., Scicluna, B.P., Peppelenbosch, M.P., Van 'T Veer, C., et al.

(2019). Kinase activity is impaired in neutrophils of sepsis patients. Haematologica *104*, e233-e235. 10.3324/haematol.2018.201913.

120. Raffaghello, L., Bianchi, G., Bertolotto, M., Montecucco, F., Busca, A., Dallegri, F., Ottonello, L., and Pistoia, V. (2008). Human Mesenchymal Stem Cells Inhibit Neutrophil Apoptosis: A Model for Neutrophil Preservation in the Bone Marrow Niche. Stem cells (Dayton, Ohio) *26*, 151-162. 10.1634/stemcells.2007-0416.

121. Hall, S.R.R., Tsoyi, K., Ith, B., Padera, R.F., Lederer, J.A., Wang, Z., Liu, X., and Perrella, M.A. (2013). Mesenchymal Stromal Cells Improve Survival During Sepsis in the Absence of Heme Oxygenase-1: The Importance of Neutrophils. Stem cells (Dayton, Ohio) *31*, 397-407. 10.1002/stem.1270.

122. Jiang, D., Muschhammer, J., Qi, Y., Kügler, A., de Vries, J.C., Saffarzadeh, M., Sindrilaru, A., Beken, S.V., Wlaschek, M., Kluth, M.A., et al. (2016). Suppression of Neutrophil-Mediated Tissue Damage—A Novel Skill of Mesenchymal Stem Cells. Stem cells (Dayton, Ohio) *34*, 2393-2406. 10.1002/stem.2417.

123. Mittal, S.K., Mashaghi, A., Amouzegar, A., Li, M., Foulsham, W., Sahu, S.K., and Chauhan, S.K. (2018). Mesenchymal Stromal Cells Inhibit Neutrophil Effector Functions in a Murine Model of Ocular Inflammation. Invest Ophthalmol Vis Sci *59*, 1191-1198. 10.1167/iovs.17-23067.

124. Margraf, S., Lögters, T., Reipen, J., Altrichter, J., Scholz, M., and Windolf, J. (2008). Neutrophil-derived circulating free DNA (cf-DNA/NETs): a potential prognostic marker for posttraumatic development of inflammatory second hit and sepsis. Shock (Augusta, Ga.) *30*, 352-358. 10.1097/SHK.0b013e31816a6bb1.

125. Maruchi, Y., Tsuda, M., Mori, H., Takenaka, N., Gocho, T., Huq, M.A., and Takeyama, N. (2018). Plasma myeloperoxidase-conjugated DNA level predicts outcomes and organ dysfunction in patients with septic shock. Critical Care *22*. 10.1186/s13054-018-2109-7.

126. Pena, O.M., Hancock, D.G., Lyle, N.H., Linder, A., Russell, J.A., Xia, J., Fjell, C.D., Boyd, J.H., and Hancock, R.E.W. (2014). An Endotoxin Tolerance Signature Predicts Sepsis and Organ Dysfunction at Initial Clinical Presentation. EBioMedicine *1*, 64-71. 10.1016/j.ebiom.2014.10.003.

127. Cavaillon, J.-M., and Adib-Conquy, M. (2006). Critical Care *10*, 233. 10.1186/cc5055.

128. Cavaillon, J.-M., and Adib-Conquy, M. (2006). Bench-to-bedside review: endotoxin tolerance as a model of leukocyte reprogramming in sepsis. Crit Care *10*, 233. 10.1186/cc5055.

129. Jiang, X.-X., Zhang, Y., Liu, B., Zhang, S.-X., Wu, Y., Yu, X.-D., and Mao, N. (2005). Human mesenchymal stem cells inhibit differentiation and function of monocyte-derived dendritic cells. Blood *105*, 4120-4126. 10.1182/blood-2004-02-0586.

130. Jiang, D., Singh, K., Muschhammer, J., Schatz, S., Sindrilaru, A., Makrantonaki, E., Qi, Y., Wlaschek, M., and Scharffetter-Kochanek, K. (2020). MSCs rescue impaired wound healing in a murine LAD1 model by adaptive responses to low TGF-β1 levels. EMBO reports *21*. 10.15252/embr.201949115.

131. Liotta, F., Angeli, R., Cosmi, L., Filì, L., Manuelli, C., Frosali, F., Mazzinghi, B., Maggi, L., Pasini, A., Lisi, V., et al. (2008). Toll-Like Receptors 3 and 4 Are Expressed by Human Bone Marrow-Derived Mesenchymal Stem Cells and Can Inhibit Their T-Cell Modulatory Activity by Impairing Notch Signaling. Stem Cells *26*, 279-289. 10.1634/stemcells.2007-0454.

132. Lin, T., Pajarinen, J., Nabeshima, A., Lu, L., Nathan, K., Jämsen, E., Yao, Z., and Goodman, S.B. (2017). Preconditioning of murine mesenchymal stem cells synergistically enhanced immunomodulation and osteogenesis. Stem Cell Research & Therapy *8*. 10.1186/s13287-017-0730-z.

133. Franchi, L., Eigenbrod, T., Muñoz-Planillo, R., and Nuñez, G. (2009). The inflammasome: a caspase-1-activation platform that regulates immune responses and disease pathogenesis. Nature Immunology *10*, 241-247. 10.1038/ni.1703.

134. Li, Y., and Jiang, Q. (2023). Uncoupled pyroptosis and IL-1β secretion downstream of inflammasome signaling. Frontiers in immunology *14*, 1128358-1128358. 10.3389/fimmu.2023.1128358.

135. Martinon, F., and Tschopp, J. (2004). Inflammatory Caspases. Cell *117*, 561-574. 10.1016/j.cell.2004.05.004.

136. Madouri, F., Guillou, N., Fauconnier, L., Marchiol, T., Rouxel, N., Chenuet, P., Ledru, A., Apetoh, L., Ghiringhelli, F., Chamaillard, M., et al. (2015). Caspase-1 activation by NLRP3 inflammasome dampens IL-33-dependent house dust mite-induced allergic lung inflammation. Journal of molecular cell biology *7*, 351-365. 10.1093/jmcb/mjv012.

137. Sarkar, A., Hall, M.W., Exline, M., Hart, J., Knatz, N., Gatson, N.T., and Wewers, M.D. (2006). Caspase-1 RegulatesEscherichia coliSepsis and Splenic B Cell Apoptosis Independently of Interleukin-1β and Interleukin-18. American Journal of Respiratory and Critical Care Medicine *174*, 1003-1010. 10.1164/rccm.200604-546oc.

138. Vanden Berghe, T., Demon, D., Sze Men, C., Meyer, E., Krautwald, S., Declercq, W., Takahashi, N., Cauwels, A., Vandenabeele, P., Bogaert, P., et al. (2014).

Simultaneous Targeting of IL-1 and IL-18 Is Required for Protection against Inflammatory and Septic Shock. American journal of respiratory and critical care medicine *189*, 282-291. 10.1164/rccm.201308-1535OC.

139. Giamarellos-Bourboulis, E.J., Van De Veerdonk, F.L., Mouktaroudi, M., Raftogiannis, M., Antonopoulou, A., Joosten, L.A., Pickkers, P., Savva, A., Georgitsi, M., Van Der Meer, J.W., and Netea, M.G. (2011). Inhibition of caspase-1 activation in gram-negative sepsis and experimental endotoxemia. Critical Care *15*, R27. 10.1186/cc9974.

140. Wang, L., Chen, K., Wan, X., Wang, F., Guo, Z., and Mo, Z. (2017). NLRP3 inflammasome activation in mesenchymal stem cells inhibits osteogenic differentiation and enhances adipogenic differentiation. Biochemical and biophysical research communications *484*, 871-877. 10.1016/j.bbrc.2017.02.007.

141. Zhang, C., Zhao, C., Chen, X., Tao, R., Wang, S., Meng, G., Liu, X., Shao, C., and Su, X. (2020). Induction of ASC pyroptosis requires gasdermin D or caspase-1/11-dependent mediators and IFNβ from pyroptotic macrophages. Cell Death & Disease *11*. 10.1038/s41419-020-2664-0.

142. Ahn, J.-S., Seo, Y., Oh, S.-J., Yang, J.W., Shin, Y.Y., Lee, B.-C., Kang, K.-S., Sung, E.-S., Lee, B.-J., Mohammadpour, H., et al. (2020). The activation of NLRP3 inflammasome potentiates the immunomodulatory abilities of mesenchymal stem cells in a murine colitis model. BMB Reports *53*, 329-334. 10.5483/bmbrep.2020.53.6.065.

143. Wang, Y., Chen, X., Cao, W., and Shi, Y. (2014). Plasticity of mesenchymal stem cells in immunomodulation: pathological and therapeutic implications. Nature immunology *15*, 1009-1016. 10.1038/ni.3002.

144. Shi, Y., Wang, Y., Li, Q., Liu, K., Hou, J., Shao, C., and Wang, Y. (2018). Immunoregulatory mechanisms of mesenchymal stem and stromal cells in inflammatory diseases. Nature reviews. Nephrology *14*, 493-507. 10.1038/s41581-018-0023-5.

145. Abreu, S.C., Rolandsson Enes, S., Dearborn, J., Goodwin, M., Coffey, A., Borg, Z.D., Dos Santos, C.C., Wargo, M.J., Cruz, F.F., Loi, R., et al. (2019). Lung inflammatory environments differentially alter mesenchymal stromal cell behavior. American Journal of Physiology-Lung Cellular and Molecular Physiology *317*, L823-L831. 10.1152/ajplung.00263.2019.

146. Moll, G., Ankrum, J.A., Kamhieh-Milz, J., Bieback, K., Ringdén, O., Volk, H.-D., Geissler, S., and Reinke, P. (2019). Intravascular Mesenchymal Stromal/Stem Cell Therapy Product Diversification: Time for New Clinical Guidelines. Trends in Molecular Medicine *25*, 149-163. 10.1016/j.molmed.2018.12.006.

147. Hass, R., Kasper, C., Böhm, S., and Jacobs, R. (2011). Different populations and sources of human mesenchymal stem cells (MSC): A comparison of adult and neonatal tissue-derived MSC. Cell Communication and Signaling *9*, 12. 10.1186/1478-811x-9-12.

148. Dwyer, R.M., Potter-Beirne, S.M., Harrington, K.A., Lowery, A.J., Hennessy, E., Murphy, J.M., Barry, F.P., O'Brien, T., and Kerin, M.J. (2007). Monocyte Chemotactic Protein-1 Secreted by Primary Breast Tumors Stimulates Migration of Mesenchymal Stem Cells. Clinical Cancer Research *13*, 5020-5027. 10.1158/1078-0432.ccr-07-0731.

149. Hanahan, D., and Coussens, M., Lisa (2012). Accessories to the Crime: Functions of Cells Recruited to the Tumor Microenvironment. Cancer Cell *21*, 309-322. 10.1016/j.ccr.2012.02.022.

150. Joyce, J.A., and Fearon, D.T. (2015). T cell exclusion, immune privilege, and the tumor microenvironment. Science (American Association for the Advancement of Science) *348*, 74-80. 10.1126/science.aaa6204.

151. Ostrand-Rosenberg, S. (2008). Immune surveillance: a balance between protumor and antitumor immunity. Current opinion in genetics & development *18*, 11-18. 10.1016/j.gde.2007.12.007.

152. Polchert, D., Sobinsky, J., Douglas, G., Kidd, M., Moadsiri, A., Reina, E., Genrich, K., Mehrotra, S., Setty, S., Smith, B., and Bartholomew, A. (2008). IFN-γ activation of mesenchymal stem cells for treatment and prevention of graft versus host disease. European Journal of Immunology *38*, 1745-1755. 10.1002/eji.200738129.

153. Sheng, H., Wang, Y., Jin, Y., Zhang, Q., Zhang, Y., Wang, L., Shen, B., Yin, S., Liu, W., Cui, L., and Li, N. (2008). A critical role of IFNγ in priming MSC-mediated suppression of T cell proliferation through up-regulation of B7-H1. Cell Research *18*, 846-857. 10.1038/cr.2008.80.

154. Chacko, S.M., Ahmed, S., Selvendiran, K., Kuppusamy, M.L., Khan, M., and Kuppusamy, P. (2010). Hypoxic preconditioning induces the expression of prosurvival and proangiogenic markers in mesenchymal stem cells. American Journal of Physiology: Cell Physiology *299*, C1562-C1570. 10.1152/ajpcell.00221.2010.

155. Lan, Y.-W., Choo, K.-B., Chen, C.-M., Hung, T.-H., Chen, Y.-B., Hsieh, C.-H., Kuo, H.-P., and Chong, K.-Y. (2015). Hypoxia-preconditioned mesenchymal stem cells attenuate bleomycin-induced pulmonary fibrosis. Stem Cell Research & Therapy *6*. 10.1186/s13287-015-0081-6.

156. Bustos, M.L., Huleihel, L., Meyer, E.M., Donnenberg, A.D., Donnenberg, V.S., Sciurba, J.D., Mroz, L., Mcverry, B.J., Ellis, B.M., Kaminski, N., and Rojas, M. (2013).

Activation of Human Mesenchymal Stem Cells Impacts Their Therapeutic Abilities in Lung Injury by Increasing Interleukin (IL)-10 and IL-1RN Levels. Stem Cells Translational Medicine *2*, 884-895. 10.5966/sctm.2013-0033.

157. Martínez-González, I., Roca, O., Masclans, J.R., Moreno, R., Salcedo, M.T., Baekelandt, V., Cruz, M.J., Rello, J., and Aran, J.M. (2013). Human mesenchymal stem cells overexpressing the IL-33 antagonist soluble IL-1 receptor-like-1 attenuate endotoxin-induced acute lung injury. American journal of respiratory cell and molecular biology *49*, 552-562. 10.1165/rcmb.2012-0406oc.

158. Monsel, A., Zhu, Y.-G., Gennai, S., Hao, Q., Hu, S., Rouby, J.-J., Rosenzwajg, M., Matthay, M.A., and Lee, J.W. (2015). Therapeutic Effects of Human Mesenchymal Stem Cell–derived Microvesicles in Severe Pneumonia in Mice. American Journal of Respiratory and Critical Care Medicine *192*, 324-336. 10.1164/rccm.201410-1765oc.

159. Shah, T.G., Predescu, D., and Predescu, S. (2019). Mesenchymal stem cells-derived extracellular vesicles in acute respiratory distress syndrome: a review of current literature and potential future treatment options. Clinical and Translational Medicine *8*. 10.1186/s40169-019-0242-9.

160. Kou, M., Huang, L., Yang, J., Chiang, Z., Chen, S., Liu, J., Guo, L., Zhang, X., Zhou, X., Xu, X., et al. (2022). Mesenchymal stem cell-derived extracellular vesicles for immunomodulation and regeneration: a next generation therapeutic tool? Cell Death & Disease *13*. 10.1038/s41419-022-05034-x.

161. Wang, J., Huang, R., Xu, Q., Zheng, G., Qiu, G., Ge, M., Shu, Q., and Xu, J. (2020). Mesenchymal Stem Cell–Derived Extracellular Vesicles Alleviate Acute Lung Injury Via Transfer of miR-27a-3p. Critical care medicine *48*, e599-e610. 10.1097/CCM.0000000000004315.

162. Chen, W., Huang, Y., Han, J., Yu, L., Li, Y., Lu, Z., Li, H., Liu, Z., Shi, C., Duan, F., and Xiao, Y. (2016). Immunomodulatory effects of mesenchymal stromal cells-derived exosome. Immunologic research *64*, 831-840. 10.1007/s12026-016-8798-6.

163. Moser, E.K., Hufford, M.M., and Braciale, T.J. (2014). Late Engagement of CD86 after Influenza Virus Clearance Promotes Recovery in a FoxP3+ Regulatory T Cell Dependent Manner. PLoS Pathogens *10*, e1004315. 10.1371/journal.ppat.1004315.

164. Akbari, A., and Rezaie, J. (2020). Potential therapeutic application of mesenchymal stem cell-derived exosomes in SARS-CoV-2 pneumonia. Stem Cell Research & Therapy *11*. 10.1186/s13287-020-01866-6.

165. Wang, X., Gu, H., Qin, D., Yang, L., Huang, W., Essandoh, K., Wang, Y., Caldwell, C.C., Peng, T., Zingarelli, B., and Fan, G.-C. (2015). Exosomal miR-223 Contributes

to Mesenchymal Stem Cell-Elicited Cardioprotection in Polymicrobial Sepsis. Scientific Reports *5*, 13721. 10.1038/srep13721.

166. Yao, M., Cui, B., Zhang, W., Ma, W., Zhao, G., and Xing, L. (2021). Exosomal miR-21 secreted by IL-1β-primed-mesenchymal stem cells induces macrophage M2 polarization and ameliorates sepsis. Life sciences (1973) *264*, 118658-118658. 10.1016/j.lfs.2020.118658.

167. Song, Y., Dou, H., Li, X., Zhao, X., Li, Y., Liu, D., Ji, J., Liu, F., Ding, L., Ni, Y., and Hou, Y. (2017). Exosomal miR-146a Contributes to the Enhanced Therapeutic Efficacy of Interleukin-1β-Primed Mesenchymal Stem Cells Against Sepsis. Stem Cells *35*, 1208-1221. 10.1002/stem.2564.

168. Kotecha, N., Krutzik, P.O., and Irish, J.M. (2010). Web-based analysis and publication of flow cytometry experiments. Curr Protoc Cytom *Chapter 10*, Unit10.17. 10.1002/0471142956.cy1017s53.